POLITECNICO DI MILANO

Facoltà di Ingegneria dei Sistemi
Corso di Laurea Magistrale in Ingegneria Biomedica

STAND-ALONE INTRAOPERATIVE ULTRASOUND IMAGING FOR NEUROSURGERY

Relatore: Prof. Giancarlo Ferrigno
Correlatore: Dott. Roberto Israel Foroni

Tesi di Laurea di:
CARLO GIRELLI
Matricola: 766565

Anno Accademico 2012-2013

A papà e mamma:

i miei migliori insegnanti.

Sommario

Il campo della neurochirurgia è sempre stato all'avanguardia nell'innovazione e nella ricerca, e la strumentazione per aiutare il neurochirurgo nella cura del malato è molto vasta. Sono attualmente presenti, nelle sale operatorie della neurochirurgia di Verona, dove ho svolto il mio lavoro, il microscopio, il neuronavigatore e il monitoraggio neurofisiologico. Nella pratica neurochirurgica è inoltre possibile ricorrere a metodologie di imaging avanzato in fase di pianificazione dell'intervento, sfruttando la tecnica della trattografia da Diffusion Tensor Imaging (DTI). Nella neurochirurgia più che in altre specialità chirurgiche, gli strumenti di imaging sono divenuti essenziali. Un nuovo e vasto campo di ricerca riguarda l'acquisizione di immagini in fase intraoperatoria le quali possono rivelarsi molto utili poiché forniscono informazioni sullo stato della procedura chirurgica durante l'intervento. Il neurochirurgo è messo nelle condizioni di valutare con più accuratezza la percentuale di rimozione della lesione, oltre alla collocazione spaziale nell'encefalo dell'area di intervento. Esistono diversi strumenti in grado di effettuare imaging intraoperatorio. I più conosciuti sono radiografie e risonanze magnetiche le quali si distinguono tra alto (> 1.5 Tesla) e basso campo (< 0.8 Tesla). I principali difetti comuni a queste tecniche sono l'alto costo, i lunghi tempi di acquisizione, la necessità di interrompere l'intervento durante l'esame e la realizzazione di immagini che rimangono lontane dall'essere in real-time. Alle tecniche di imaging che sfruttano i raggi X si va inoltre ad aggiungere la problematica della dose a cui sono sottoposti il paziente e gli operatori.

In questo studio ho valutato le possibilità offerte dalla tecnica di imaging che sfrutta il principio della ultrasonografia (US). L'imaging intraoperatorio ecografico supera tutti gli svantaggi delle tecniche citate precedentemente, ha costi economici molto inferiori e necessita di tempi di acquisizione molto ridotti. Uno scanner ecografico è venduto a un prezzo di $150,000$ euro più un costo di circa $10,000$ euro a sonda, una risonanza magnetica supera il milione di euro, senza contare il costo del necessario adeguamento dei locali. Nella mia esperienza con l'ecografo e in quella di molti altri autori non sono mai stati spesi più di 5 minuti per intervento. Inoltre non necessita dell'interruzione dell'intervento chirurgico, non fornisce dose ulteriore al paziente e non è necessario, come per le tecniche che sfruttano il principio di risonanza magnetica, adeguare i locali o le strumentazioni per il suo utilizzo. L'unico limite di questa tecnica risiede nella più complessa lettura da parte del chirurgo delle immagini. Questo limite può essere superato con l'esperienza o con un adeguato addestramento. Al contrario, una risonanza magnetica ha tempi di acquisizione molto superiori (mediamente 8 minuti per ogni acquisizione pesata in T1 o in T2), e l'intervento deve essere momentaneamente interrotto.

Lo studio è stato svolto presso il dipartimento di neurochirurgia dell'ospedale maggiore di Verona. Nell'ultimo anno questa tecnica è stata testata su un gruppo di pazienti per valutarne l'utilità e l'efficacia. Nel primo capitolo è descritta la situazione del sistema sanitario italiano, per comprendere la necessità di rinnovamento e di innovazione a basso costo. E' inoltre descritta l'importanza delle tecniche di imaging in neurochirurgia ed esposto lo scopo del lavoro. Nel secondo capitolo si trova la descrizione della fisica degli ultrasuoni allo scopo di comprenderne le interazioni con la materia e la modalità di generazione delle immagini. E' anche mostrato lo stato dell'arte nell'utilizzo di questa metodologia a livello mondiale. Nel terzo capitolo sono descritti gli strumenti a disposizione e i metodi utilizzati per l'acquisizione delle immagini. Nel quarto capitolo vi è una trattazione delle problematiche riscontrate e delle soluzioni proposte. Sono inoltre analizzati i dati con tecniche statistiche. Nel quinto capitolo sono tratte le conclusioni e sono descritti possibili miglioramenti e sviluppi futuri realisticamente perseguibili. In appendice si trovano tutte le immagini estratte e l'analisi dettagliata di esse. Lo studio mostra come l'imaging ecografico intraoperatorio porti informazione real-time fruibile e utile al chirurgo, a tutto beneficio del malato.

Parole chiave

- Neurochirurgia;
- Ultrasuoni;
- Correlazione MRI-US;
- Imaging intraoperatorio in tempo reale;
- Elaborazione di immagini.

Abstract

Neurosurgery has always been at the forefront in innovation and research, and instrumentation to help the neurosurgeon in the care of the patient is very wide. Are currently present in the operating rooms of neurosurgery in Verona, where I did my work, the microscope, the neuronavigation and neurophysiological monitoring. In neurosurgical practice is also possible to use advanced imaging methodologies in the planning stage of the intervention, using the technique of tractography from Diffusion Tensor Imaging (DTI). In neurosurgery, more than in other surgical specialties, imaging tools have become essential. A new and large field of research concerns the acquisition of images during surgery which can be very useful because they provide information on the status of the surgical procedure during surgery. The neurosurgeon can assess more accurately the proportion of removal of the lesion and the spatial location of the intervention area. There are several technologies that can perform intraoperative imaging. The best known are X-rays and MRIs which are distinguished between high ($>$ 1.5 Tesla) and low-field ($<$0.8 Tesla). The main issues common to these techniques are the high cost, the acquisition times, the need to interrupt the operation during the exam and the creation of images that remain far from being in real-time. Imaging techniques that use X-rays also add to the problem of the dose to which patient and operators are subjected. In this study I evaluated the possibilities offered by the imaging technique that uses the principle of ultrasound (US). The intraoperative ultrasound imaging overcomes all disadvantages of

the techniques mentioned above. It costs much lower and requires littler acquisition times. An ultrasound scanner is sold at a price of $150,000$ euros plus a cost of around $10,000$ euros for each probe. An MRI scanner costs over than a million euros, not counting the cost of the necessary adaptation of the rooms. In litterature, and in my experience, more than 5 minutes per intervenction with ultrasound, have never been spent. Ultrasound does not require the interruption of surgery, does not provide further dose to the patient and is not necessary, as for techniques that use the principle of magnetic resonance, adapt the rooms or the instrumentation for its use. The only limitation of this technique resides in the more complex reading by the surgeon of the images. This limitation can be overcome with the proper training or experience. In contrast, an MRI acquisition times is much higher (average 8 minutes per each T1 or T2 weighted acquisition), and the operation must be stopped.

This study was carried out at the department of neurosurgery of Verona. In the last year, this technique was tested on a group of patients to evaluate its usefulness and effectiveness. The 1^{st} chapter describes the state of the Italian health care system, to understand the need of renewal and innovation at low cost. It is also described the importance of imaging techniques in neurosurgery and exposed the purpose of the work. 2^{nd} chapter contains a description of the physics of ultrasound, in order to understand the interactions with tissues and image generation. Is also shown the state of the art in the use of this methodology. 3^{rd} chapter describes the tools available and the methods used to acquire the images. In the 4^{th} chapter there is a discussion of problems encountered and solutions proposed. They also analyzed the data using statistical techniques. In the 5^{th} chapter the conclusions are drawn and described possible improvements and future developments. Appendix contains all the extracted images and detailed analysis of them. The study shows that intraoperative ultrasound imaging brings real-time information accessible and useful to the surgeon, for the benefit of the patient.

Keywords

- Neurosurgery;
- Ultrasound;
- Correlation MRI-US;
- Real-time intraoperative imaging;
- Image processing.

Contents

Chapter 1

Introduction

“ ʼΕν ἀρχῆ ῆν ὁ λόγος,
καὶ ὁ λόγος ῆν πρὸς τὸν θεόν,
καὶ θεὸς ῆν ὁ λόγος.”

Johannes 1,1

1.1 Healthcare in Italy

Italy is a democratic republic but throughout its history it has experienced different forms of government that influenced the evolution, and current status, of its national health system. [24]

Health Indicators

Health indicators are quantifiable characteristics of a population which researchers use as supporting evidence for describing the health of a population. Health status in Italy is excellent. All indicators are among the best in the world. For the World Health Organization (WHO) life expectancy is 82 years in 2008, second only to Japan. Health-Adjusted Life Expectancy (HALE) is 74 years in 2007, infant mortality is 3 out of 1000 in 2008, and 20% of population is over 65. Many studies have shown that these successes are due in particular to the lifestyle but there is little doubt that having adopted a system of health care organization modeled on the British national health service, has certainly had a positive impact on these indices. [24]

Expenditure and Financing

The Italian health care expenditure is currently similar to the European avarage. Generally speaking, the Italian expenditure measured as a percentage of Gross Domestic Product (GDP) is equal to or higher than the Organisation for Economic Co-operation and Development (OECD) average, the per capita is lower. In Italy, spending on health care for the hospital sector is relevant. In 2009 was 45.4% of the total health expenditure. In most of other European countries is between 35% and 40%. The distribution of expenditure across regions is strongly influenced by patient mobility. In general, migration health goes from south to north, and is especially true for the more affluent social classes. About 79% of the total expenditure is supported by general taxation, 20% by direct fees, and 1% by private insurance.[24]

European sovreign-debt crisis

The financial crisis of 2007–2008, as well as the great depression of 2009-2013, and other factors, generated the european sovreign-debt crisis.
Many European countries embarked on austerity programs, reducing their budget deficits relative to GDP from 2010 to 2011. Iceland, Italy, Ireland, Portugal, France, and Spain improved their budget deficits from 2010 to 2011 relative to GDP. However, with the exception of Germany, each of these countries had public-debt-to-GDP ratios that increased from 2010 to 2011, as indicated in figure 1.1. As consequence of these austerity programs, invesment on innovation and research was limited.

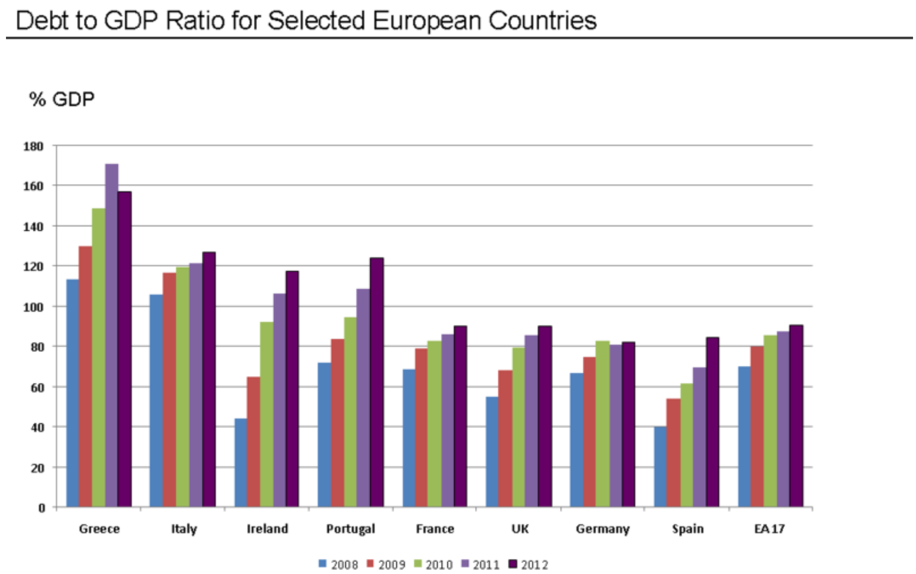

Figure 1.1: Public Debt to GDP Ratio for Selected European Countries - 2008 to 2012. [1]

Innovation

Due to all these factors, finding resources and funds to pursue technological innovation in the public sector has become very complicated in recent years. In this study I found the way to achieve a good level of innovation, with excellent prospects for the future, in surgical procedures, with a limitated budget.

1.2 Hospital institute of Verona

The Hospital Trust of Verona is very renowned in the Veneto region and nation-wide recognized as a Health Center for its excellent specialities as well as for its research, assistance and training.[2]

Structures

The Trust consists of two hospitals: the Ospedale Civile Maggiore (OCM) in Borgo Trento and the Ospedale Policlinico Giambattista Rossi in Borgo Roma, plus 13 regional reference centers. Here, many extraordinary operations are performed such as transplants, brain surgeries, heart surgery, chest surgeries, scald center and onco-haematology.
The Hospital Trust of Verona offers the main surgery and medical specialities in the operative centers and the diagnosis and cure centers. Hospitalization, speciality wards with visits, exams and lab diagnosis are offered as well. Visits and exams are also available on payment.[2]

Statistics

Over 5000 people work in the Trust, among these, hospital and university doctors, nurses, sanitary operators, technicians and administration employees. The two hospitals in town offer assistance, hospitalization and emergency wards 24 hours a day to the almost 500 people who daily need it. Every year 60.000 people are hospitalized in the hospitals of the Trust, among these 10.000 come from outer regions and over 3000 from other provinces. Every day 1300 patients are hospitalized, 400 people are treated in day hospital. Every day 100 surgeon operations are performed, one third of these takes place on a day hospital basis - 3000 people are daily visited in wards. 211 patients are discharged, 34 of these come from regions other than Veneto. 1082 people are treated daily in the emergency ward, 185 people are dialyzed, 12 are hospitalized in intensive therapy, 9 babies are born.[2]

Excellence

The hospitals are specialized in the organ and tissue transplants, as well as heart, cornea, marrow, lung and liver transplants. The fist kidney transplant was occurred in 1968. The hospital, in cooperation with the Medicine and Surgery University in Verona, offers an ever increasing quality in diagnosis and treatments, as research, as well as innovation and updating, play and important role.
The constant cooperation of the hospital with the university grants life long learning to doctors and operators of higher quality standards.[2]

1.3 Importance of gross total removal for survival rate

One of the main object in neurosurgical tumor resection is to achieve gross total removal of the lesion. Perform a total removal resection is very important for survival rate and intraoperative imaging may help the surgeon in this way.
The extent of resection (EOR) is a known prognostic factor in patients with brain tumor [26] [37] [38]. However, gross-total resection (GTR) is not always achieved. A work performed in Michigan University, published in 2012, tried

to identify demographic tumor-related and technical factors that influence EOR and to define the relationship between the surgeon's impression of EOR and the radio graphically determined resection. The authors conclude that EOR is affected by tumor location and suggest that it may also be influenced by the surgeon's ability to judge the presence of residual tumor diring surgery. Furthermore, they declared that this ability to judge the completeness of resection during surgery is commonly inaccurate.
In order to assist surgeons in evaluating the EOR they will require more information. The most valued information that could be given to surgeons is intraoperative imaging. If surgeons can directly evaluate the EOR during the surgery procedure they can easily achieve GTR. Intraoperative imaging could assist surgeons to be more accurate in surgical procedure, and therefore minimizing damage on the healthy tissue. [25]

1.4 Importance of intra-operative imaging in neurosurgery

Neurosurgery is the medical specialty concerned with the prevention, diagnosis, treatment and rehabilitation of disorders that affect the entire nervous system including the spinal column, spinal cord, brain and peripheral nerves. In every medical speciality imaging is important, however in this particular field it is of great imporrtance. The importance of imaging in this specialty is given by:

- The extreme sensitivity of brain tissue to external damage;
- The importance that the brain plays in the body;
- The lack of reference points clearly identifiable by the surgeon during surgery procedure.

1.4.1 Image-guidance for neuro-surgical procedures

Image-guidance in surgical procedures is used in much the same way that navigational technology is employed to guide an airplane pilot when a direct view of the landing site is unavailable.
Many surgical interventions involve significant trauma to the patient. To ensure minimal trauma is necessary to define accurately the target and to plan a route that offers minimal disturbance to the intervening tissue. To define target and trajectory it is necessary to register multi-modal pre-operative images to each other and to the patient, and to track instruments in real-time. It is also important to provide the surgeons with high quality images that explain not only normal anatomy and pathology, but also vascularity and function. [41]

1.4.2 Imaging techniques

X-ray fluoroscopy and DSA

Fluoroscopy is used to guide catheters during interventions in the brain. With DSA we are able to see the vascular system clearly without the interference of overlying structures. These systems are sometimes unable to visualize the soft-tissue targets. This led combines x-ray fluoroscopy with pre-operative 3D models. This allows the catheter tip to be placed in the appropriate position. [41]

Computed Tomography

CT scanners are present in some operating rooms (OR) for their capacity to acquire high resolution 3D images. However there are significant problems limiting the use of CT in the OR as an intra-operative imaging modality. The first one is the radiation dose delivered to both patient and surgeon. The second one is the difficulty to justify the use of intra-operative CT

economically. The third one is the low capacity in distinguishing the soft tissue. Another one is the image could be corrupted by bleeding. The lastly is that the acquired images do not occur in real-time and spends a lot of time to obtain them.
The standard CT image is intrinsically and geometrically accurate, although errors in patients or gantry alignment may result in errors in relating image coordinates to reference coordinates. The recent adoption of CT scanners capable of acquiring up to 64 simultaneous slices has removed many of the issues related to non-isotropic image resolution and slice alignment. [41]

Magnetic Resonance Imaging

Except for radiation dose, many of the problems of the CT intra-operative imaging are also found in intra operative MRI.
We can distinguish two different situations concerning intraoperative MRI: Low-Field MRI (<0.8 T) and High-Field MRI (>1.5 T).
Low-Field MRI provides lower resolution images compared to the pre-operative datasets. They can be used in the OR while the surgical action is proceeding but all the surgical instruments have to be non-ferromagnetic.
High-Field MRI provides high resolution images, however they can not be placed in the surgical environment, so it is necessary to interrupt the surgical procedure and to transport the patient in another room where the MRI system is located.
These limitations and the unacceptable economic investment has limited this solution in ordinary clinical environment in the majority of the Italian hospitals.
When MRI arrived on the scene, certain metallic components had to be replaced by non-metallic components to avoid creating magnetic field perturbations that would distort the images. The most probable cause of image distortion in MRI is the main magnetic field lack of homogeneity across the

volume of interest. It could be caused by spatial nonlinearities of the gradients or by locals perturbations by the presence of either an internal or external influence. Even the deviation of tens of part per million of the field strength from the ideal can have a significant impact on the geometrical integrity of the images, and the effect of gradient nonlinearities tends to be particularly noticeable towards the periphery of the field of view. Distortions due to the gradient design limitations are often automatically corrected by the scanner software. [41]

Ultrasound

The main advantages of ultrasounds are:

- Real-time imaging;
- Lower economical investment compared to intraoperative CT and MRI;
- Short extra-time during the surgical procedure;
- Increased identification accuracy of structures observed in the US images even if the registration accuracy (7-13 mm) is less then ideal;

Although ultrasound is inexpensive and unobtrusive, it has its own limitations. One immediate obstacle to its use in some circumstances is that intimate contact between the transducer and the tissue must be maintained at all times, usually via water or gel acoustic matching medium. Furthermore, image quality is somewhat operator dependent, and resolution is lower than MRI and CT. Another problem could be caused by the propagation velocity, if it is different from the supposed (1497 m/s), significant image distortion may result.

Ultrasound will probably be the future of image guidance for surgical procedures for their benefits. [41]

1.5 Aim of the work

The aim of this study is to improve the surgery procedure in the neurosurgery department of Verona, through the use of an intraoperative ultrasound imaging system, and to demonstrate that information given by intraoperative US are correlated and comparable to the preoperative Magnetic Resonance Imaging (MRI). Type of surgery that has been studied are removals of intracranial brain lesion. At the hospital a US scanner (Aloka $\alpha 7$ prosound), was available, and used for reasearch, so work was focused on bringing that system, as a choice for the surgeon, in the standard surgical procedure. As intraoperative imaging system, US is not the only one in litterature. Many others imaging systems could be use. The decision to use the US was a result of the following reasons:

- The availability of this imaging system without any additional costs;
- Adaptibility of this system in the surgical environment;
- Little additional time taken during the procedure to perform ultrasound acquisitions;
- Minimlly invasive for patient;
- No additional radiation dose to patient and operators;
- Possible future development that could be adapted in the future to the clinical environment.

1.5.1 Similarity between MRI weighted in T1 with contrast agent and US

MRI weighted in T1 with contrast agent and US imaging perform comparable images in term of grayscale. But the reason to that is not of immediate comprhension. As shown before, these imaging systems are very different

from each other, which be expected to illustrate different images.
The most commonly used compounds for contrast enhancement in MRI are gadolinium-based. They work throught shortening the T1 relaxation times of protons within body tissues where they are present after oral or intravenous administration. Therefore, the zones in which gadolinium is present, are brighter in MRI. Gadolinium binds easily to water, therefore this kind of MRI contrast agent is most commonly used for enhancement of vessels in MR angiography or for brain tumor enhancements associated with the degradation of the blood–brain barrier, where the presence of blood is relevant. Areas where gadolinium-rich blood (or water) is absent, appears darker than the other ones. Examples are cystic component of a lesion and the necrotic regions.

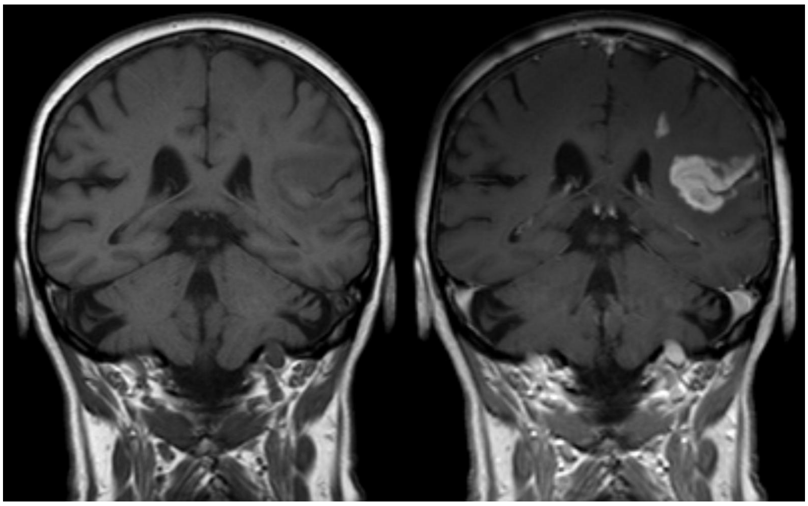

Figure 1.2: Effect of contrast agent on images: Defect of the blood–brain barrier after stroke shown in MRI. T1-weighted images, left image without, right image with contrast medium administration.

On US imaging the echogenicity of a certain region is represented in grayscale. Hyperechoic areas are represented with lighter grays, hypoechoic

regions with darker gray. In this way, the peripheral areas of the lesion, are hyperechogenic and lighter, the cystic/necrotic regions are hypoechoic and darker.
Making a summary, MRI weighted in T1 with Gadolinium and US:

- Are able to represent soft tissue well;
- Outline peripheral and proliferating regions of the lesion in light gray;
- Represent cystic part and necrotic areas of the lesion in dark gray.

For all this stuff we can suppose that MRI weighted in T1 with contrast agent and US are similar and comparable.

Chapter 2

State of art

"A few observation and much reasoning lead to error;
many observations and a little reasoning to truth."

Alexis Carrel (1873 - 1944)
Nobel Prize in Physiology or Medicine (1912)

2.1 Ultrasound

In neurosurgery, due to the properties of brain tissue in the propagation of the ultrasound waves, ultrasounds can be used in many important ways in imaging. Intraoperative ultrasound imaging may be effective in tumor localization, evaluation of brain shift, and visualization of blood vessels. [18] [20] [22] [40]

2.1.1 Physics of ultrasound

Ultrasound is a mechanical vibration of physical medium that perturbs the particles, generating around them regions of compression and rarefaction. In practical systems the ultrasound frequencies used are between 2 and 20 MHz's, that are above the audible range. This oscillation pressure propagates

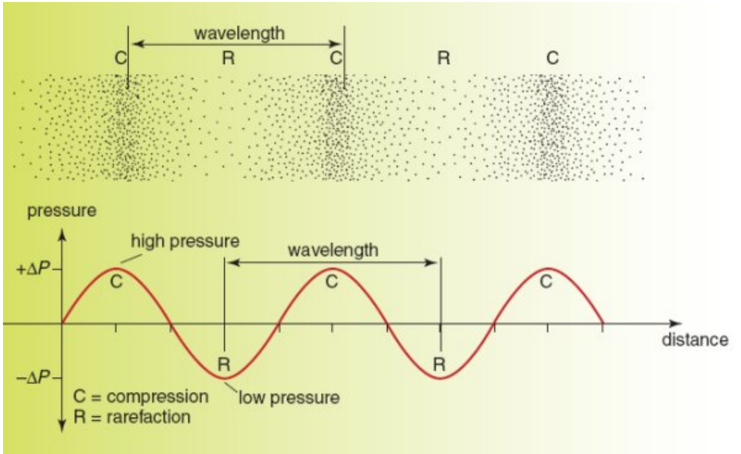

Figure 2.1: Ultrasound wave [3]

in space at a variable speed, in proportion to the density of the material in which the wave moves. When an ultrasound wave passes between tissues that have different acoustic impedances, only a percentage of wave energy passes through. The remaining energy is reflected with a reflection coefficient R_a that depends on the impedances (equation 2.5) of the two tissues. The reflected wave can be revealed by a transducer and gives us information about variation of tissue density. [18] [20] [22] [40]

Parameters of sound waves

An ultrasound wave can have different parameters that characterize the behaviour in relation to the matter in which it diffuses. The main parameters are:

- Amplitude A [m];
- Period T [s];
- Wavelenght λ [m];

Time frequency is a parameter related with period:

$$f = \frac{1}{T} \tag{2.1}$$

Spatial frequency is related with wavelenght:

$$\nu = \frac{1}{\lambda} \tag{2.2}$$

Speed of sound c is independent from the ultrasound wave, it depends only on the matter, in particular on density ρ and adiabatic compressibility κ.

$$c = \sqrt{\frac{1}{\bar{\rho}\kappa}} = \sqrt{\frac{B}{\bar{\rho}}} \tag{2.3}$$

Where $\bar{\rho}$ is the mean density and B is the adiabatic bulk modulus.
The characteristic acoustic impedance Z_0 $[\frac{kg}{m^2 \cdot s}]$ of a medium is an inherent property of a medium. Is calculated as:

$$Z_0 = \bar{\rho} \cdot c \tag{2.4}$$

When a sound wave passes through two zones with different acoustic impedance (Z_1 and Z_2), only a percentage of the wave energy passes through. The reflection R_a and the transmission T_a coefficient for an incident wave normal to the boundary are defined as:

$$R_a = \frac{Z_2 - Z_1}{Z_2 + Z_1} \tag{2.5}$$

$$T_a = 1 - R_a \tag{2.6}$$

To be able to extract useful information from the reflected wave it is necessary that the reflection rate ($R_{100} = \frac{R_a}{R_a + T_a} \cdot 100$) will be above -10% to $+10\%$. For this reason medical applications of ultrasound are limited to the soft tissues.

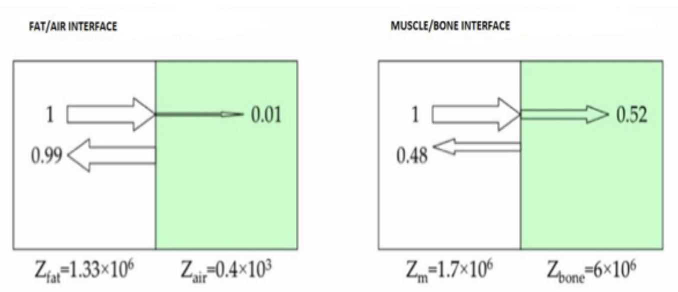

Figure 2.2: Difference of acoustic impedence [40]

Attenuation A $[\frac{dB}{MHz \cdot cm}]$ is another important property of the medium that strongly influence the usefullness of ultrasound in medical practice. While a sound wave is propagating in a tissue, it loses part of its energy for scattering and absorption. The attenuation is depended both on the medium and the frequency of the propagating wave.

$$A(f, d) = e^{-2\pi\beta f d} \tag{2.7}$$

d is the distance that the wave has propagated in the tissue. [40] [22] [18] [20]

2.1.2 Desctiption of basic system of ultrasound imaging

Generation of ultrasound

Ultrasound are generated using properties of piezoelectric crystals. Voltage high frequency input signal in a piezoeletric transducer generates an ultrasound acoustic wave. [18] [20] [22] [40]

Ultrasound transducer

Ultrasound transducers are used as emitters and receivers of ultrasound waves. In the figure below 2.3 a scheme of a typical ultrasound tranducer.

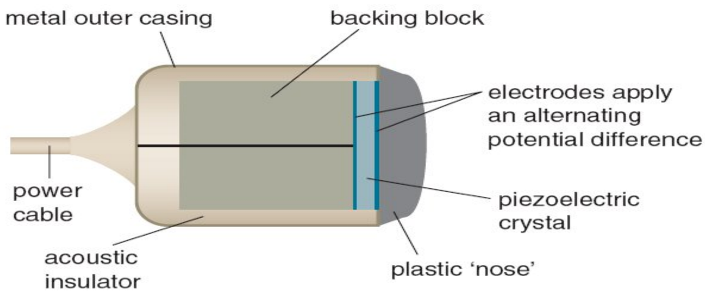

Figure 2.3: Ultrasound tranducer scheme [3]

Ultrasound systems operate in a frequency range of 1 to 30 MHz, depending on application. 5 to 10 MHz are used in brain surgery. The piezoelectric material commonly used is barium titanate or lead zirconate titanate which is piezoceramics. Advent of piezocomposites in the transducer technology has improved the ultrasound performance. They have a larger bandwidth and smaller acoustic impedance, without loss in sensitivity. [18] [20] [22] [40]

Types of transducer

The beam shape generated by the probe is determined by type of transducers and by their disposal. Also many transducers can be combined to have different geometries of the overall beam. Two types of transducers exist: flat crystals and concave crystals. With the first type you can build linear arrays or phased array. Concave crystals are usually disposed in convex arrays, to have another different form of ultrasound beam. Each kind of beam is used in different situations and for specific tasks. [18] [20] [22] [40]

Signal revelation

If a piezoelectric material is mechanically stressed it replies with a voltage signal, proportional to its spatial variation speed. When a surface reflects a wave, this returning ultrasound stresses the transducer generating a variation

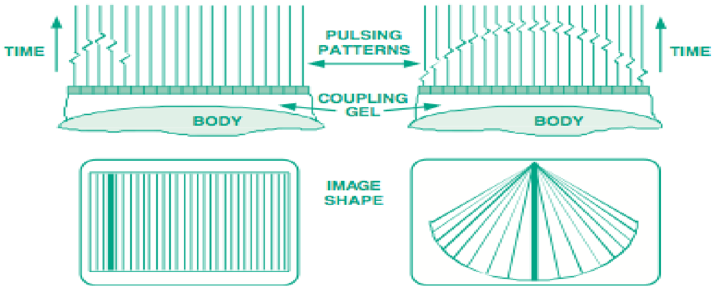

Figure 2.4: Linear and phased-array transducer [20]

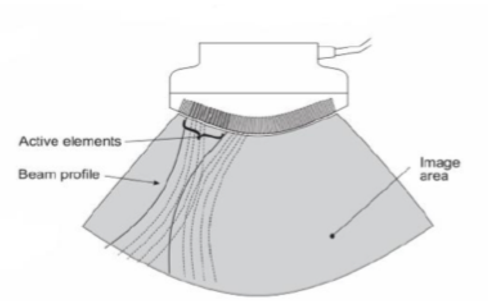

Figure 2.5: Shaped array transducer [40]

of potential in it. The time that has passed between generation of wave and generation of returning signal is used in order to calculate the distance between the transducer and the surface that has generated the reflected wave, given the speed of sound. This electric signal is used to find the intensity of reflected ultrasound wave, which bring us information about reflection rate and attenuation. The signal depends on this two parameters, in particular the attenuation depends also on frequency and material. Frequency is known and attenuation in matter is tabulated, so we can get the reflection rate and the transmission rate. [18] [20] [22] [40]

Ways of depict

Spatial information and the reflecting rate can be displayed in different ways.

- A-mode: is used in order to measure distances. A transducer emits an ultrasonic pulse and the time taken for the pulse to bounce off an object and come back is graphed in order to determine how far away the object is. A-scans only give one-dimensional information and therefore are not useful for imaging.

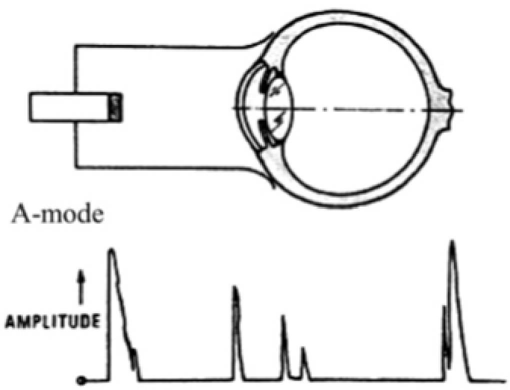

Figure 2.6: US A-mode image [40]

- B-scans: is used to take an image of a cross-section through the body. The transducer is swept across the area and the time taken for pulses to return is used to determine distances, which are plotted as a series of dots on the image. B-Scans will give two-dimensional information about the cross-section.

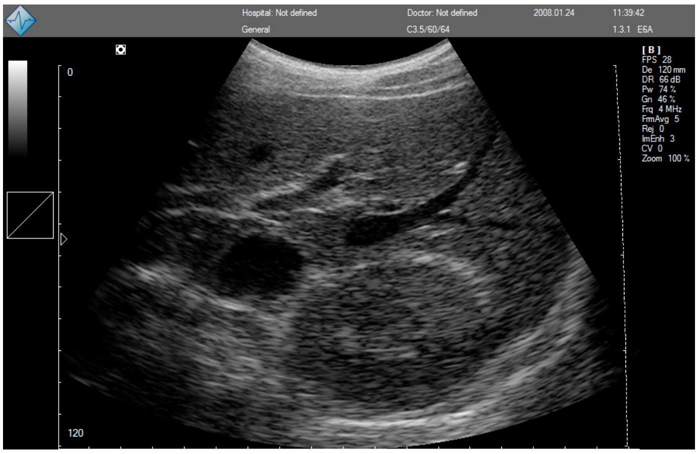

Figure 2.7: US B-mode image [4]

- M-mode: is an evolution of A-mode. Provides information about the motion. In the M-mode several lines were emitted in the same direction and the backscattered echo was recorded (A-lines). By acquiring several lines and displaying each one side by side, information about the motion was seen. The acquired lines were presented in x-y axis, where x-axis corresponds to time and y-axis to the depth.

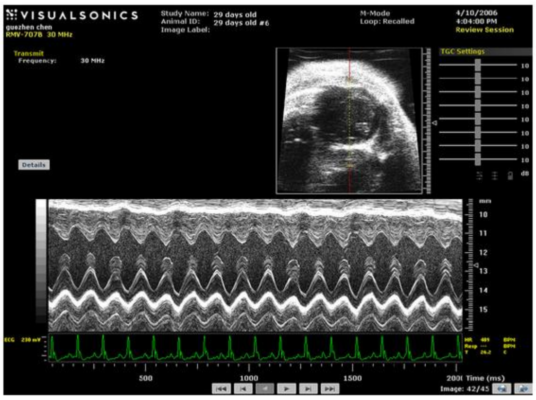

Figure 2.8: US M-mode image [5]

2.1.3 Properties of ultrasound images

Beamforming

Each ultrasound transducer can generate a different beam form. This different beam shape can be performed in two different ways. The first one is to modify the disposal of the array transducer, the second one is achieved electronically by changing the time delay and the amplitude of the voltage applied on each element. Different shapes are used to enhance focusing and directivity of the beam. [18] [20] [22] [40]

Focusing

In all array transducers focusing is achieved by applying delays in excitation pulses. It's also possible to have multiple transmit focal zone if multiple lines are transmitted in the same direction with different focusing depth. [18] [20] [22] [40]

Image resolution

Image resolution is the ability of an imaging system to distinguish between closely-spaced scatterers. In system's Point Spread Function (PSF) the resolution is evaluated by the acoustic pulse interrogation of a medium with a single point scatterers places at the focus point. It has mainly three components:

- Axial resolution;
- Lateral resolution;
- Elevation resolution.

[18] [20] [22] [40]

Speckle

Each ultrasound image has a characteristic grainy texture. Homogeneous tissue does not have a constant gray level, but structures that are imaged, like tissue and cells, are much smaller than the wavelength of an ultrasound signal. This generates constructive and destructive interference of scattered wave and this problem cannot be fixed. [18] [20] [22] [40]

Blood flow imaging

One of the big assets of ultrasound imaging is the ability to detect blow flow in real-time, using the Doppler effect. The estimation of flow direction is displayed on the B-mode imaging modality with colours. A common convention is red or flow moving towards the transducer and blue for moving away from it. The brightness of the colour shows the magnitude of velocity. [18] [20] [22] [40]

2.1.4 Safety of ultrasound

Some studies tried to determinate the effects of ultrasound in population. In particular they tried to determine if there's any effect of ultrasound on the foetus. These studies focused their attention on some effects like brain development, growth, and childhood cancers. There is no conclusive evidence that any of these traits are caused by pre-born ultrasound imaging.
However ultrasound are not free from other effects. First of all is the heat effect. In one study on newborns, ultrasound caused a temperature increase of 1.3 degrees Celsius, and blood circulated through the infant brain's more quickly. In addition to heat, scientists have begun to learn more about the various types of mechanical effects that ultrasound can have on the body. These effects are acoustic cavitation, changes in pressure, force, torque and streaming.
Acoustic cavitation is an effect caused by the presence of air bubbles. Due to an ultrasound wave, if the bubbles collapse, they can generate very high temperatures and pressures for a few tens of nanoseconds. These high temperatures and high pressures can produce highly reactive chemicals called free radicals. These could theoretically cause genetic damage.
Other effects could generate electrical changes in cell membrane, redistribution of liquid and cell damage. [18] [20] [22] [39] [40]

Ultrasound systems estimate risks

To estimate ultrasound risks the United States Nations Council on Radiation Protection and Measurements (NCRP) has identified two indexes. One for Thermal risk (TI) and one for Mechanical risk (MI). Manufacturers began incorporating these displays into ultrasound systems in order to meet the U.S. government's 1991 new regulations allowing them to increase ultrasound system outputs. If they used the Index displays, they could increase outputs. When the MI is above 0.5 or the TI is above 1.0, the NCRP recommends that the risks of ultrasound be weighed against the benefits. The physician and technician who is using the ultrasound system must interpret these numbers in order to weigh the risks against the benefits of getting a better ultrasound image.

Unlike ionizing radiation, there has been little international safety standard on the clinical use of ultrasound. There are many studies about biological effects of ultrasound however they are difficult to interpret because exposure conditions are not clinically relevant. It is also difficult to find biological end-points that are sufficiently sensitive to respond to the low powered acoustic wave that are used in diagnostic systems. [18] [20] [22] [39] [40]

2.1.5 Standardization in diagnostic ultrasound

There are three kind of standards:

- Fundamental standard;
- Engineering standard;
- User oriented operational standard.

Fundamental standards try to define measurements of fundamental quantity like peak and average acoustic intensity. These quantities are difficult to perform and there is no unanimity about the best method for measuring it.

Traditional engineering methods and standards measure gain, band width, noise level, electrical leakage, etc. These measures are available and simpler to perform.

User-oriented operational methods check the performance of a complex ultrasound system on a daily or weekly basis. Standards for hospital technologist must be simple and easy to use since they will often be used by people with little or no background in science or engineering. The test must use a simple low cost device and should test the whole system as a black box to avoid manufacturers' complaints. The traditional method in medicine is to employ a phantom to be scanned. [18] [20] [22] [39] [40]

2.2 Usefulness of Ultrasonography

In literature the use of ultrasound intraoperative imaging in neurosurgery has been deeply studied, illustrating the many uses of the ultrasound [13] [14] [16] [17] [19] [28] [29] [43] [49]. Each research and surgical team has developed a different workflow in order to utilize them. Different instrumentation can be used, and diferent information can be extracted. In order to understand what is necessary in order to improve the surgical procedures, it was essential to do an extensive literature review.

2.2.1 A milestone in intraoperative use of real-time ultrasonography in neurosurgery: The Michigan experience, 1982

In this paper authors describe their first experience in the use of ultrasound real-time technology in a neurosurgical environment. Real-time describes that the image on the monitor at any given point in time, which is precisely the image produced by the ultrasound unit at that instant. Thus, any movement of structures being imaged can easily be seen. It was proven [cit 3-5] that real-time ultrasonography is very useful in detecting intracerebral or interventricular hemorrhage, hydrocephalus, and porencephaly in premature or other infants, but this technology is limited by the inability of the ultrasound beam to penetrate the human skull. In the case of infants, advantages of the open fontanel allow the brain to be ultrasounded in multiple directiones. In adults, it is necessary to remove a portion of the skull in order to overcome this physical limitation. In this study the authors have investigated the imaging capabilities of real-time ultrasonography during a wide variety of neurosurgical procedures, and have found this technique to be extremely helpful and easy to perform. [47]

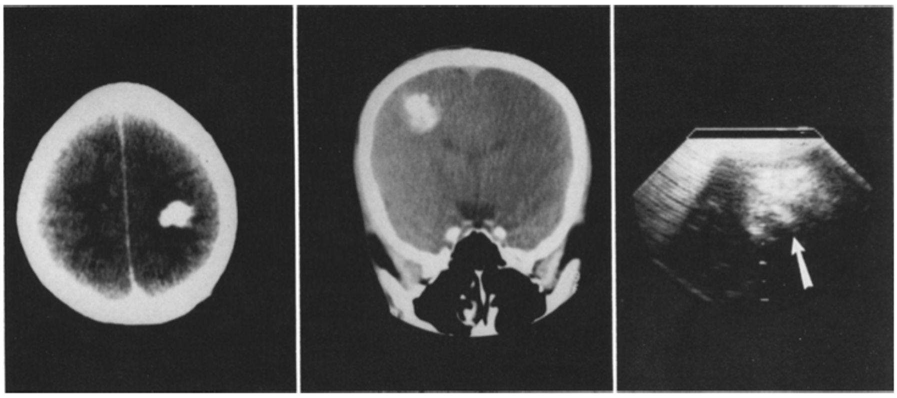

Figure 2.9: Plain computerized tomography, axial scan (left) and coronal scan (center), demonstrates a calcified right parietal lesion. Intraoperative ultrasonography demonstrates this subcortical ganglioglioma (right, arrow) [47]

Equipment

Ultrasound imaging was performed with an ATL real-time sector scanner (Advance Technology Laboratories, Inc., Bellevue, Washington). The depth of the brain imaged may be as shallow as from the surface to just 3 cm deep or from the surface to the opposite side of the brain. The depth is determined by a selector switch on the instrument. A video recorder and a Polaroid camera are used to store videos and images of interest. [47]

Intraoperative Technique

To assure sterile conditions, ultrasound transducer is placed in a sterile rubber glove partially filled with a coupling gel. Transducer head is 2 x 2 cm in size and can be placed either on the dura or directly on the exposed brain surface moistened with a saline solution. There was no difference in quality image with the dura intact or opened. Before opening dura, they tested image acquisition in order to determine the optimum site for opening. [47]

Summary of cases

This technique has been tested with many different cerebral neoplasm cases. Meningiomas and large superficial gliomas were not studied. The most significant result of this investigation into the intraoperative use of real-time ultrasound imaging was that the pathology was clearly identified and localized in every case. The solid subcortical metastatic neoplasms were readily identified as hyperechoic masses. Furthermore, there was no intraoperative complications related to the use of real-time ultrasonography, and no post-operative infections were noted. The time demands on the equipment are minimal, generally 30 to 45 minutes. [47]

Discussion and conclusions

The authors believe that the advent of real-time ultrasound scanning could provide great opportunity for its use as a localizing instrument during neurosurgical procedures. Overall, they have found real-time ultrasonography to be extremely helpful for the localization and identification of every lesion in which ultrasound was attempted.
In conclusion the following advantages have been identified:

- It can provide assistance in localization of subcortical metastatic neoplasms;
- This technique is very useful for the identification of deep lesions, providing information about their solid and cystic components;
- The system is highly accurate in visualizing ventricular catheters;

- The system is inherently safe for the patient and the operating room personnel since there is no radiation exposure.

[47]

2.2.2 Ultrasound-guided surgery of deep seated bran lesions: The Homburg experience, 2000

Computer aided navigation systems have been introduced to optimize the neurosurgical strategies minimizing the damage to the healthy brain tissue but brain shift phenomenon alter the position of the lesion and of the structure in the external reference system. In this paper the authors presented their experiences with ultrasound, which represents a real-time navigation system, in order to overcome this problem. In particular they have studied 45 patients with subcortical intracerebral lesions: 17 cavernomas, 12 metastases and 16 gliomas. [35]

Technique

Thw following ultrasound imaging system was used: an ATL 3000 HDI with three different kinds of probes: a 2 to 4 MHz phased array probe, a 4 to 7 MHz phased array probe and a 5 to 12 MHz linear array probe. The last one was used in particular in cases of highly superficial subcortical lesions. For sterile usage a sheath was filled with contact gel and as a coupling agent sterile saline solution was used on the surface or within a cavity. [35]

Results

In all cases the use of intraoperative ultrasound did not result in any adverse event or reaction to the brain and deep seated brain tumors could be easily detected. [35]

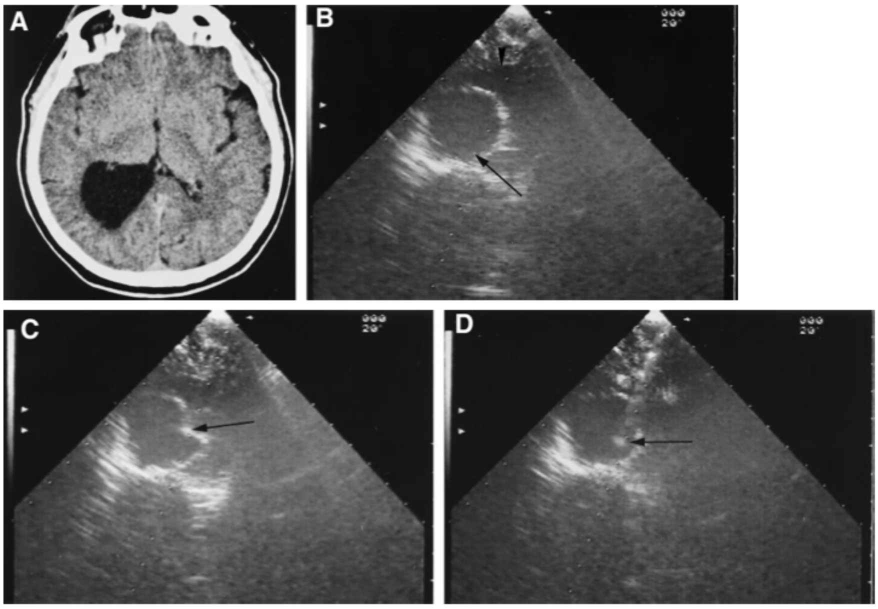

Figure 2.10: A 49-year-old man harboring a large intraventricular cyst. A. Preoperative CT-scan shows enlargement of the posterior horn of the right lateral ventricle due to an intraventricular cyst. B. Intraop- erative ultrasound image via an occipital burr hole. The intraventric- ular cyst (straight arrow) and the trigone of the lateral ventricle (ar- rowhead) are clearly depicted. C. Introduction of the puncture needle. The tip of the needle dents the wall of the cyst just before penetration (straight arrow). D. Penetration of the cyst wall. The tip of the needle, outlined by a small hyperechoic artifact, is clearly depicted inside the cyst (straight arrow) [35]

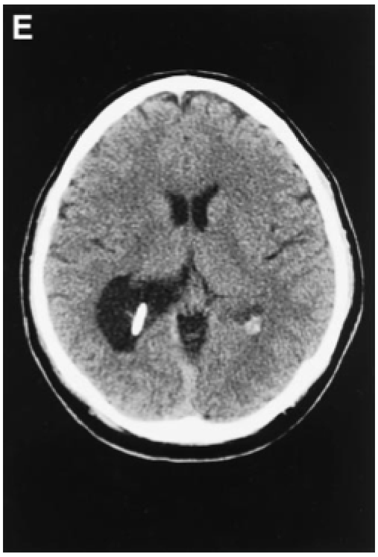

Figure 2.11: E. Postoperative CT scan. Internal connection between cyst and lateral ventricle is achieved by the implanted catheter [35]

Conclusion

Intraoperative ultrasound is a reliable intraoperative guidance tool in the localization of deep seated brain tumors because it operates in real-time, thus increasing the safety of the surgical procedure and of the tumor resection. [35]

2.2.3 Real-Time Two-Dimensional Ultrasound: The Trondheim experience, from 1997 to 2001

In 1995 in Trondheim, Norway, started a project to investigate various possibilities of using ultrasound in brain surgery. They explored the essential clinical parameters required for the successful use of ultrasonic guidance. In this period many surgical setups were designed to optimize the use of intraoperative ultrasonic imaging. These different solutions included various positions of the ultrasound probe in relation to both the operation cavity and the lesion. As a result they were able to depict all 114 lesions studied, with the exception of two cases, with the use of ultrasound imaging. In particular they found ultrasounds very useful in the detection of remaining tumor tissue at the conclusion of surgery. In this study, in 14 low vascular tumors, the operation is guided only by ultrasound imaging. This study, for his completeness, was a milestone for many other studies. [27]

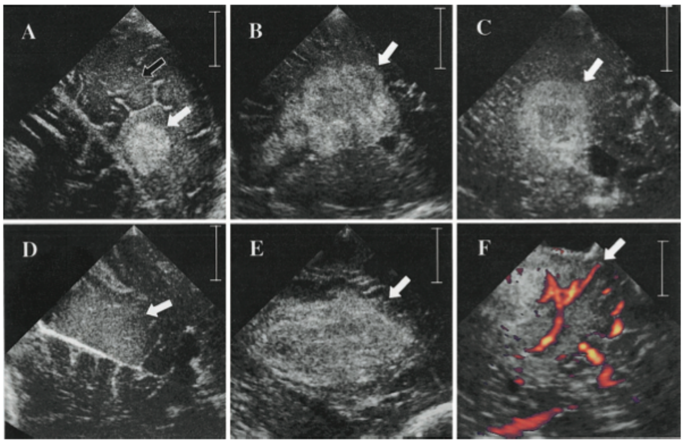

Figure 2.12: Intraoperative images of the lesions that we resected from 1997 to 2001 at our clinic. These lesions (white arrows) were depicted well by the use of ultrasound, except in two cases. A, metastasis with surrounding edema (black arrow); B, glioblastoma; C, anaplastic astrocytoma; D, low-grade astrocytoma; E, hematoma; F, ves- sels in a tumor detected with the use of ultrasound power Doppler. Scale bars, 2 cm. [27]

Equipment

Ultrasound imaging was performed using a System FiVe high-performance ultrasound scanner (GE Vingmed Ultrasound, HOrten, Norway). For deep-seated or subcortical lesions, a 4 to 8 MHz phased-array probe was used for some of the superficial lesions, a 10 MHz linear array probe was used in addition to the previous probe. All the probes were covered by a sterile condom with sterile gel before it was introduced into the operative field. [27]

Positioning the probe

There are to ways to positioning the probe to achieve the highest possible image quality. The first one is to perform an enlarged craniotomy, the second one is to perform another minicraniotomy. Sterile gel was placed between the probe and the dura to ensure satisfactory contact for optimal wave propagation. [27]

Positioning the patient

Patient position adducts the angle of the resection cavity in relation to the vertical gravity line and hence the amount of air trapped in the cavity during the resection. [27]

Additional items that cause reverbation

Cotton padding and spatulas were removed from the resection cavity during ultrasound imaging. These items cause undesirable echoes, shadows, and reverberation in the images. [27]

Results

Before resection of the dura, ultrasound imaging was useful for locating different brain tumors and hematomas in relation to surrounding anatomic structures. All 114 lesions less two were depicted well.
During the operation, after resection of the dura, ultrasound was used extensively for guiding the surgical tools to the lesion. A problem in the use of 2D ultrasound for navigating surgical tools into the lesion is the position and orientation of the ultrasound 2D plane in relation to the tip of the surgical tool. Inexperienced users may misinterpret a small reverberation in the

ultrasound image at the tip of the surgical tool. [27]

Discussion

It may seem controversial to perform an additional mini craniotomy or an enlarged craniotomy to allow for intraoperative guidance. On the basis of the study the authors are convicted that the extra time involved in making the additional incision are rewarded by an increase in image quality, which enhances the performance and hence the outcome of surgery.
The vertical operative channel was found useful to prevent trapping air in the cavity and thus provide optimal conditions for ultrasound imaging.
Ultrasonographic images seems to be able to provide high-quality image information regarding tumor and lesion extension and location, especially in the supratentorial brain, but not in cases of posterior fossa lesions. [27]

Future Technology

For authors Navigational technology and three-dimensional imaging could be useful to overcome the problem of orientation and for improving tumor resection. Another powerful possibility is in characterizing brain shift during surgery. [27]

2.2.4 Stand-alone ultrasonography: The Nagasaky experience, 2012

Due to the particular instrumentation they used, this work put the bases to my work. They have tools very similar to those available in Verona Hospital. They worked with a portable ultrasonography scanner (Aloka SSD-2000; HitachiAloa Medical, Ltd. Tokyo) and a small transducer with bayonet-style handle and straight, untapered head (Aloka UST-5268P-5, 3.0-8.0 MHz, phased-array sector probe; HItachi Aloka Medical, Ltd). The ultrasound is not co-registered with intraoperative MRI, is as stand-alone imaging system.

[32]

Methods and Results

The transducer, after sterilization, was used without sterile drape. After opening a standard burr-hole, the transducer was placed in the operative field and the ultrasonography scanner was positioned so that the surgeon can easily view the display screen.

The transducer was in contact with the dura surface and before opening it the time-gain compensation was adjusted to improve the image quality. Furthermore, color Doppler imaging was used to identify important vasculatures.

The sector probe provided fan-shaped views ranging from 45 to 135 degrees and the region from 1 cm to approximately 10 cm was visualized clearly. Intraoperative ultrasonography provided immediate ongoing information about the anatomy and pathological lesion.

Total examination time was approximately 5 minutes, and no procedure-related complication was noted with minimal problems. However, there was only minor alterations in the standard surgical techniques. [32]

Discussion

The authors believed that this methodology could be useful to identify cystic lesions and to localize hematomas. They found this procedure minimally invasive and fast to perform. Disadvantages associated with the burr-hole ultrasonography technique include additional operation time needed to perform ultrasound imaging, and introduction of an additional foreign body. [32]

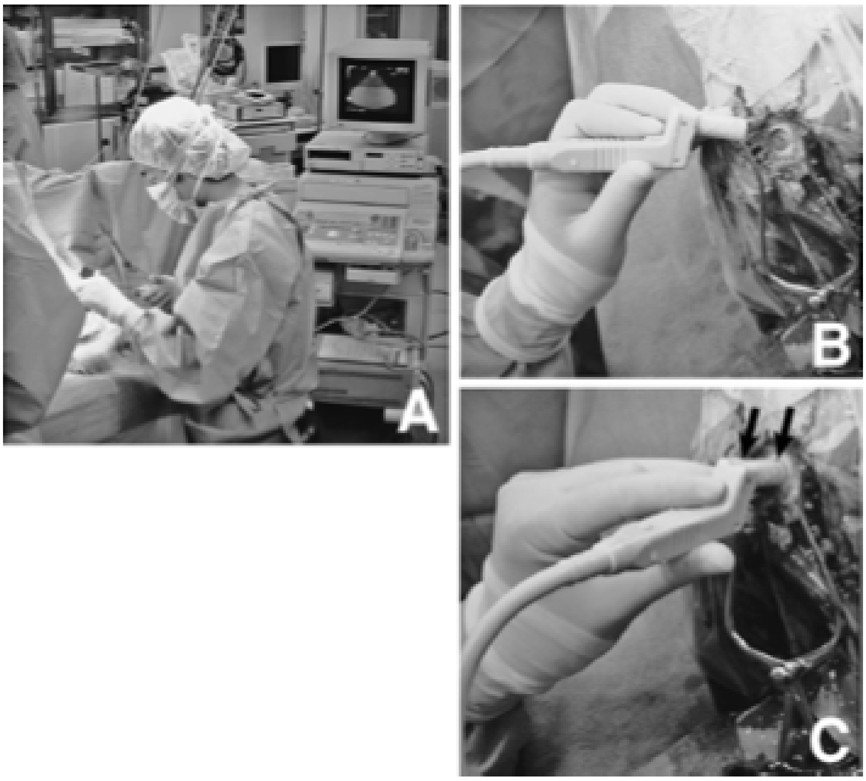

Figure 2.13: Photograms showing use of the system. Operative theater (A) with ultrasonography scanner. After creating a burr-hole (B), the ransducer was inserted into the burr-hole (C). A slot is present in the head of the transducer (arrows). [32]

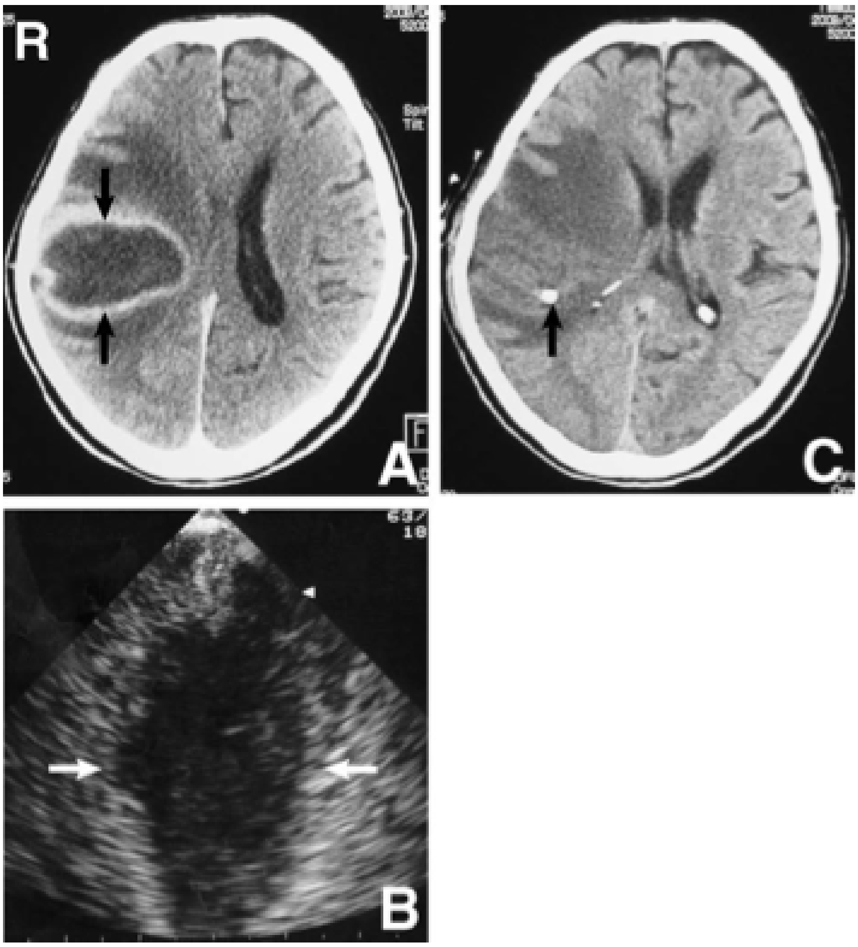

Figure 2.14: A: Computed Tomography scan demonstrating a ring-enhanced lesion in the right parietal lobe (arrows). B: Ultrasonogram showing a hypoechoic cystic lesion with hyperechoic margin just under the burr-hole (arrows). C: Postoperative CT scan showing shrinkage of the lesion and correct placement of the tube (arrow). [32]

Chapter 3

Material and methods

*"Who does not admit to the unfathomable mystery
cannot even be a scientist."*

Albert Einstein (1879 - 1955)
Nobel Prize in Physics (1921)

3.1 Instrumentation for imaging

3.1.1 Aloka α7 Prosound

The US scanner adopted is Aloka α7 Prosound, produced by Hitachi Aloka Medical, Ltd. Hitachi Aloka has been the world's leading pioneer of ultrasound systems for the healthcare industry. They provide obstetrics/gynaecology, radiology, surgical, cardiology, urology, vascular, veterinary and other applications with a broad array of innovative ultrasound technologies.
This is a portable high-performance scanner, equipped with wheels. It is provided with a touch screen, a QWERTY keyboard, a track pad and many others input devices. [6] [7] [8] [9]

Figure 3.1: Aloka α7 Prosound

Figure 3.2: Burr-hole probe

Burr-hole probe

Transducer is an ultrasound phased-array probe. It is waterproof and compatible with "STERRAD® system" for sterilization. Insertion diameter is 12mm with a scan angle of 90 degrees. It works in multifrequency from 3 to 7.5 MHz [6] [7] [8] [9]. I've always used the transducer at a frequency of 6.67 MHz. The ideal resolution expected is equal to the wave lenght that corresponds to 0.224 mm. Is calculated with equation 3.1 where λ is the wave lenght, v is propagation speed ($v = 1497$ m/s in water), and f is frequency.

$$\lambda = \frac{v}{f} \tag{3.1}$$

3.1.2 Magnetic resonance scanners

MRI machines make use of the fact that body tissue contains huge amounts of of water, and hence protons (1H nuclei), which are then aligned in a large magnetic field.[10] In the hospital of Verona there are two different scanners available.

3.2 Imaging acquisitions

3.2.1 MRI preoperative acquisition

Before going into the surgery room it is necessary to plan the intervention. Planning is perfomed on preoperative MRI imaging and on patient's clinical situation. Imaging exams are not always performed in the hospital. Patients who come from outside the region always have their own MRI exams that were performed in other hospitals. Usually MRI acquisitions are performed between two weeks and one month before the intervenction. For this, the preoperative imaging dataset is very heterogeneus in terms of resolution and acquisition parameters. Each MR exam has a different image resolution. The best case has a voxel volume of 0.185 mm^3, the worst of 1.10 mm^3.

3.2.2 US imaging acquisition

When introducing a new technology in the operating room it is important to take into consideration the costs - benefits ratio it brings to the surgeon. The ultrasound scanner is a device relatively small and easy to transport, but still has a footprint that may interfere with surgery. It is important to carefully plan its positioning in the operating room in order to limit the inconvenience for the surgeon. Other aspects to consider in the preoperative phase are the timing of use and the time spent in the use of technology, which will add on the total time of the surgical procedure. In the end, is important to have an idea of which will be the parameters of US acquisitions.

Environment

Environment plays a fundamental role in order to perform the surgery procedure in safety conditions. The first limitation is imposed by the lenght of cable that connects the probe to the scanner, is long 2.5 meters. The scanner has to be placed near to the sterile region. Around the operating field, in addition to the US, need to take place two surgeons and the scrub nurse with her sterile table. The situation is not always comfortable. In order to makes easier for the surgeon to view US images, an additional monitor is connected to the scanner. The monitor shows in real-time the images extracted from the scanner. The situation can be more complicated when many different technologies have to be available at the same time to the surgeon. Example is when the surgeon wants to use microscope, neuronavigator and neurophysiological monitoring. In these situations the positioning of all items has to be deeply studied. In pictures below 3.3 and 3.4 is shown one of these situations.

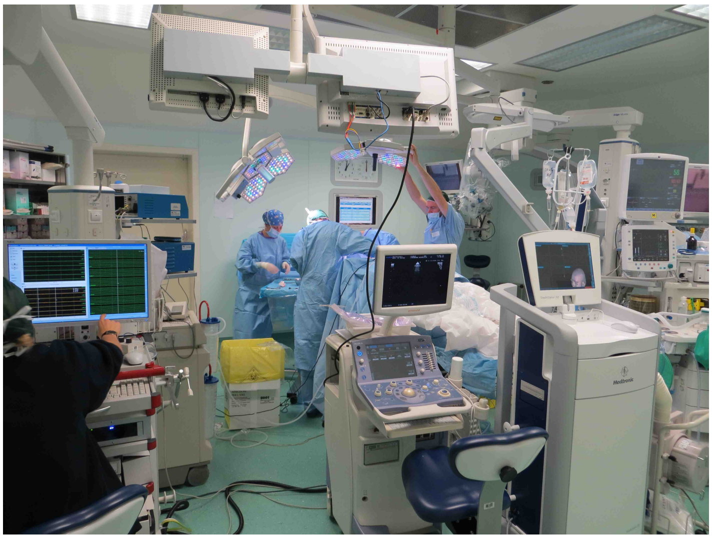

Figure 3.3: Left: Neurophysiological monitoring, Center: Echo scanner, Right: Neuronavigator

Figure 3.4: Additional monitor mounted in front of the surgeon

Timing

One of the main advantages of US imaging technology is the little time that adds to the surgical procedure. In our experience is estimated at a maximum of five minutes of effective use for surgery. This advantage is also underlined by other studies in the literature. [35] [49]
The US acquisitions are performed in three different times during surgery. The first one is after skull resecition, when the dura mater is exposed. Probe is placed on the dura while second operator washes with sterile water the contact area. Second acquisition is performed after opening dura, before start the using of microscope. In this situation is possible to obtain the best quality images of the lesion. As before, second operator still washes the contact region, in order to improve adherence of probe to the brain. All imaging analysis were performed on images obtained in these conditions. If necessary, during the intervenction, the surgeon uses again the US, in order to obtain real-time intraoperative imaging.

Parameters

The only parameter that is essential to set is the depth of scan field. All the other parameters like angle gain works well with the default value. The depth of scan field is evaluated before the surgery, looking at the preoperative MRI. This value is fixed in such a way that the field of view is sufficient to display the entire lesion, but the smallest possible.

3.3 Image registration process

In order to compare the US and the MR images it is necessary to overlap them. This procedure is called registration. In a registration process, each

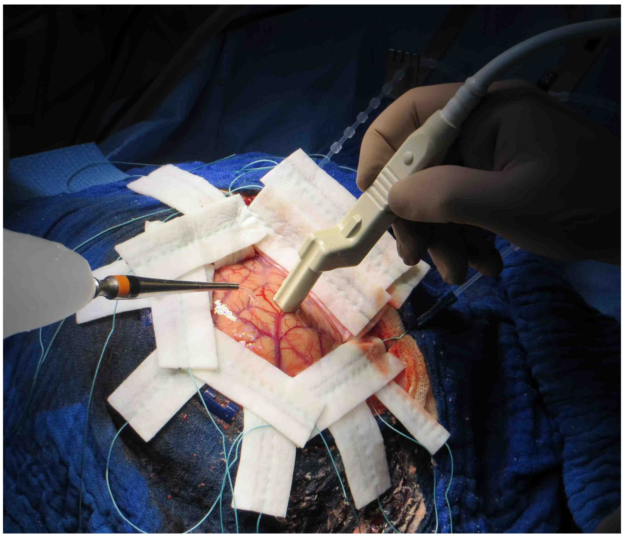

Figure 3.5: US imaging acquisition on brain surface, after opening dura mater

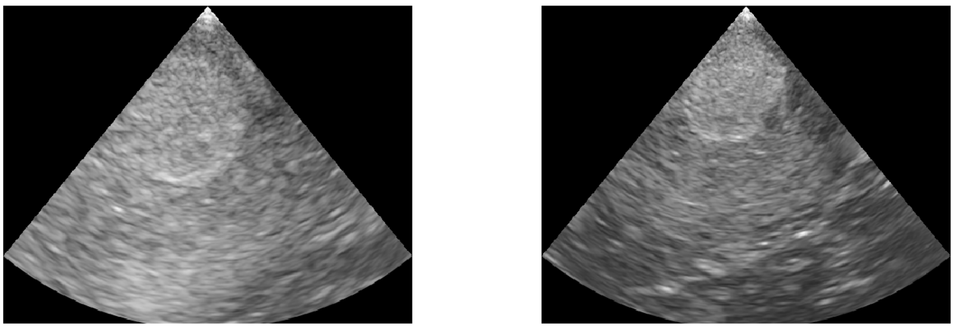

Figure 3.6: Depth of scan field. Left 40 mm, right 50 mm

of the two images have its own role, one is the reference image and the other one is the test image.[36]

Reference image

Reference image is the one which remains static throught cut the registration process. It is preferable to use an image with higher resolution, out of the two images to be registered as a reference image. The transformation is then calculated and optimized based on the coordinate system of this image. For these reasons we had choosen the US image as the reference image.

Test image

Test image is the one which is iteratively spatially transformed (be it rigid, affine or non-rigid deformation) until a most similar arrangement is found with respect to the reference image. MR volume was choosen to be the test image.

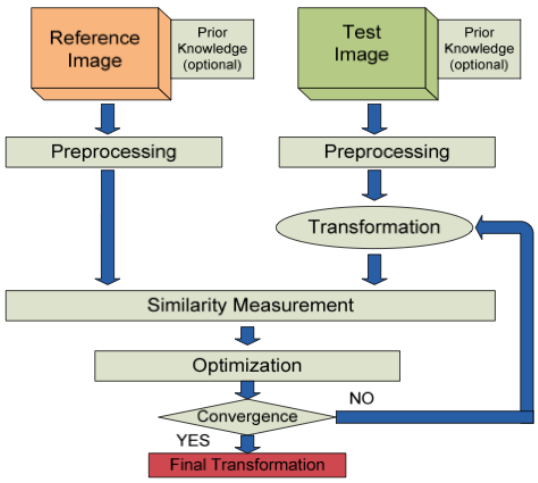

Figure 3.7: System diagram of general image registration process

3.3.1 Preprocessing

The preprocessing stage in the registration pipeline can include trivial tasks like padding correction in the images. More sophisticated tasks can also form a part of preprocessing stage like filtering of the images and/or feture extraction utilizing the prior knowledge linke manually segmented structures in the images. Hence, this stage can be used to perform all kinds processing on the images before they are fed in to the iterative loop of similarity measurement, transofmation and optimization. This is a key step in order to be able to confront two different images.[36]
In our study preprocessing was performed with MATLAB. [11]

US preprocessing

Ultrasound images are used as reference images. Aloka saves images in DICOM files. They include in the field of view many unnecessary data. For this reason was required to cut the image in order to save only necessary data.

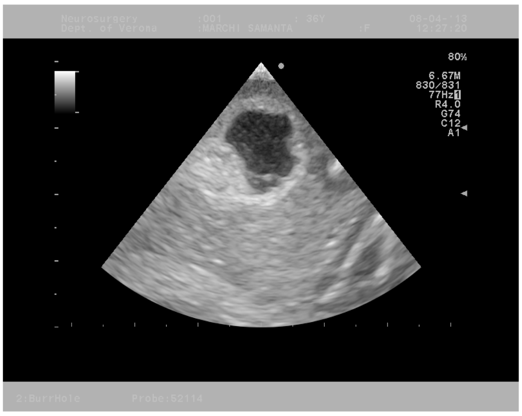

Figure 3.8: US image before preprocessing: there are many useless information

Moreover, the size of the image is always 800x600 pixels, even if the radius of the US beam is variable. For this reason is important to extract from each dicom file, the value of the ray of the US beam. Changing the depth of scan field, pixels can represent a different spatial measurement. In order to perform the registration process is necessary known how each pixel of each image describes a physical measurement.
US images are represented in gray scale. The ultrasound system uses different encoding in gray values depending on different acquisition. It is necessary to have a unique representation method of the gray intensity so all gray values were transformed in the interval [0 1].

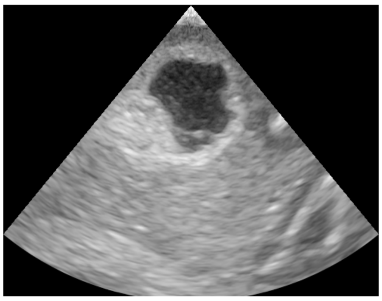

Figure 3.9: US image after preprocessing: the image was cut and the gray levels normalized in order to be comparable with the MRI

MR preprocessing

MR image is the test image. For this reason preprocessing is more complicate than the previous one. The first step is loading the MRI exam performed in T1 with contrast (all the slices), and also its DICOM header file. From the header is extracted the spatial resolution of the image. Each pixel represent an area of space in the patient reference system. Pixels dimension is rescaled considering that each pixel in MRI have to represent the same area of the US pixel in order to be able to compare them.

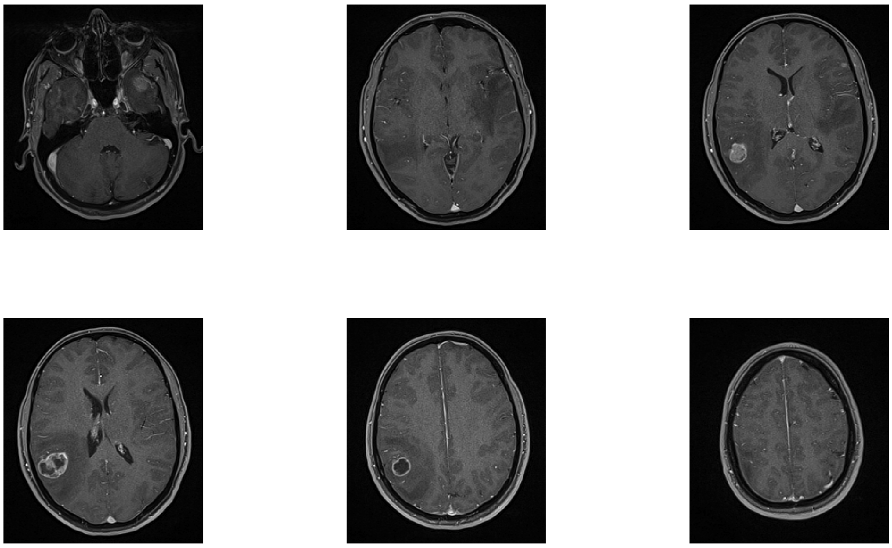

Figure 3.10: A selection of MR slices

After rescaling, it is time to extract a slice that can be compared with the US image. In an ideal situation the surgeon will try to direct the US beam in one of axial, sagittal or coronal plane. It is simpler for the surgeon to recognize structures or lesions. Unfortunately, depending on the position of the burr-hole and patient, is not always possible to acquire these planes. In these situations is necessary to reslice the MRI volume in order to extract the same slice, in the same direction, that was acquired by US. Is not simple to do that: is necessary to know the positioning of the probe during acquisition in the reference system of the patient. Home made solutions are difficult to perform in the surgery room environment, in particular due to the problem of sterilization. For all these reasons we have tried to reconstruct the positioning of the probe after the intervention. This is performed with three instruments:

- Photos of operating field and probe;
- Asking the surgeon how he perfomed the acquisitions in relation to the

brain anatomy;

- If available, place the pointer of the neuronavigator and save its position.

About this choice, another fundamental reason was the unnecessary - for surgeon - knowledge of probe position in the reference system of patient. In this situation, an innovation for most of surgeons, the only important data was the direction of US beam in the reference system of the probe. They are able to obtain the position of the lesion merging their spatial knowledge of brain structures and what they see with the US intraoperative imaging.

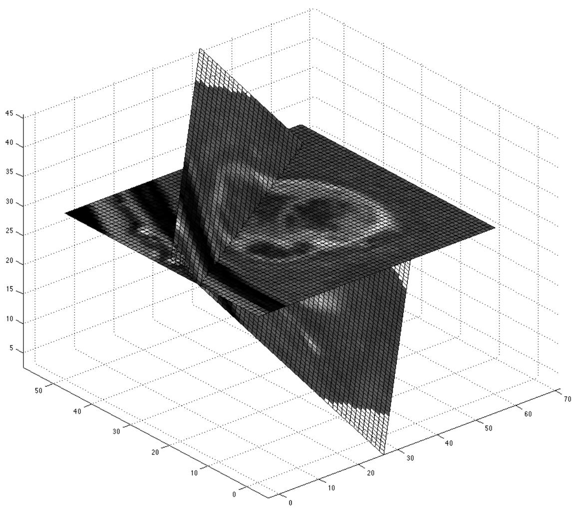

Figure 3.11: Axial view and new extracted slice

3.3.2 Alignment

After preprocessing, overlap between the images is achieved manually. This choice was obliged by the impossibility to know the exact transformation from the coordinate system of the probe to the coordinate system of the

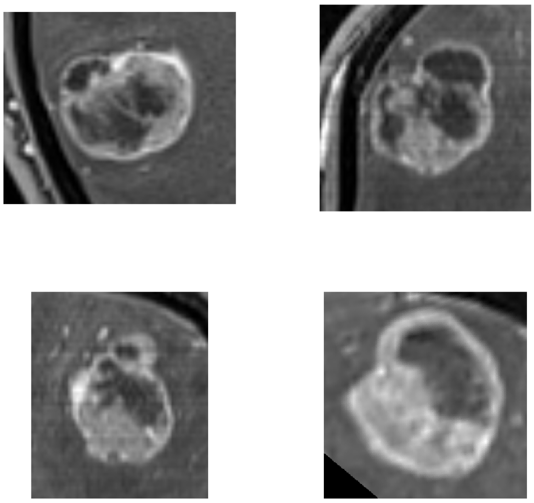

Figure 3.12: Top-left: Axial view, Top-right: Coronal view, Down-left: Sagittal view, Down-right: New extracted slice

head. Due to the effects of brain shift, in our study, it is most important to compare how these two different technologies are able to represent the lesion, in face of their ability to reproduce the spacial positioning of the structures.

3.4 Dataset description

Dataset is composed by 30 images acquired by 5 different patiens, 3 US and 3 MRI per patient.

3.4.1 Case 1

Surgery information

- Sugeon: Dr. Angelo Musumeci
- Data of intervenction: 04/08/2013
- Pathology: Melanoma metastases
- Patient age: 36 years
- Gender: Female

MRI information

- Magnetic field strenght: 1.5 Tesla
- Voxel dimension (mm x mm x mm): 0.75 x 0.75 x 0.80
- Space between slices (mm): 0.00
- Number of slices: 208
- Slices orientation: Axial
- Acquisition mode: T1 with contrast (Gadolinium)
- Exam data: 03/27/2013

US information

- Wave frequency (MHz): 6.67
- Wave lenght (mm): 0.224
- Pixel dimension (mm x mm): 0.102 x 0.102
- Depth of scan field (mm): 40
- Original image resolution: 800 x 600

3.4.2 Case 2

Surgery information

- Sugeon: Dr. Riccardo Damante
- Data of intervenction: 04/19/2013
- Pathology: Glioblastoma, grade 4^{th}
- Gender: Female
- Patient age: 57 years

MRI information

- Magnetic field strenght: 1.5 Tesla
- Voxel dimension (mm x mm x mm): 0.47 x 0.47 x 5.00
- Space between slices (mm): 6.00
- Number of slices: 24
- Slices orientation: Axial
- Acquisition mode: T1 with contrast (Gadolinium)
- Exam data: 04/08/2013

US information

- Wave frequency (MHz): 6.67
- Wave lenght (mm): 0.224
- Pixel dimension (mm x mm): 0.204 x 0.204
- Depth of scan field (mm): 80
- Original image resolution: 800 x 600

3.4.3 Case 3

Surgery information

- Sugeon: Dr. Angelo Musumeci
- Data of intervenction: 05/14/2013
- Pathology: Right rolandic metastases
- Gender: Female
- Patient age: 43 years

MRI information

- Magnetic field strenght: 3.0 Tesla
- Voxel dimension (mm x mm x mm): 0.43 x 0.43 x 1.00
- Space between slices (mm): 0.00
- Number of slices: 176
- Slices orientation: Axial
- Acquisition mode: T1 with contrast (Gadolinium)
- Exam data: 04/16/2013

US information

- Wave frequency (MHz): 6.67
- Wave lenght (mm): 0.224
- Pixel dimension (mm x mm): 0.127 x 0.127
- Depth of scan field (mm): 50
- Original image resolution: 800 x 600

3.4.4 Case 4

Surgery information

- Sugeon: Dr. Riccardo Damante
- Data of intervenction: 05/16/2013
- Pathology: Lung metastases
- Gender: Male
- Patient age: 47 years

MRI information

- Magnetic field strenght: 1.5 Tesla
- Voxel dimension (mm x mm x mm): 0.83 x 0.83 x 1.00
- Space between slices (mm): 1.00
- Number of slices: 160
- Slices orientation: Axial
- Acquisition mode: T1 with contrast (Gadolinium)
- Exam data: 04/26/2013

US information

- Wave frequency (MHz): 6.67
- Wave lenght (mm): 0.224
- Pixel dimension (mm x mm): 0.204 x 0.204
- Depth of scan field (mm): 80
- Original image resolution: 800 x 600

3.4.5 Case 5

Surgery information

- Sugeon: Prof. Francesco Sala
- Data of intervenction: 11/06/2013
- Pathology: Metastases
- Gender: Female
- Patient age: 65 years

MRI information

- Magnetic field strenght: 3.0 Tesla
- Voxel dimension (mm x mm x mm): 0.43 x 0.43 x 1.00
- Space between slices (mm): 0.00
- Number of slices: 176
- Slices orientation: Axial
- Acquisition mode: T1 with contrast (Gadolinium)
- Exam data: 05/06/2013

US information

- Wave frequency (MHz): 6.67
- Wave lenght (mm): 0.224
- Pixel dimension (mm x mm): 0.127 x 0.127
- Depth of scan field (mm): 50
- Original image resolution: 800 x 600

Chapter 4

Analysis

"Research leads to truth."

Socrates (c.470 BC - 399 BC)
Greek philosopher

4.1 Assumption to anlysis

Before proceeding with data analysis is necessary to clarify which are the problems encountered and possible solutions. The dataset is composed by 30 images acquired by 5 different patiens, 3 US and 3 MRI per patient. Complete information about dataset are placed in appendix.

4.1.1 Issues

Normalization

In order to compare different images from different acquisition system is necessary to normalize them to some reference values. Normalization is based on the assumption of having an image that represent the entire brain. This is verified with MRI but with US this is not possible for two reasons: depth of scan field and high reflection rate of bone tissues. There are two

types of normalization: spatial and intensity.
Spatial normalization is non applicable for these reasons:

- The images do not match each other (reslicing is approximate, there are no spatial reference to overlap, has not been made a co-registration because the scanner does not produce a coregistrable dataset);
- We do not have informations about any bias caused by the ultrasound imaging;
- Is impossible to compare images to atlas because lesions deform brain tissue.

For all these reasons we are not sure that each pixel (from MRI and US) correspond each other and neither to the same brain region.
Intensity normalization is a chapter even more difficult. Normalization of MRI is one of the most controversial part of imaging reasearch. Better works concern Alzheimer and Parkinson disease. In this area imaging techniques are very heavy, for this intensity normalization of MRI is not simple. [33]
We are not in the situation of creating features based on MRI and US directly correlated.

4.1.2 Solutions

All these bad conditions are not totally bad news. In this study I demonstrated that the distinction between healty tissue and pathological tissue is possible applying spacial imaging filters. With these methods I demonstrated that ultrasound imaging can be useful as the magnetic resonance. This is very interesting because it permits to have an useful instrument, not depending on pre-operatory MRI, that can be useful in the surgery room. Furthermore ultrasound reduces costs in therm of time and money compared

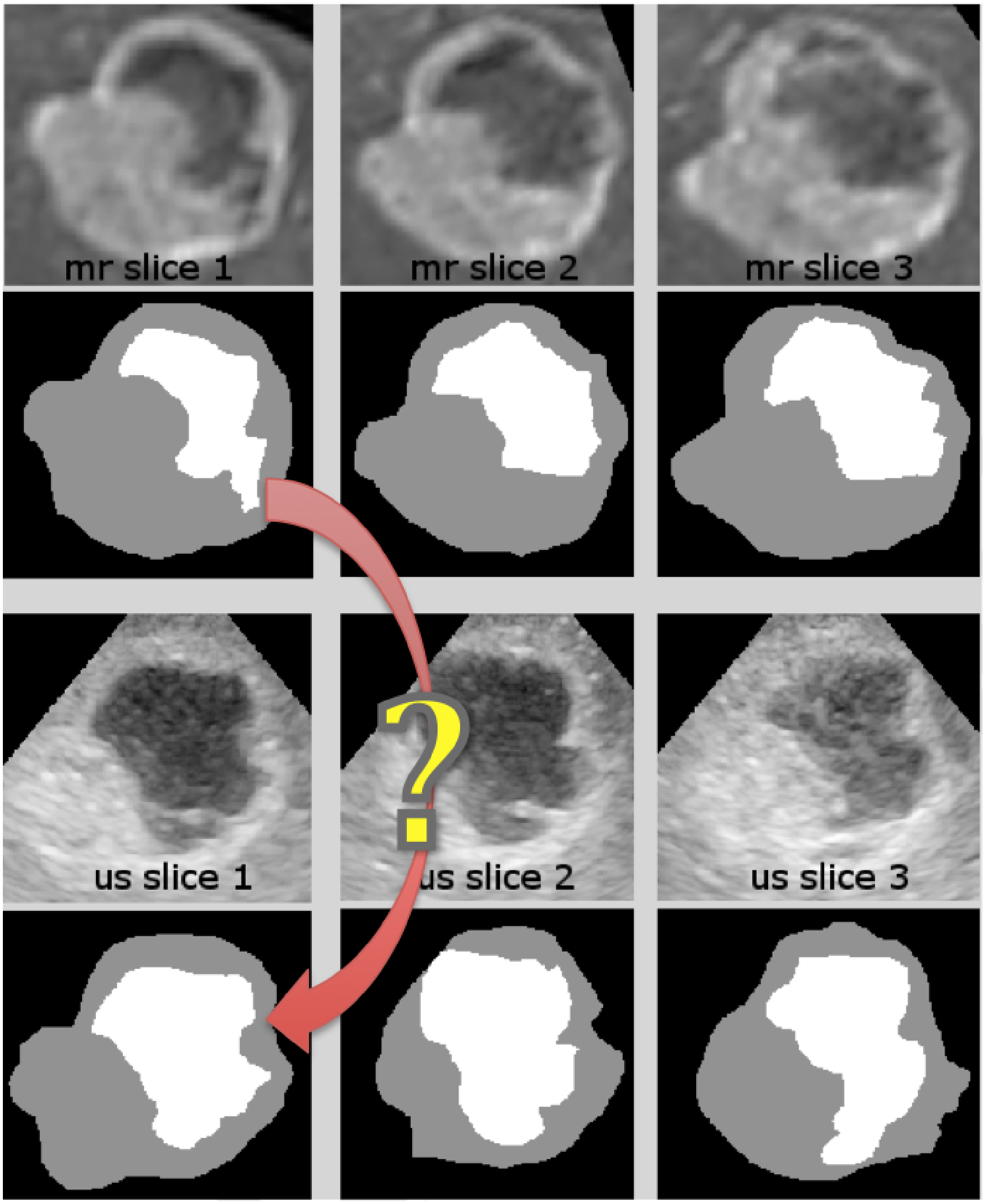

Figure 4.1: This picture shows how is difficult to compare the images and the manual tracking confirms

to a low-field intraoperatory MR scanner.

To reach these conclusions I have following these steps:

- Apply a chain of filters to images (US and MR);
- Using an automatic instrument to segment three regions;
- Assign a label to each region (healty or pathological tissue);
- Compare to the segmentation performed by the surgeon;
- Calculate the percentage error of the automatic segmentation;
- Compare the results obtained with ultrasound to those obtained with MRI.

4.2 Pre-processing

4.2.1 Filtering

Ultrasound imaging are affected by artifacts. First of all is "speckle noise". It overlaps on the image a widespread grain, similar to classic "salt and pepper" effect. This noise is generated by the transducer when it release electromagnetic waves. Was necessary to process the image because is not possible acting on the physical acquisition. [12] [23] [31] [42] The goal is to remove noise in order to obtain sharper images. This not for an aesthetic reason. This kind of noise reduce the possibility to extract contours and regions from the image. See also figure 4.2

To remove speckle noise and obtain a sharper image the litterature suggest to use Fourier Filter.

Using these filters and extracting magnitude of gradient is easy to segment the necrotic part of the lesion.

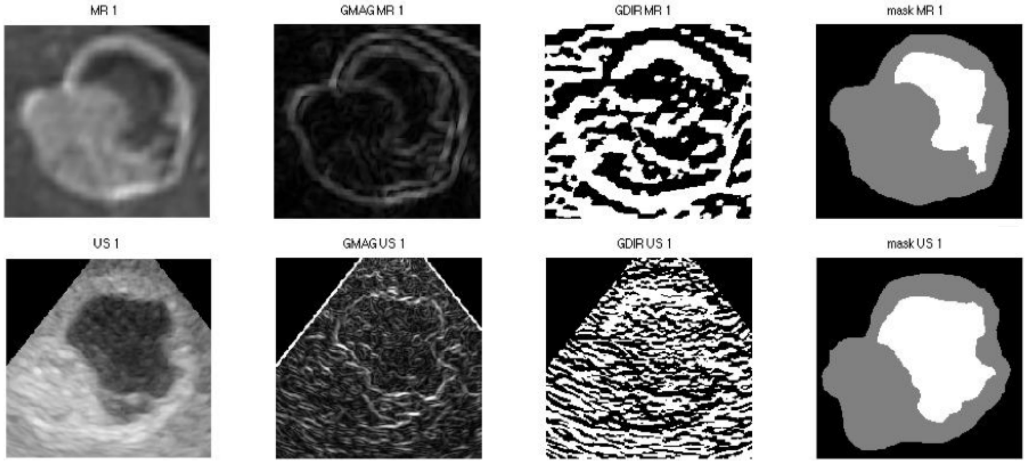

Figure 4.2: Magnitude applied on the MR image (up) and on US (down). The extraction of the contours is more difficult with US that is affected by speckle noise

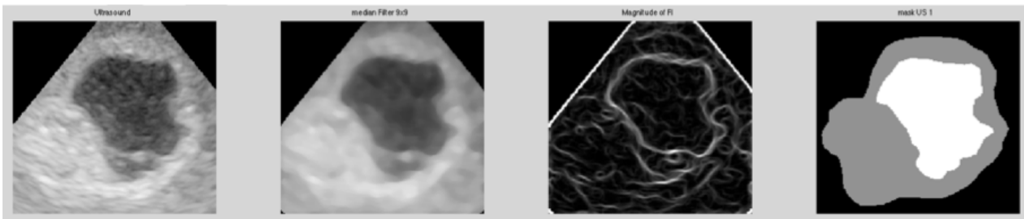

Figure 4.3: Median filter 9x9. Using the median filter and extracting magnitude of gradient is easy to extract che necrotic part of the lesion.

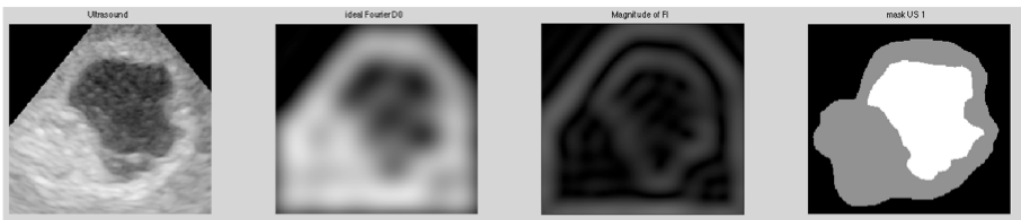

Figure 4.4: Ideal Fourier filter $d_0 = 10$

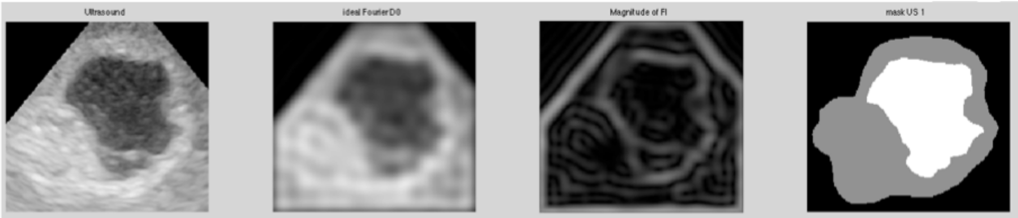

Figure 4.5: Ideal Fourier filter $d_0 = 20$

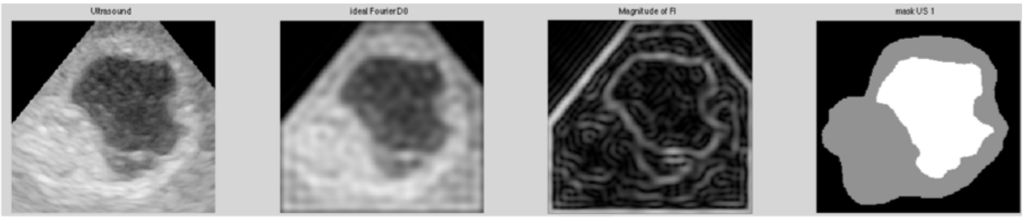

Figure 4.6: Ideal Fourier filter $d_0 = 30$

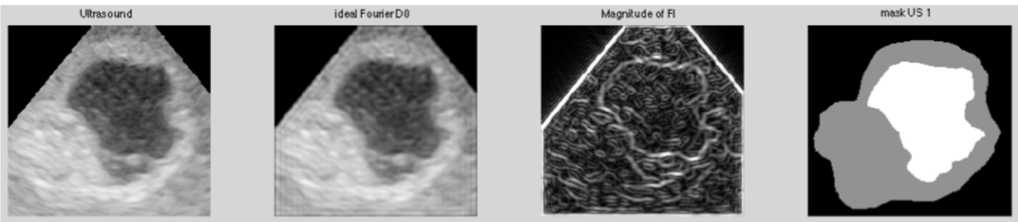

Figure 4.7: Ideal Fourier filter $d_0 = 70$

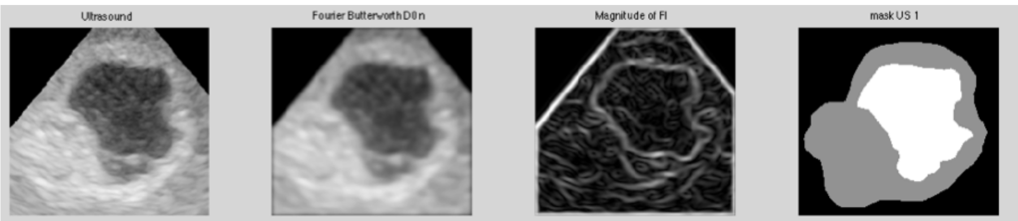

Figure 4.8: Fourier Butterworth $d_0 = 40, n = 2$

Figure 4.9: Homomorphic Butterworth $d_0 = 15, n = 3$. 4th picture represent the application of direction filter.

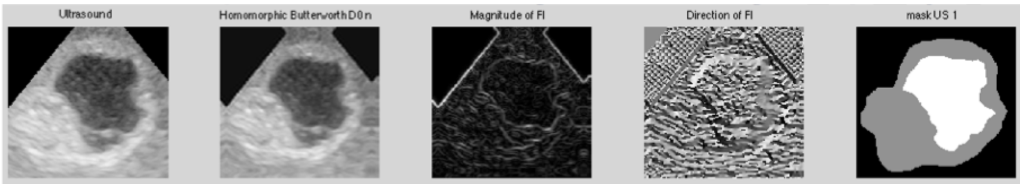

Figure 4.10: Homomorphic Wavelet Bi-Orthogonal 2nd Level High Frequency. 4th picture represent the application of direction filter.

Histogram equalization

After seeing how to improve the visualization of the necrotic component of the lesion is necessary to consider how to emphasize the pathological component.

In image processing is possible to obtain benefits by applying a filter able to distribute the gray levels over the entire available spectrum. In Computed Axial Tomography (CAT) the grey levels corresponds to a physical measured value. In MRI and US imaging they don't have a physical meaning, so is possible to adapt the histogram to our needs. In figure **??** necrosis part of the lesion remains equally visible, the pathological area is more evident.

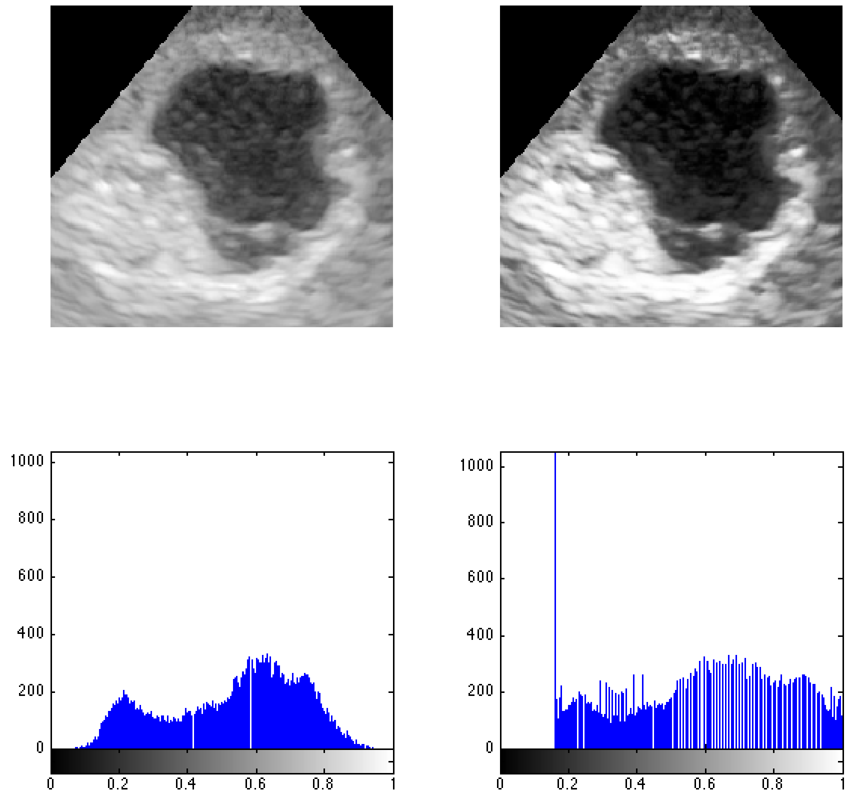

Figure 4.11: Upper-Left: Original image, Bottom-Left: Histogram of the original image, Upper-Right: Image after histogram equalization, Bottom-Right: Histogram of the equalized image. Pathological area is emphasized after filtering.

Order

At this step, it is necessary to evaluate the best order of filters to apply.

Figure 4.12: Hist EQ, Fourier/Butterworth $d_0 = 20, n = 2$ and magnitude.

Figure 4.13: Fourier/Butterworth $d_0 = 20, n = 2$, Hist EQ and magnitude.

Looking at the combined effect of the magnitude of the previous filters, is evident that equalization is more effective after applying Fourier/Butterworth filter. This filter is indicated as one of the best to remove speckle noise, as the Ideal Fourier filter.

4.2.2 Segmentation and clustering

Magnitude and direction filters use the instruments of contours extraction like Sobel or Prewitt operator. They emphasize contours instead of homogeneous areas. This step is necessary to prepare data for segmentation.
Many instruments for segmentation exist. In this study the approach was based on features space. Segmentation can be performed using different properties of the image. A simple and powerful method is based on grey

levels. This because also human vision is based on contours and shadows. This operation of segmentation and classification is called clustering.

The decision was to divide the pixels in three classes. Each pixel has to be assigned to a particular class. The assignment is based on feature space with a c-means fuzzy logic. This kind of logic consider both local and global properties of the pixel in order to assign it to a class. An example is shown in figures 4.14 and 4.15.

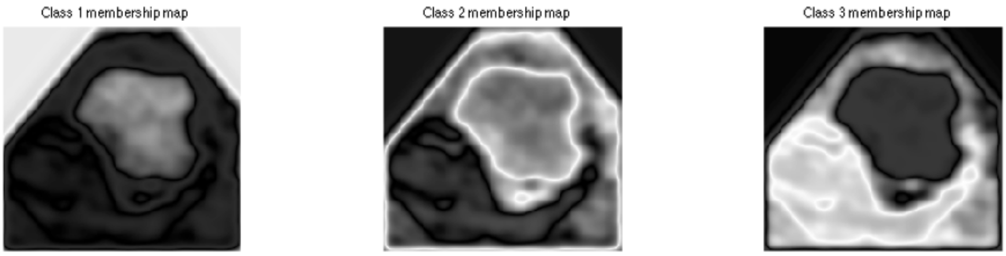

Figure 4.14: From left to right: class 1,2 and 3 membership.

Figure 4.15: Fuzzy c-means ($C = 3$).

4.3 Analysis

After clustering is necessary to evaluate the goodness of classification. The instrument adopted is the statistic diagnostic test.

4.3.1 Diagnostic test

After surgery, I asked to the surgeons to track the areas of the image in wich is represented the lesion. Then I choose wich classes can represent the lesion in the automatic segmentation image. I assigned to each class the label of pathologic or non-pathologic tissue. After that I performed a pixel-to-pixel comparison in order to obtain sensitivity and specificity of this test. Test is the automatc segmentation and surgeon's track is considered the real shape of the lesion. To each pixel in both images is assigned a label: patologic or non-pathologic. Pixel of coordinates ($\bar{x}$,$\bar{y}$) in automatic segmentation is compared to the same pixel ($\bar{x}$,$\bar{y}$) in the surgeon segmentation. If the first pixel is pathologic and the second is non-pathologic the return of the test is a false positive value. If the first pixel is non-pathologic and the second is pathologic the return of the test is a false negative value. If both are pathologic is a true positive value, and if both are non-patologic is a true negative value. All these results are saved, sensitivity and specificity are calculated with equations 4.1 and 4.2. FN, FP, TN and TP are the number of times in which they occurred previously.

$$Sensitivity = \frac{TP}{TP + FP} \tag{4.1}$$

$$Specificity = \frac{TN}{TN + FN} \tag{4.2}$$

Filtering was applied both on MR and US. As expected, the best automatic segmentation is performed in MR images then in US. Five kinds of filtering was applied in order to evaluate wich one is the best. Both sensitivity and specificity are important. In surgery procedure is better to have fewer false negative cases as possible. For this reason sensitivity is more important than specificity that however have to be kept in mind. Having low specificty means indentify all the image as lesion tissue. The results are visible in figures 4.16 and 4.18. To choose wich is the best filter I used the Mattews Correlation Coefficient (MCC).

Mattews Correlation Coefficient

The MCC is used in machine learning as a measure of the quality of binary classifications. It takes into account true and false positives and negatives ad is generally regarded as a balanced measure which can be used even if the classes are of very different sizes. The MCC is a correlation coefficient between the observed and predicted binary classifications. It returns a value between -1 and $+1$. A coefficient of $+1$ represents a perfect prediction, 0 is no better than random prediction and -1 indicates total disagreement between prediction and observation. It can be calculate using equation 4.3.

$$MCC = \frac{TP \cdot TN - FP \cdot FN}{\sqrt{(TP + FP) \cdot (TP + FN) \cdot (TN + FP) \cdot (TN + FN)}} \tag{4.3}$$

Considering the results obtained by MCC analysis the best filter is Fourier / Butterworth for US imaging and Homomorphic / Butterworth for MRI. For ultrasound imaging Fourier / Butterworth MCC performs a value of 0.6867 (figure 4.17), for magnetic resonance imaging Homomorphic / Butterworth MCC performs 0.8741 (figure 4.19). As we aspected, results obtained in MRI analysis are better than in US. This result does not question our study, indeed it highliths our premises. Infact it demonstrates that althought MRI is more readble for surgeon, US is still an useful information source. This study is focused on US automatic segmentation so the choosen filter is Fourier / Butterworth.

4.3.2 Conclusions

This small dataset is not sufficient to have a firm guarantee about this study but is a starting point for future works in this research area. Anyway this study prove the strong correlation between information extracted by surgeon and classification performed with an automatic algorithm. Morever, it shows that information that US brings intraoperatively are easily accessible by surgeon.

	Median 3x3	Ideal Fourier	Fourier/ Butterworth	Homomorphic/ butterworth	Homomorphic wavelet Dau
Specificity	0,8730	0,8461	0,8956	0,7394	0,7554
Sensitivity	0,7538	0,7755	0,8135	0,9110	0,8492

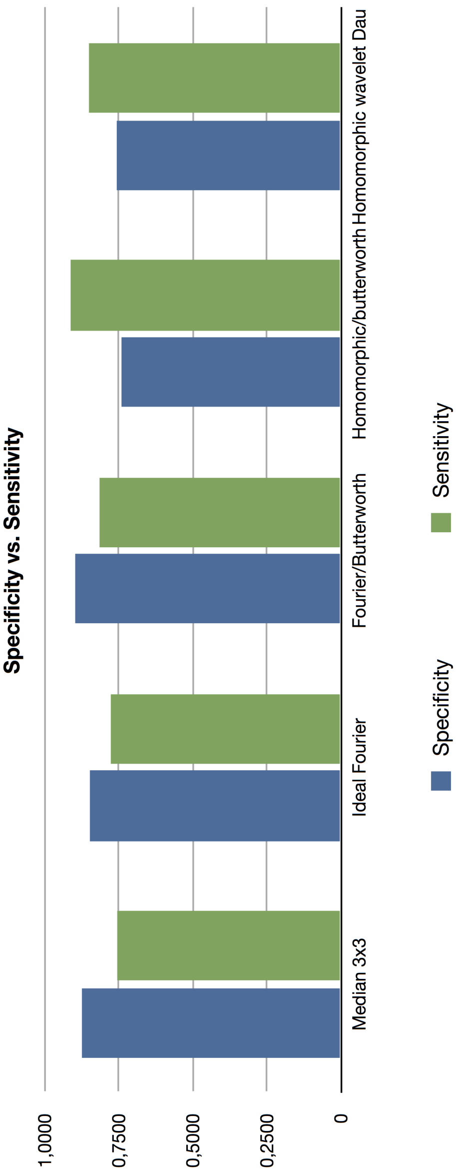

Figure 4.16: Diagnostic test on US images. From left to right where evaluated these filters: Median 3x3, Ideal Fourier, Fourier/Butterworth, Homomorphic/Butterworth, Homomorphic wavelet Daubechies.

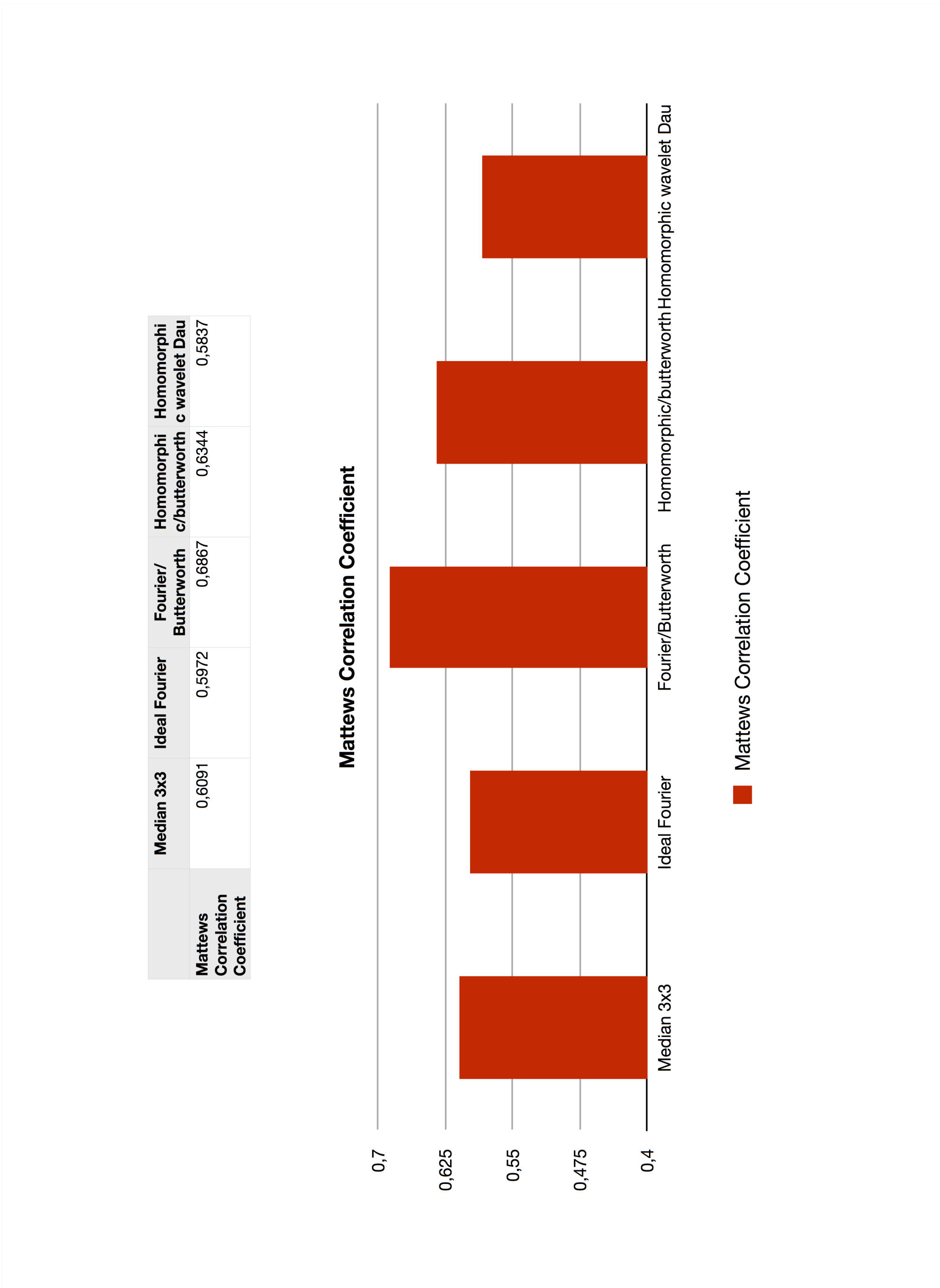

Figure 4.17: Mattews Correlation Coefficient for US filtered images.

	Median 3x3	Ideal Fourier	Fourier/ Butterworth	Homomorphic/ butterworth	Homomorphic wavelet Dau
Specificity	0,9239	0,9228	0,9225	0,9711	0,9747
Sensitivity	0,9016	0,9028	0,9033	0,8849	0,8034

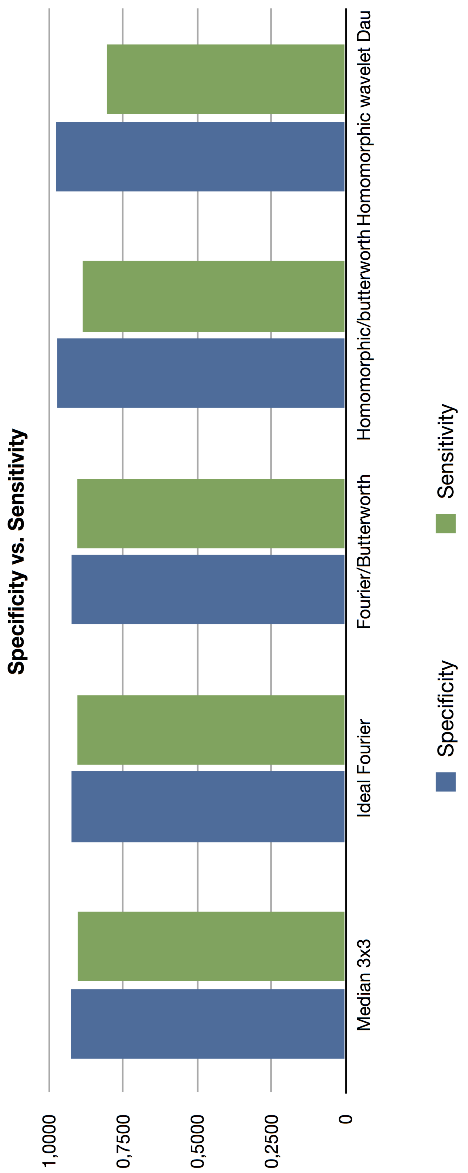

Figure 4.18: Diagnostic test on MR images. From left to right where evaluated these filters: Median 3x3, Ideal Fourier, Fourier/Butterworth, Homomorphic/Butterworth, Homomorphic wavelet Daubechies.

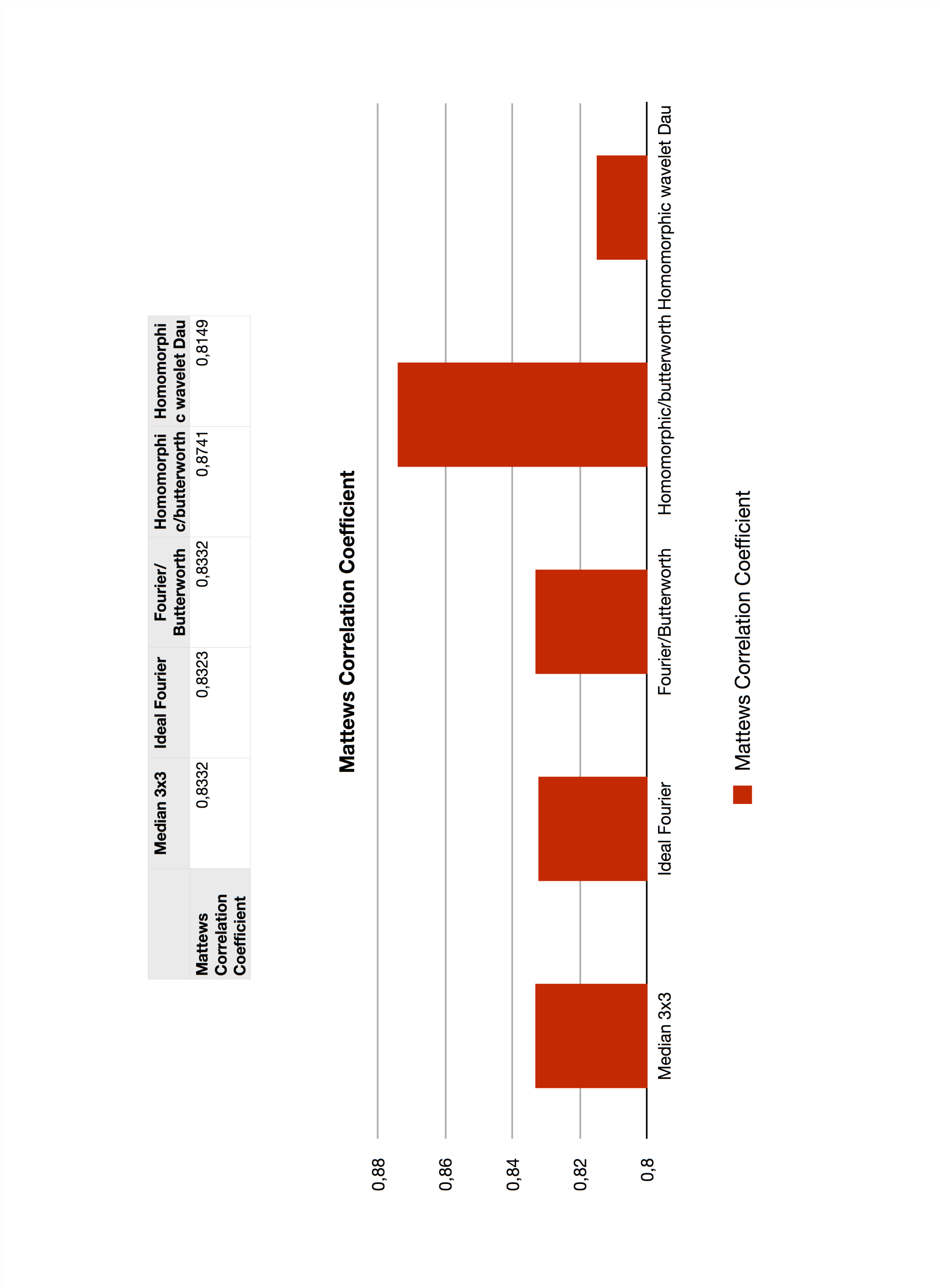

Figure 4.19: Mattews Correlation Coefficient for MR filtered images.

Figure 4.20: The surgeon watching both US and microscope.

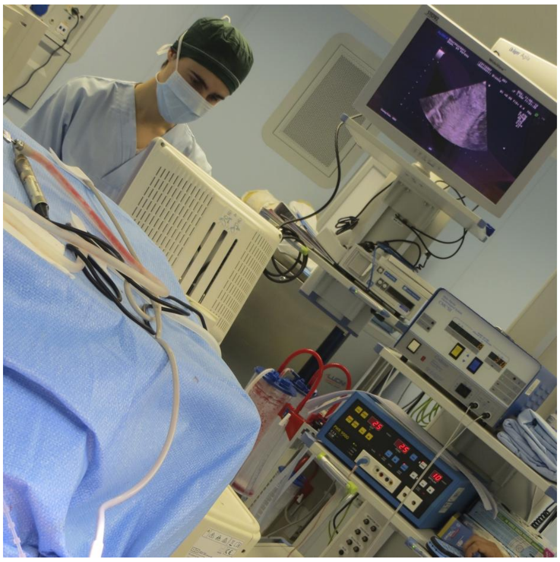

Figure 4.21: While I'm setting US parameters.

Chapter 5

Conclusions

"Criterion of truth is beauty."

Hans Urs von Balthasar (1905 - 1988)
Jesuit, Theologian, Cardinal of the Holy Roman Church

5.1 Possible improvements

On-line video segmentation

After this study a new research area can be opened. First of all is the possibility to implement an on-line filter, in order to help the surgeon in distinguishing and classification of tissues. Neurosurgeons are usualy not skilled in reading echographic imaging. Morover, US images are not easily interpretable, and have long learning curve. This instrument can help the surgeon in learning faster and may allow less frustration during the first uses that may discourage a further future use. An instrument like this can be extremely innovative. My hope is to have the possibility to continue my studies in this way. With the experience I have gained during this years and during my bachelor degree thesis project [21] I think that is possible to achieve this object in the coming years.

5.2 Future developments

5.2.1 Three-dimensional (3D) Ultrasound

Three-dimensional ultrasound is increasingly being introduced in the clinic, both for diagnostics and image guidance. Two ways exist to obtain a 3D US acquisition. Using dedicated 3D probes or obtaining 3D volumes with 2D probes in a two-step process. The first step is to fix to the probe a positioning sensor. It could be electromagnetic, optical, mechanical or acoustic. The second step is to apply a reconstruction algorithm, merging 2D acquisitions and positioning informations. Accuracy depends on:

- Reconstruction algorithm;
- Quality of the input 2D images;
- Accuracy of the position data. [15]

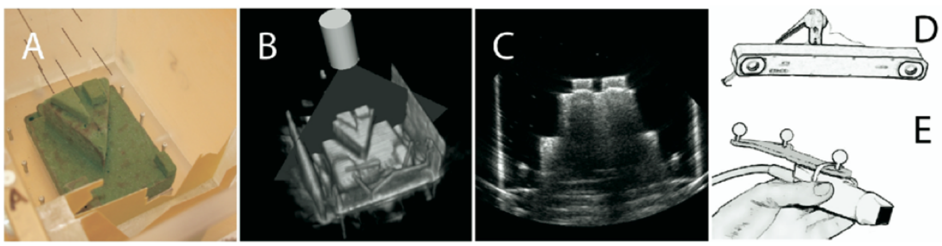

Figure 5.1: A; Photograph of a laboratory-phantom. B: Illustration of the US probe position and US 2D scan plane position in relation to the reconstructed phantom. C: Input 2D image scan. D: Illustration of the optical position tracking. E: Illustration of the US probe with an attached frame with reflecting spheres. [15]

Description of reconstruction algorithms

Reconstruction algorithms can be divided in three main groups based on implementation: Voxel-Based Methods (VBM), Pixel-Based Methods (PBM) and Function-Based Methods (FBM). VBMs traverse each voxel in the target voxel grid and gather information from the input 2D images to be placed in the voxel. In the different algorithms, one or several pixels may contribute to the value of each voxel. PBMs traverse each pixel in the input images and assign the pizel value to one ore several voxels. FBMs choose a particular function and determine coefficients to make one ore more functions pass through the input pixels. Afterwards, the function(s) are used to create a regular voxel array by calculationg the function(s) at regular intervals.
When choosing and implementing the algorithms for clinical use, it is important to take certain aspects into account, especially due to the practical application in which the algorithm is to be used. Each kind of algorithm can be evaluated according to: Analog versus digital US image import, VBM versus PBM, deciding Region-of-Interest (ROI), algorithm computation time, reconstruction quality, real-time versus high-quality implementations, post-preocessing supporting algorithms and practical considerations. Different practical applications will require different solutions, leading to the conclusion that future 3D ultrasound applications should probably consist of several reconstruction algorithms. [15]

5.2.2 Rigid US-MRI Registration

Multi-modal registration between 3D ultrasound and Magnetic Resonance Imaging is motivated by aims such as image fusion for improved diagnostics or intra-operative evaluation of brain shift. It's possible to perform a rigid region-based registration between US and MRI based on the segmentation of equivalent anatomic structures in both modalities. This kind of registration is a particularly difficult challenge due to the different source of information

delivered from the different imaging modalities. Moreover, the shape of image, the resolution and the pixel density are not the same. Many approaches have been proposed in literature, e.g. for non-linear registration in cardiac [48] and orthopaedic surgery [44] as well as pre-operative planning [30].
During surgery, after the opening of the dura mater, brain shift leads to a non-linear deformation of the brain tissue. In their work Ahmadi et al. has demonstrated the feasibility of region-based rigid US-MRI registration using a pair of corresponding transcranial US and MRI image volumes. This can be the first step for more complex (e.g. deformable) registration [45].
Ultrasound acquisitions are transcranial performed, using the temporal bone window of the skull. This is a complete non-invasive method. After acquisition is used an accurate, easy-to use, and robust 3D-TCUS midbrain segmentation method [46]. The segmented midbrain region was proposed to serve as a region-of-interest (ROI), for a later step of segmenting the substantia nigra (SN) for Parkinson's Disease (PD) diagnosis. For segmentation of the midbrain structure in MRI, was applied an atlas-based segmentation approach.

From registration experiment and the qualitative evaluation of the registration performance, it can be seen that this approach is possible. There are good results for both segmentation methods. In proximity of the midbrain structure, the registration is sufficiently high and a future image-based US-MRI deformable registration method will be possible [45].

5.2.3 Integration with neuronavigator

IIntegration between ultrasound intraoperative imaging and neuronavigation could offer a quick, helpful and economical method to extent tumour resection. It is known that long-term survival of patients with recurrent gliomas strictly depends on extent of resection. [26] [37] [38] This work was done in Philipps University, Marburg, Germany and explains the usefulness of navi-

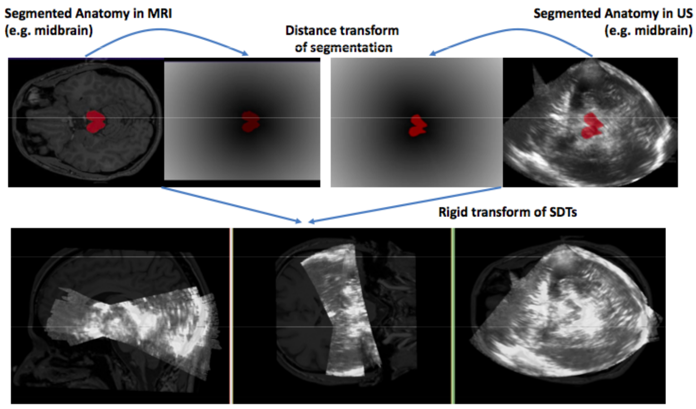

Figure 5.2: Illustration of the rigid registration approach for T1-MRI (top left) and 3D-TCUS (top right), using signed distance transforms (SDT) of the segmented surfaces. The bottom row shows an exmaple registration result. [45]

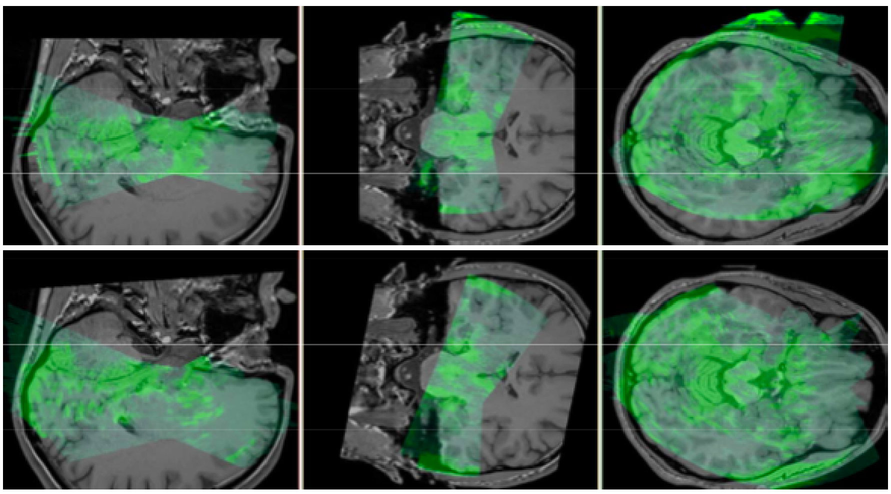

Figure 5.3: Results from the region-based registration experiment with initialization (top row) and registration (bottom row). Ultrasound is overlaid in green. [45]

gated ultrasound in a surgical environment during tumour resection of cystic gliomas.
The study was performed with an image guidance system (VectorVision2, BrainLab, Heimstetten, Germany) and with an ultrasoun device (IGSonic), integrated into the VectorVision2 navigation system. The probe (IGSonic Probe 10V5, 5-7.5 MHz frequency, max. 120 mm depth at 5 MHz) is connected to VectorVision2 via an IGSonic Device Box. THe IGSSonic Reference Star, which is equipped with three markers is fixed to the probe by an adapter in a predefined position. Moreover, the probe is pre-calibrated by the manufacturer's engineers. The surgeon has the opportunity to recalibrate the probe using a specific phantom if the previous calibration is not sufficiently accurate. MR preoperative images and US intraoperative images are rigidly overlapped by the navigation system. To facilitate the reading of the images, the US is displayed overlapped to the MR image, but is represented in green scale [49].

5.2.4 Brain shift estimation

Brain shift estimation can be an important feasible innovation in a neurosurgery procedure, in 2005 a team of researcher in Nederland studied the possibility of using intraoperative ultrasonography. [34]
Intraoperative brain deformation is one of the most important causes affecting the overall accuracy of image-guided neurosurgical procedures. Estimation of brain shift using intraoperative ultrasound imaging can be very useful to improve accuracy of the surgical procedure. The idea is to update the information provided by the preoperatively acquired MR data using the intraoperative imaging dataset. This technique requires a intraoperative 3D ultrasound. These acquisitions are used to update the presurgical planning to the new intraoperatory conditions. Preoperatory datasets are MRI T1-

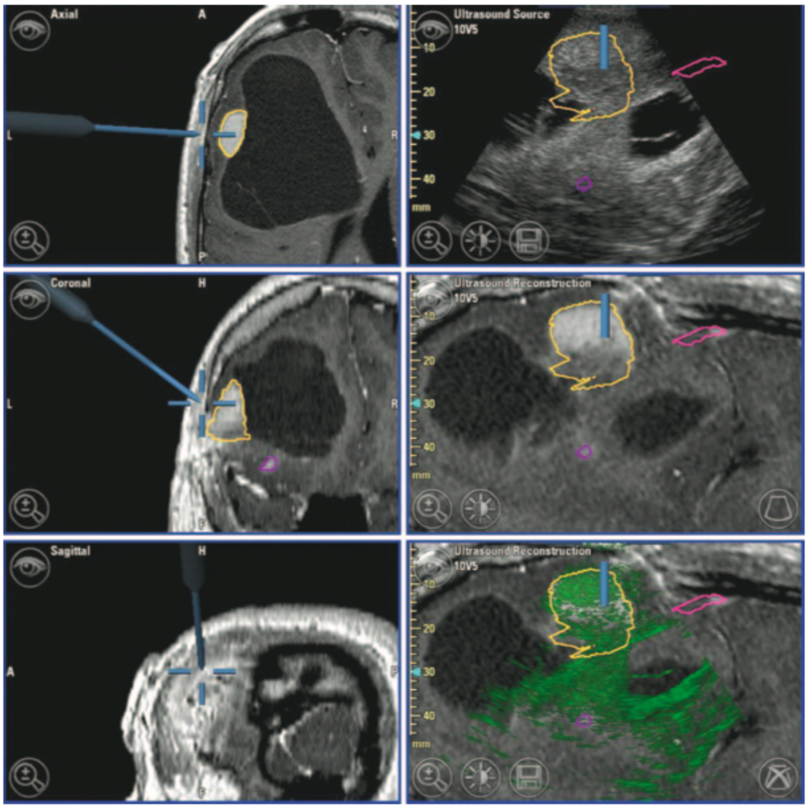

Figure 5.4: Example of an intra-operative screenshot during surgery for a left frontal recurrent cystic astrocytoma. Left side: Axial, coronal and sagittal MRI views. Right side: The ultrasound image (upper), its corresponding reconstructed MRI plane (center) and its corresponding reconstructed MRI plane with the superimposed semi-transparent green overlay image (lower), wich offers a good visualization of the hyper-echogenic tumour in a composite (ultrasound and MRI) image, are displayed. Preoperatively, the tumour has been utlined (yellow) in the MRI dataset and is superimposed onto the US image (upper right). Note the specific ultrasounic characteristics of the solid and the cystic parts of the tumours, enabling neurosurgeons without major experience in intra-operative ultrasound to understand the patients individual pathological anatomy. [49]

weighted acquisitions, gadolinium-enhanced. They have to be transferred from the MRI scanner to the neuronavigation workstation prior to surgery. During the procedure, the patient's head is fixed to the operating table so the skull is immobilized. Markers for identification of the reference system are rigidly attached to the head clamp. These markers have to be positioned in the field of view of camera system for navigation. To relate the coordinate system of the MR image to the reference arc coordinate system (arc or patient coordinate system) is determined a rigid transformation. A least-square fitting algorithm was used to relate the markers in MR coordinates to the markers in arc coordinates, and a rigid transformation could be calculated.

$$\begin{bmatrix} x_{arc} \\ y_{arc} \\ z_{arc} \end{bmatrix} = \begin{bmatrix} T_{MR \rightarrow arc} \end{bmatrix} \cdot \begin{bmatrix} x_{MR} \\ y_{MR} \\ z_{MR} \end{bmatrix} \tag{5.1}$$

An ultrasound scanner is connected to the neuronavigator. During intervention at least two ultrasound sweeps were made, one prior to opening the dura and one after opening the dura but prior to surgery. A position tracker is fixed to the ultrasound probe. In this way, identifying position of the tracker, it is possible to track position of the ultrasound images respect to the patient's head. Calibration procedure is realized with a phantom. Calibration transformation could be determined 5.2

$$\begin{bmatrix} x_{arc_{USimage}} \\ y_{arc_{USimage}} \\ z_{arc_{USimage}} \end{bmatrix} = \begin{bmatrix} T_{arc_{UStracker}} \rightarrow arc_{USimage} \end{bmatrix} \cdot \begin{bmatrix} x_{arc_{UStracker}} \\ y_{arc_{UStracker}} \\ z_{arc_{UStracker}} \end{bmatrix} \tag{5.2}$$

After calibrating the position of the 2D ultrasound plane could be described in arc coordinates by three vectors, one describing the position of the upper left corner of the ultrasound image (which is the origin of the ultrasound image in the ultrasound coordinate system), with respect to the origin in arc coordinates, and two vectors spanning the sides of the images. From these three vectors the transformation matrix from arc coordinates to ultrasound coordinates could be determined 5.3

$$\begin{bmatrix} x_{US} \\ y_{US} \\ z_{US} \end{bmatrix} = \begin{bmatrix} T_{arc \to US} \end{bmatrix} \cdot \begin{bmatrix} x_{arc} \\ y_{arc} \\ z_{arc} \end{bmatrix} \tag{5.3}$$

in which arc i $arc_{USimage}$. When an ultrasound image of the phantom is acquired, the image position of each element of the phantom could be retrieved and compared to the room position and the calibration transformation can be determined. Now it is possible to map the preoperative MRI coordinate system to the intraoperative ultrasound coordinate system. [34]

$$\begin{bmatrix} x_{US} \\ y_{US} \\ z_{US} \end{bmatrix} = \begin{bmatrix} T_{arc \to US} \end{bmatrix} \cdot \begin{bmatrix} T_{MR \to arc} \end{bmatrix} \cdot \begin{bmatrix} x_{MR} \\ y_{MR} \\ z_{MR} \end{bmatrix} \tag{5.4}$$

Measuring the brain shift

Brain shift will be apparent by a misregistration between the preoperative MR data, transformed to ultrasound coordinates with the aid of 5.4, and the ultrasound data acquired prior to and after the opening of the dura. The shift is described by two components, one for shift in the direction of gravity and one describing the perpendicular to gravity shift. US probe is usually positioned with y-axis (or depth direction) parallel to gravity, so x-axis and z-axis (where z-axis is in the scanning direction of the ultrasound probe) are perpendicular to gravity. The tumour is segmented with manual methods and the preoperative and intraoperative images are overlapped. To check the correctness of the registration results, the authors calculate the overlap factor that is defined as $2 \cdot (V_1 \cap V_2)/(V_1 + V_2)$, where V_1 is the volume of the tumour in the MR image and V_2 is the volume of the tumor in the US image. [34]

Results

For 12 patients investigated, the position of the tumor could be located well in all ultrasound scans. The margins of the tumors could be well defined in 8 patients and moderately defined in 4. In these latter patients it was clear where the tumor was located but diffuse margins made boundary definition more difficult. As first step, the preoperative MR images were transformed to the ultrasound coordinate system according to 5.4. The preoperative MR and intraoperative 3D ultrasound data could then be displayed in the same coordinate system. Brain shift is apparent by comparing tumor contours in the preoperative MR and intraoperative ultrasound images. Next, the MR images were registered to the ultrasound image, by image registration based on MI, to measure the rigid component of brain shift that had occurred after craniotomy. This registration takes five to ten minutes. A visual inspection of the data after registration showed that the MI-based registration of the preoperative MR with the intraoperative ultrasound, and thus the quantification of brain shift, was accurate for all patients. The average difference between the estimated shift from direct registration of the preoperative MR with the post opening dura intraoperative ultrasound, and the indirect measurement by registering twice, via pre opening dura ultrasound is 1.0 mm, with a maximum of 1.6 mm, which was significantly smaller than the magnitude of brain shifts that were observed. After transforming the preoperative MR to the intraoperative ultrasound coordinate system, based on the rigid transformation provided by image-guided surgery system, the average volume overlap of tumor tissue was 72%. After MI-based rigid transformation of the preoperative MR with the intraoperative ultrasound image the average volume overload of tumor tissue increased to 83%. To estimate brain shift was used MI-based registration. The shift can be expressed in relation to the ultrasound image taken before opening the dura or in realation to the ultrasound image taken after opening the dura. [34]

Discussion

This work shown that is possible to transform the preoperatively acquired MR data in the coordinate system of the intraoperative 3D ultrasound data, thus allowing an integrated display, visualizing the brain shift in 3D. To quantify the rigid component of brain shift, a rigid image registration method based on MI was used to register the MR data to the US data. The correctness of the estimated brain shift was also determined by checking whether tumor overlap increased after correction. MI-based registration improved the overlap between the tumor segments, but the overlap did not approach 100%. Below are three discussing these factors:

- Preoperative and intraoperative data cannot be described by a rigid registration alone, is necessary to perform a nonrigid registration method;
- Registration error from MR coordinates to arc coordinates: generally the registration error on the tumour surface is around 1 mm, and the error on the brain surgace is around 1.5 mm.
- Registration error from US coordinates to arc coordinates: the worst case calculated was 1.6 mm;

Not only the sinking of the brain was measured, but also a bulking of the brain. Not only the amount of brain shift but also the direction of it is important. The main limitation of the study is the use of a small group of patients. [34]

Conclusion

A system to acquire 3D ultrasound data during image-guided neurosurgery has been described. y comparing 3D ultrasound data to preoperative MR, the rigid component of brain shift could be measured. Therefore, the current setup can be used as a basis for correction for intraoperative brain deformations. [34]

5.3 Conclusions about introperative US in neurosurgery department of Verona

Introduction of intraoperative US methodology has been very favorably received by all the medical staff. All surgeons, even the less skilled in echographic imaging, who had the chance to tried this technique, were excited about it. This because it is user-friendly, takes little time, and gives useful information. This study gave much satisfaction, as well as to me, even to the surgeons. US technology is rapidly becoming a standard in neurosurgery department, also thanks to the goodwill of surgeons who have decided to engage themself in its use.

Appendix A

Case 1

Surgery information

- Sugeon: Dr. Angelo Musumeci
- Data of intervenction: 04/08/2013
- Pathology: Melanoma metastases
- Patient age: 36 years
- Gender: Female

MRI information

- Magnetic field strenght: 1.5 Tesla
- Voxel dimension (mm x mm x mm): 0.75 x 0.75 x 0.80
- Space between slices (mm): 0.00
- Number of slices: 208
- Slices orientation: Axial
- Acquisition mode: T1 with contrast (Gadolinium)
- Exam data: 03/27/2013

US information

- Wave frequency (MHz): 6.67
- Wave lenght (mm): 0.224
- Pixel dimension (mm x mm): 0.102 x 0.102
- Depth of scan field (mm): 40
- Refresh rate (Hz): 77
- Original image resolution: 800 x 600

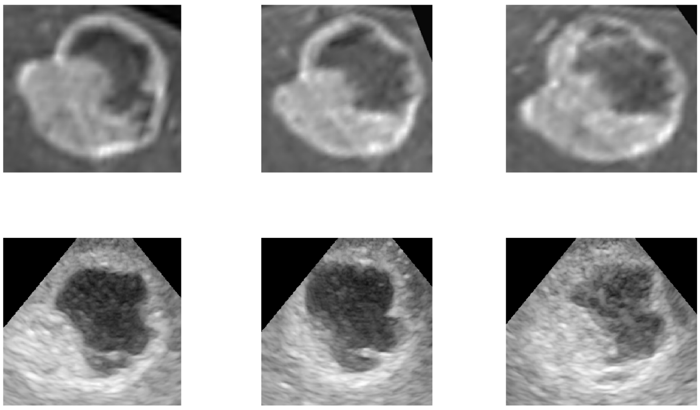

Figure A.1: Case 1. Up: MRI; Down: US.

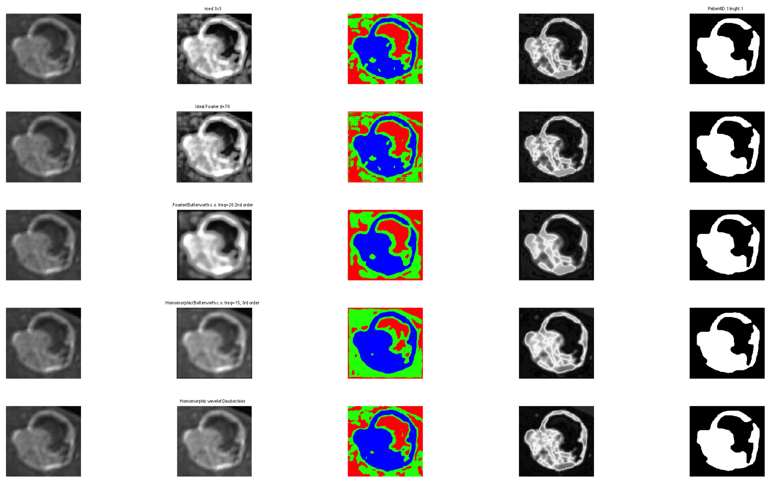

Figure A.2: MR imaging: Case 1, Image 1. In order from top to bottom: Median 3x3, Ideal Fourier, Fourier/Butterworth, Homomorphic/Butterworth, Homomorphic wavelet Daubechies filtering.

MCC 11	Median 3x3	Ideal Fourier	Fourier/Butterworth	Homomorphic/ butterworth	Homomorphic wavelet Dau
MIN	0,7010	0,6987	0,6993	0,7004	0,6597
Lesion 11	0,8766	0,8772	0,8772	0,9137	0,9122
MEAN	0,8332	0,8323	0,8332	0,8741	0,8149
MAX	0,9418	0,9306	0,9413	0,9429	0,9306

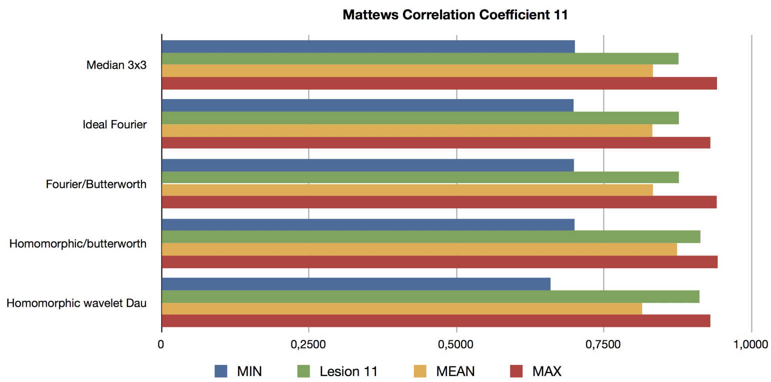

Figure A.3: MR MCC, Case 1, Image 1

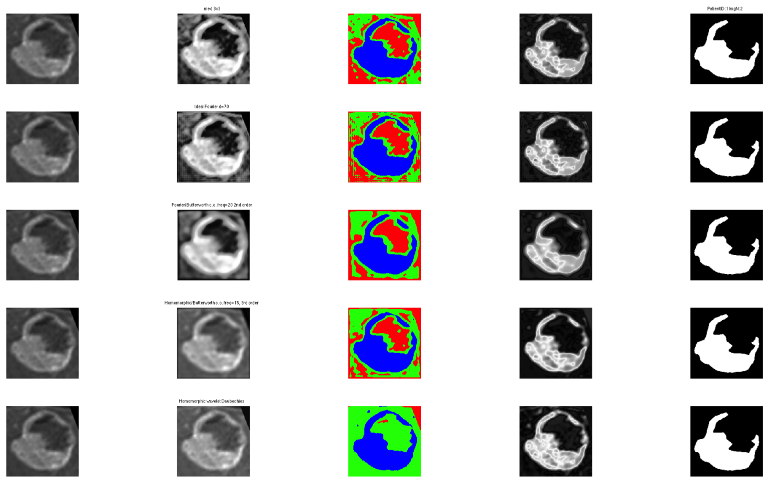

Figure A.4: MR imaging: Case 1, Image 2. In order from top to bottom: Median 3x3, Ideal Fourier, Fourier/Butterworth, Homomorphic/Butterworth, Homomorphic wavelet Daubechies filtering.

MCC 12	Median 3x3	Ideal Fourier	Fourier/Butterworth	Homomorphic/ butterworth	Homomorphic wavelet Dau
MIN	0,7010	0,6987	0,6993	0,7004	0,6597
Lesion 12	0,8926	0,8914	0,8921	0,8919	0,8833
MEAN	0,8332	0,8323	0,8332	0,8741	0,8149
MAX	0,9418	0,9306	0,9413	0,9429	0,9306

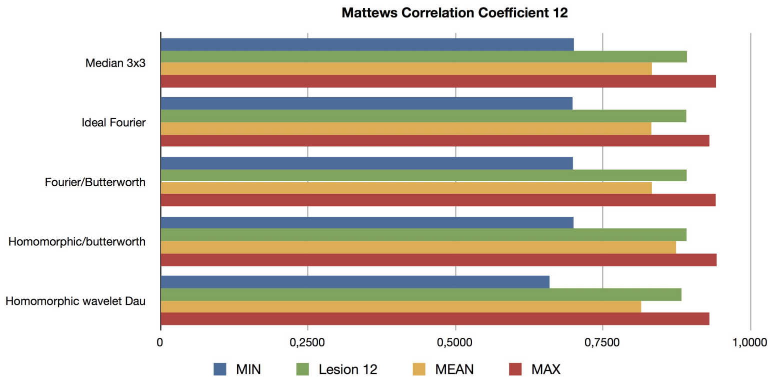

Figure A.5: MR MCC, Case 1, Image 2

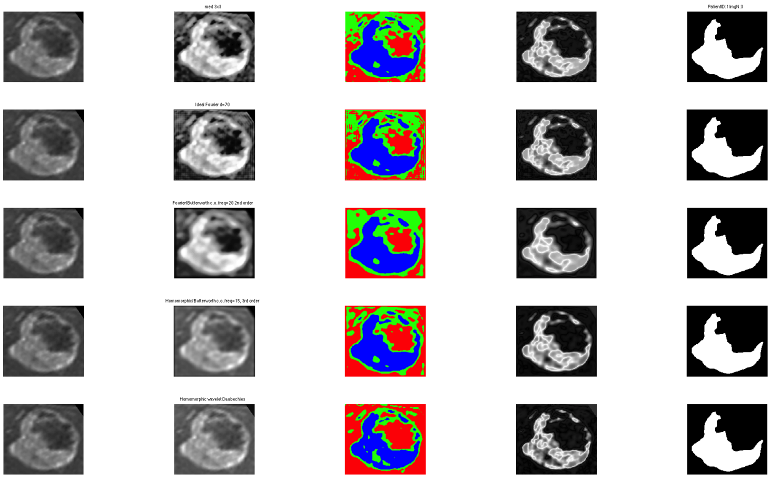

Figure A.6: MR imaging: Case 1, Image 3. In order from top to bottom: Median 3x3, Ideal Fourier, Fourier/Butterworth, Homomorphic/Butterworth, Homomorphic wavelet Daubechies filtering.

MCC 13	Median 3x3	Ideal Fourier	Fourier/Butterworth	Homomorphic/ butterworth	Homomorphic wavelet Dau
MIN	0,7010	0,6987	0,6993	0,7004	0,6597
Lesion 13	0,8463	0,8446	0,8602	0,8457	0,8211
MEAN	0,8332	0,8323	0,8332	0,8741	0,8149
MAX	0,9418	0,9306	0,9413	0,9429	0,9306

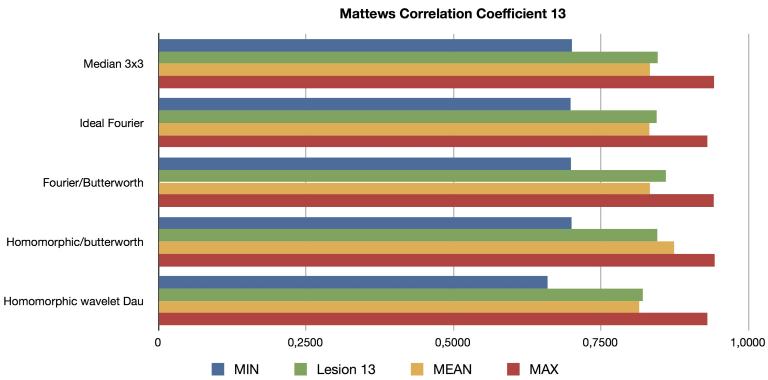

Figure A.7: MR MCC, Case 1, Image 3

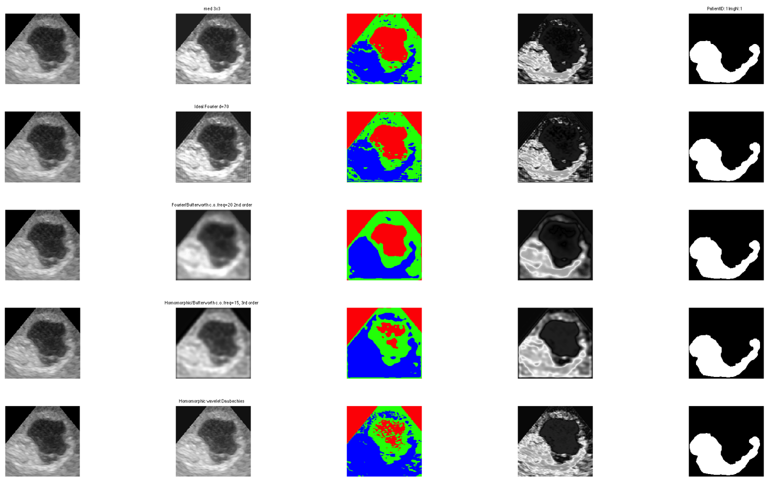

Figure A.8: US imaging: Case 1, Image 1. In order from top to bottom: Median 3x3, Ideal Fourier, Fourier/Butterworth, Homomorphic/Butterworth, Homomorphic wavelet Daubechies filtering.

MCC 11	Median 3x3	Ideal Fourier	Fourier/Butterworth	Homomorphic/ butterworth	Homomorphic wavelet Dau
MIN	0,4836	0,4989	0,5802	0,4478	0,4438
Lesion 11	0,7620	0,7521	0,7845	0,6285	0,6154
MEAN	0,6091	0,5972	0,6867	0,6344	0,5837
MAX	0,7620	0,7115	0,7992	0,7744	0,7115

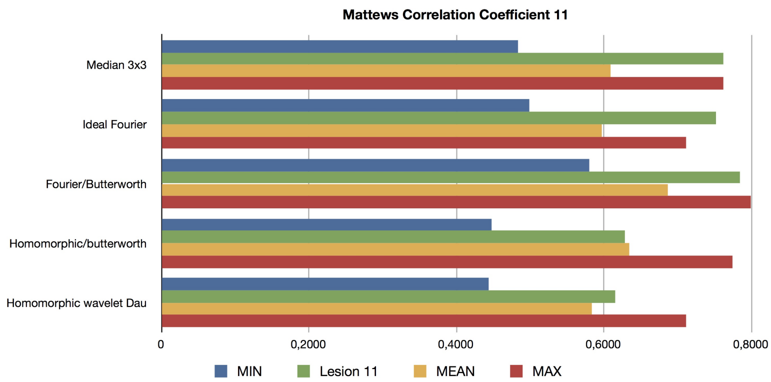

Figure A.9: US MCC, Case 1, Image 1

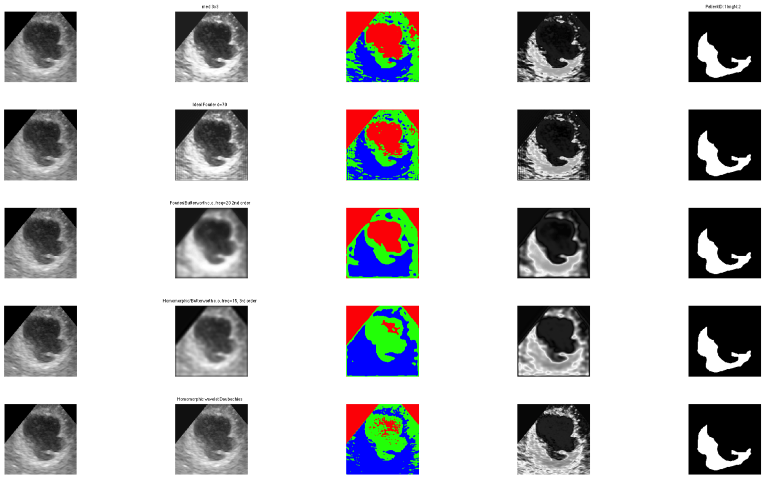

Figure A.10: US imaging: Case 1, Image 2. In order from top to bottom: Median 3x3, Ideal Fourier, Fourier/Butterworth, Homomorphic/Butterworth, Homomorphic wavelet Daubechies filtering.

MCC 12	Median 3x3	Ideal Fourier	Fourier/Butterworth	Homomorphic/ butterworth	Homomorphic wavelet Dau
MIN	0,4836	0,4989	0,5802	0,4478	0,4438
Lesion 12	0,5791	0,5682	0,5802	0,4478	0,4438
MEAN	0,6091	0,5972	0,6867	0,6344	0,5837
MAX	0,7620	0,7115	0,7992	0,7744	0,7115

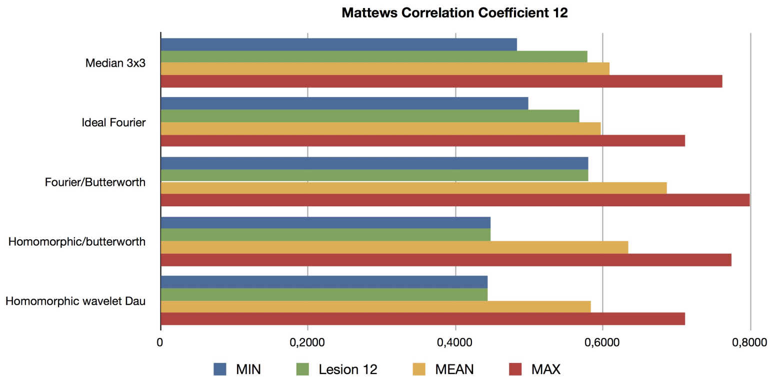

Figure A.11: US MCC, Case 1, Image 2

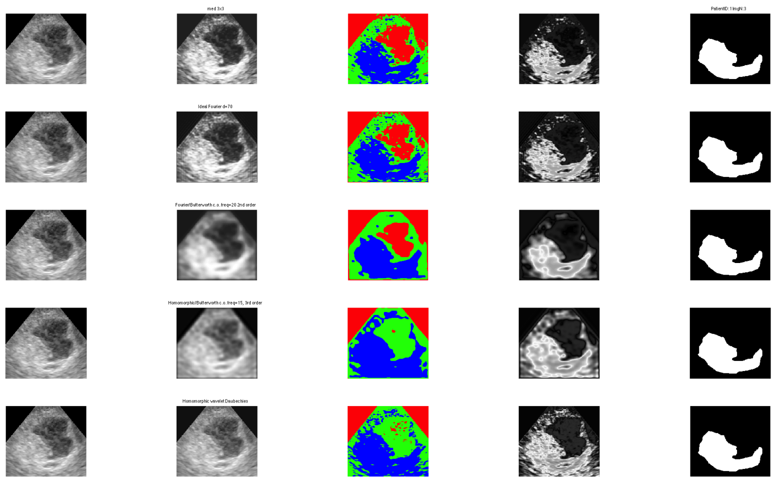

Figure A.12: US imaging: Case 1, Image 3. In order from top to bottom: Median 3x3, Ideal Fourier, Fourier/Butterworth, Homomorphic/Butterworth, Homomorphic wavelet Daubechies filtering.

MCC 13	Median 3x3	Ideal Fourier	Fourier/Butterworth	Homomorphic/ butterworth	Homomorphic wavelet Dau
MIN	0,4836	0,4989	0,5802	0,4478	0,4438
Lesion 13	0,6819	0,6729	0,7534	0,5485	0,5860
MEAN	0,6091	0,5972	0,6867	0,6344	0,5837
MAX	0,7620	0,7115	0,7992	0,7744	0,7115

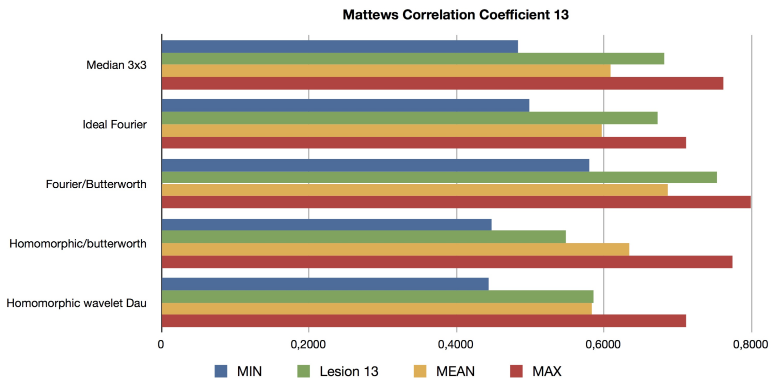

Figure A.13: US MCC, Case 1, Image 3.

Appendix B

Case 2

Surgery information

- Sugeon: Dr. Riccardo Damante
- Data of intervenction: 04/19/2013
- Pathology: Glioblastoma, grade 4^{th}
- Gender: Female
- Patient age: 57 years

MRI information

- Magnetic field strenght: 1.5 Tesla
- Voxel dimension (mm x mm x mm): 0.47 x 0.47 x 5.00
- Space between slices (mm): 6.00
- Number of slices: 24
- Slices orientation: Axial
- Acquisition mode: T1 with contrast (Gadolinium)
- Exam data: 04/08/2013

US information

- Wave frequency (MHz): 6.67
- Wave lenght (mm): 0.224
- Pixel dimension (mm x mm): 0.204 x 0.204
- Depth of scan field (mm): 80
- Refresh rate (Hz): 70
- Original image resolution: 800 x 600

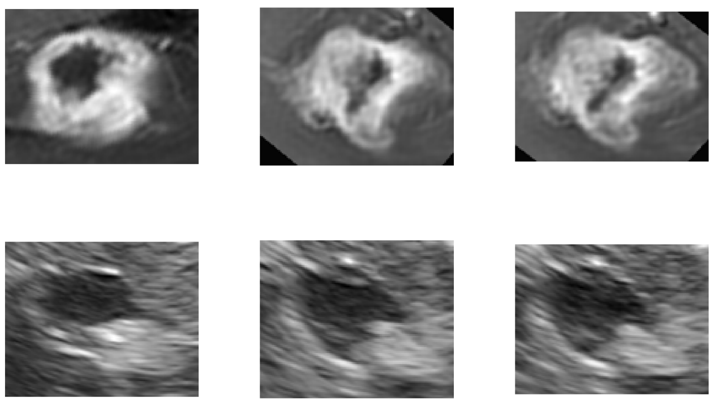

Figure B.1: Case 2. Up: MRI; Down: US.

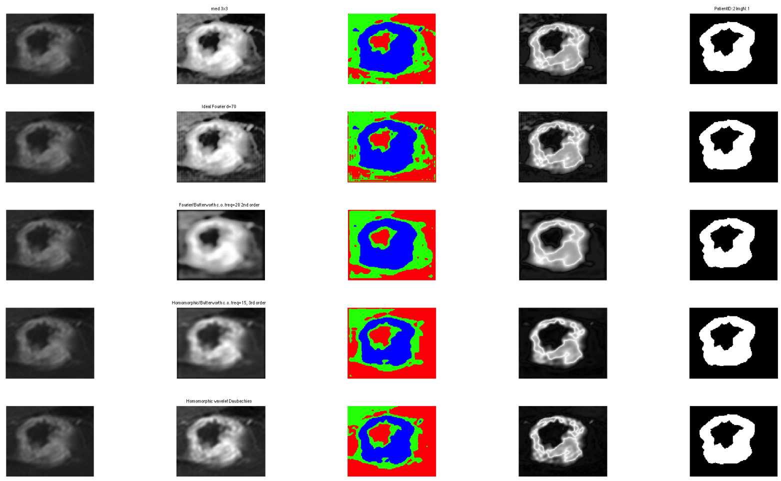

Figure B.2: MR imaging: Case 2, Image 1. In order from top to bottom: Median 3x3, Ideal Fourier, Fourier/Butterworth, Homomorphic/Butterworth, Homomorphic wavelet Daubechies filtering.

MCC 21	Median 3x3	Ideal Fourier	Fourier/Butterworth	Homomorphic/ butterworth	Homomorphic wavelet Dau
MIN	0,7010	0,6987	0,6993	0,7004	0,6597
Lesion 21	0,8525	0,8528	0,8581	0,8748	0,8704
MEAN	0,8332	0,8323	0,8332	0,8741	0,8149
MAX	0,9418	0,9306	0,9413	0,9429	0,9306

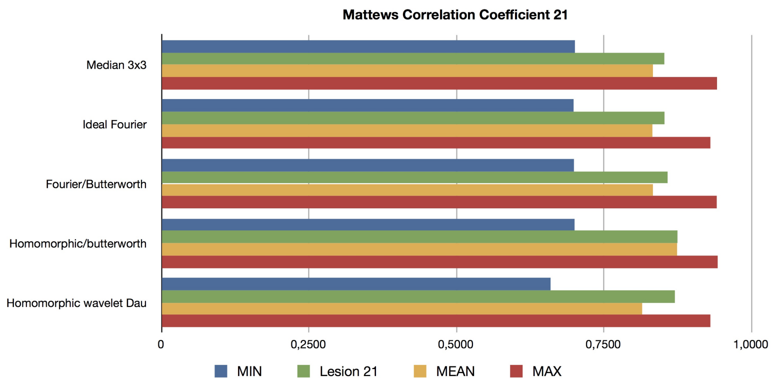

Figure B.3: MR MCC, Case 2, Image 1

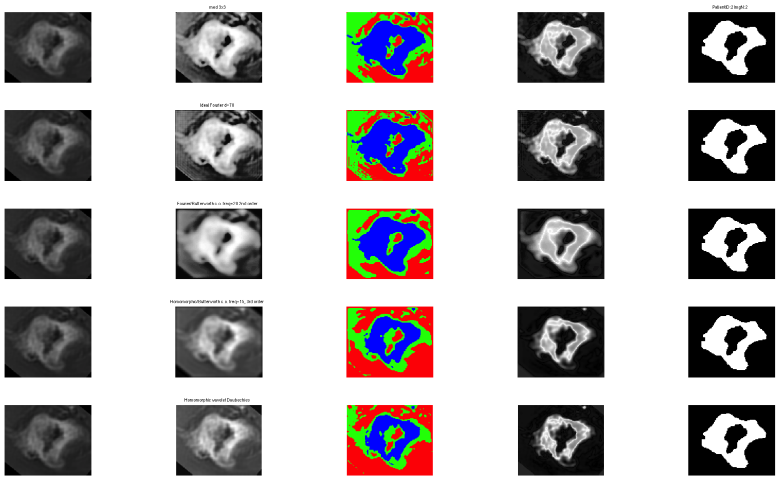

Figure B.4: MR imaging: Case 2, Image 2. In order from top to bottom: Median 3x3, Ideal Fourier, Fourier/Butterworth, Homomorphic/Butterworth, Homomorphic wavelet Daubechies filtering.

MCC 22	Median 3x3	Ideal Fourier	Fourier/Butterworth	Homomorphic/ butterworth	Homomorphic wavelet Dau
MIN	0,7010	0,6987	0,6993	0,7004	0,6597
Lesion 22	0,8377	0,8344	0,8399	0,7978	0,7874
MEAN	0,8332	0,8323	0,8332	0,8741	0,8149
MAX	0,9418	0,9306	0,9413	0,9429	0,9306

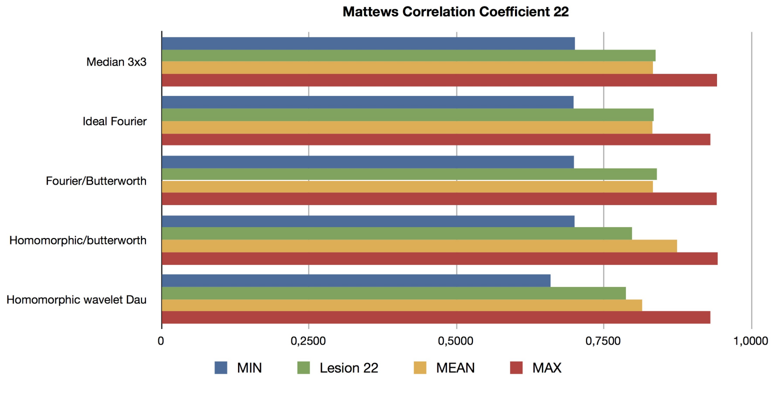

Figure B.5: MR MCC, Case 2, Image 2

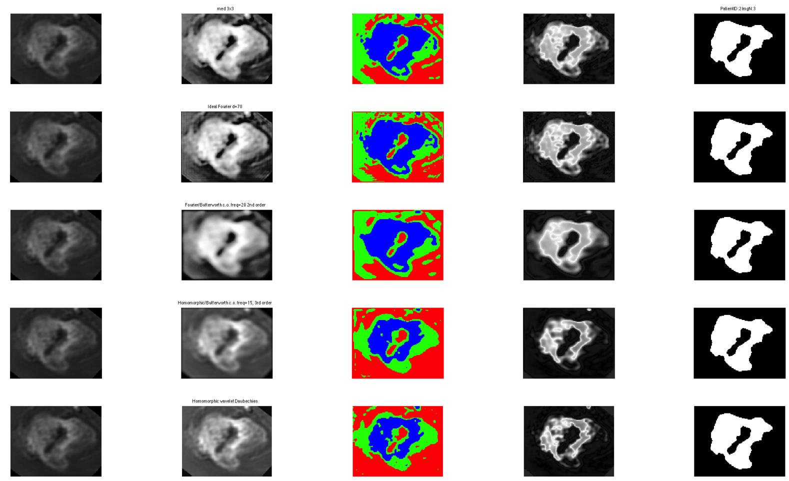

Figure B.6: MR imaging: Case 2, Image 3. In order from top to bottom: Median 3x3, Ideal Fourier, Fourier/Butterworth, Homomorphic/Butterworth, Homomorphic wavelet Daubechies filtering.

MCC 23	Median 3x3	Ideal Fourier	Fourier/Butterworth	Homomorphic/ butterworth	Homomorphic wavelet Dau
MIN	0,7010	0,6987	0,6993	0,7004	0,6597
Lesion 23	0,8399	0,8315	0,8297	0,7530	0,7410
MEAN	0,8332	0,8323	0,8332	0,8741	0,8149
MAX	0,9418	0,9306	0,9413	0,9429	0,9306

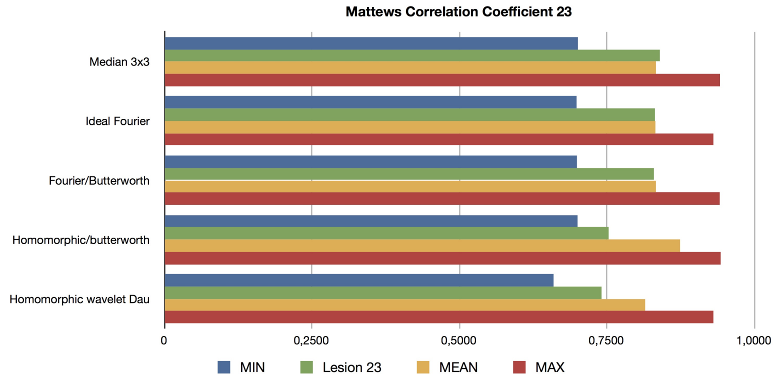

Figure B.7: MR MCC, Case 2, Image 3

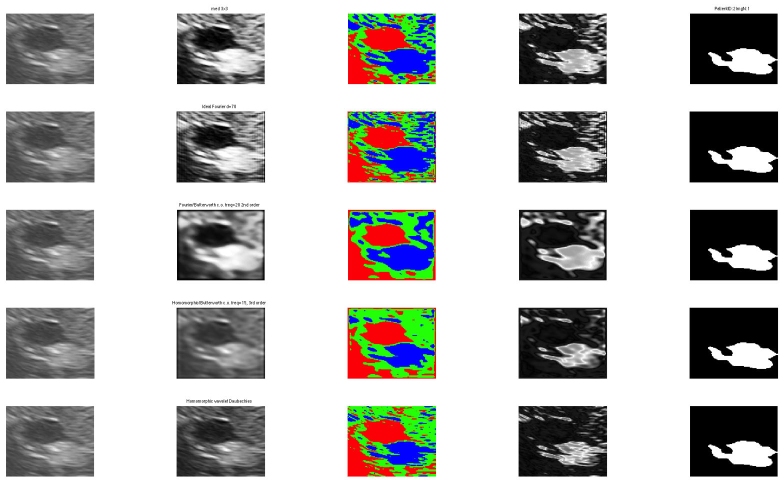

Figure B.8: US imaging: Case 2, Image 1. In order from top to bottom: Median 3x3, Ideal Fourier, Fourier/Butterworth, Homomorphic/Butterworth, Homomorphic wavelet Daubechies filtering.

MCC 21	Median 3x3	Ideal Fourier	Fourier/Butterworth	Homomorphic/ butterworth	Homomorphic wavelet Dau
MIN	0,4836	0,4989	0,5802	0,4478	0,4438
Lesion 21	0,6105	0,5725	0,6418	0,7389	0,7071
MEAN	0,6091	0,5972	0,6867	0,6344	0,5837
MAX	0,7620	0,7115	0,7992	0,7744	0,7115

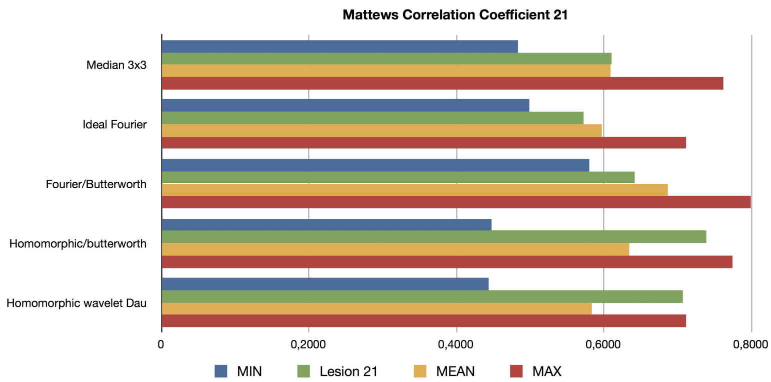

Figure B.9: US MCC, Case 2, Image 1

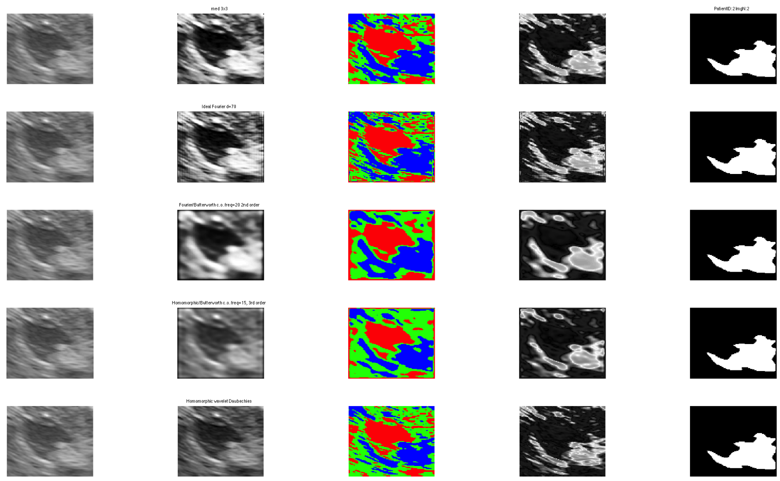

Figure B.10: US imaging: Case 2, Image 2. In order from top to bottom: Median 3x3, Ideal Fourier, Fourier/Butterworth, Homomorphic/Butterworth, Homomorphic wavelet Daubechies filtering.

MCC 22	Median 3x3	Ideal Fourier	Fourier/Butterworth	Homomorphic/ butterworth	Homomorphic wavelet Dau
MIN	0,4836	0,4989	0,5802	0,4478	0,4438
Lesion 22	0,5671	0,5483	0,6086	0,5929	0,5530
MEAN	0,6091	0,5972	0,6867	0,6344	0,5837
MAX	0,7620	0,7115	0,7992	0,7744	0,7115

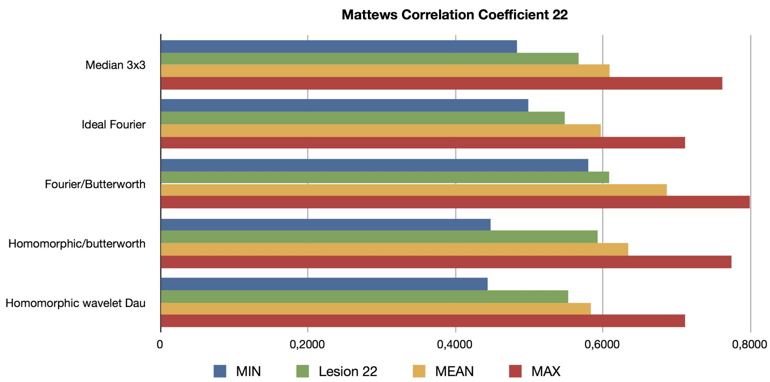

Figure B.11: US MCC, Case 2, Image 2

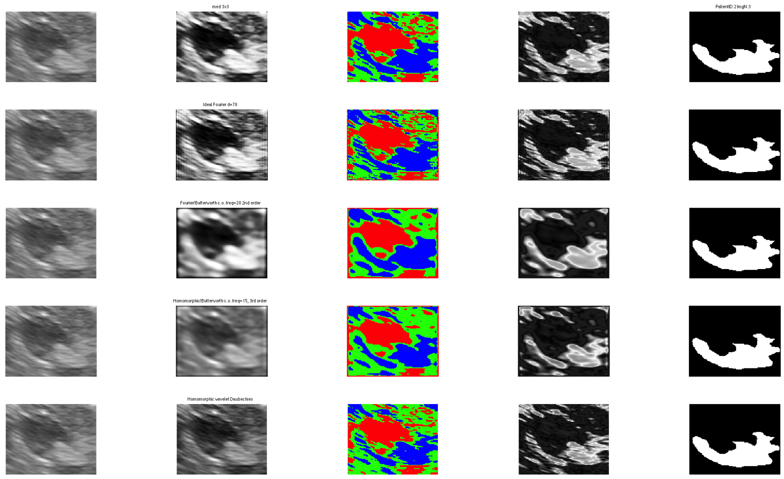

Figure B.12: US imaging: Case 2, Image 3. In order from top to bottom: Median 3x3, Ideal Fourier, Fourier/Butterworth, Homomorphic/Butterworth, Homomorphic wavelet Daubechies filtering.

MCC 23	Median 3x3	Ideal Fourier	Fourier/Butterworth	Homomorphic/ butterworth	Homomorphic wavelet Dau
MIN	0,4836	0,4989	0,5802	0,4478	0,4438
Lesion 23	0,5623	0,5431	0,5948	0,5561	0,5357
MEAN	0,6091	0,5972	0,6867	0,6344	0,5837
MAX	0,7620	0,7115	0,7992	0,7744	0,7115

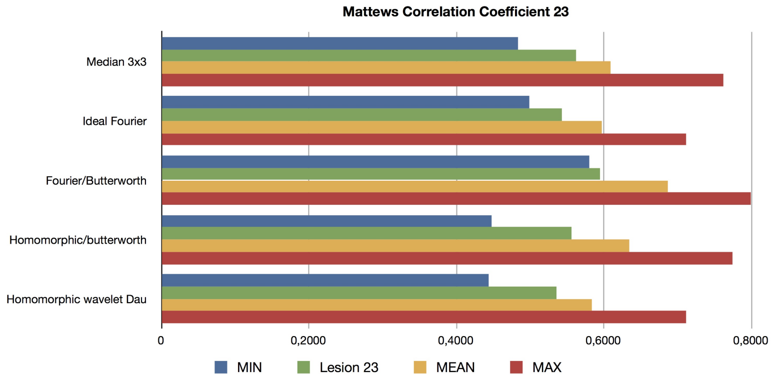

Figure B.13: US MCC, Case 2, Image 3.

Appendix C

Case 3

Surgery information

- Sugeon: Dr. Angelo Musumeci
- Data of intervenction: 05/14/2013
- Pathology: Right rolandic metastases
- Gender: Female
- Patient age: 43 years

MRI information

- Magnetic field strenght: 3.0 Tesla
- Voxel dimension (mm x mm x mm): 0.43 x 0.43 x 1.00
- Space between slices (mm): 0.00
- Number of slices: 176
- Slices orientation: Axial
- Acquisition mode: T1 with contrast (Gadolinium)
- Exam data: 04/16/2013

US information

- Wave frequency (MHz): 6.67
- Wave lenght (mm): 0.224
- Pixel dimension (mm x mm): 0.127 x 0.127
- Depth of scan field (mm): 50
- Refresh rate (Hz): 77
- Original image resolution: 800 x 600

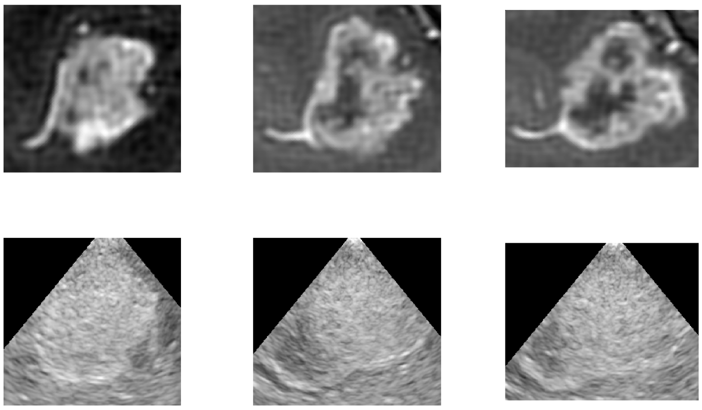

Figure C.1: Case 3. Up: MRI; Down: US.

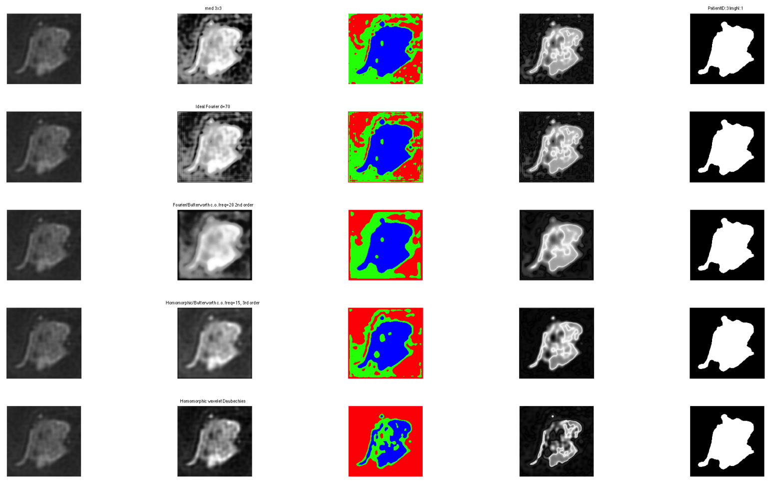

Figure C.2: MR imaging: Case 3, Image 1. In order from top to bottom: Median 3x3, Ideal Fourier, Fourier/Butterworth, Homomorphic/Butterworth, Homomorphic wavelet Daubechies filtering.

MCC 31	Median 3x3	Ideal Fourier	Fourier/Butterworth	Homomorphic/ butterworth	Homomorphic wavelet Dau
MIN	0,7010	0,6987	0,6993	0,7004	0,6597
Lesion 31	0,9418	0,9418	0,9413	0,8995	0,6597
MEAN	0,8332	0,8323	0,8332	0,8741	0,8149
MAX	0,9418	0,9306	0,9413	0,9429	0,9306

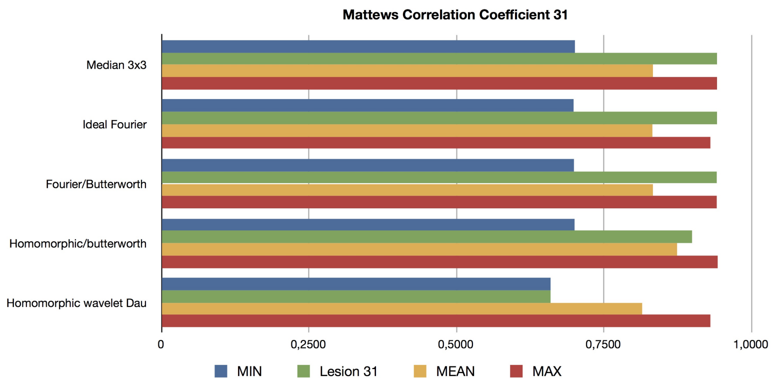

Figure C.3: MR MCC, Case 3, Image 1

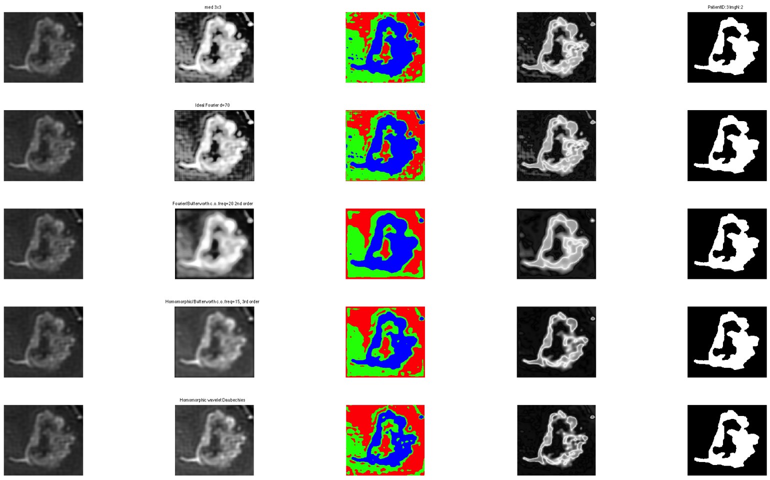

Figure C.4: MR imaging: Case 3, Image 2. In order from top to bottom: Median 3x3, Ideal Fourier, Fourier/Butterworth, Homomorphic/Butterworth, Homomorphic wavelet Daubechies filtering.

MCC 32	Median 3x3	Ideal Fourier	Fourier/Butterworth	Homomorphic/ butterworth	Homomorphic wavelet Dau
MIN	0,7010	0,6987	0,6993	0,7004	0,6597
Lesion 32	0,8568	0,8542	0,8475	0,9040	0,8848
MEAN	0,8332	0,8323	0,8332	0,8741	0,8149
MAX	0,9418	0,9306	0,9413	0,9429	0,9306

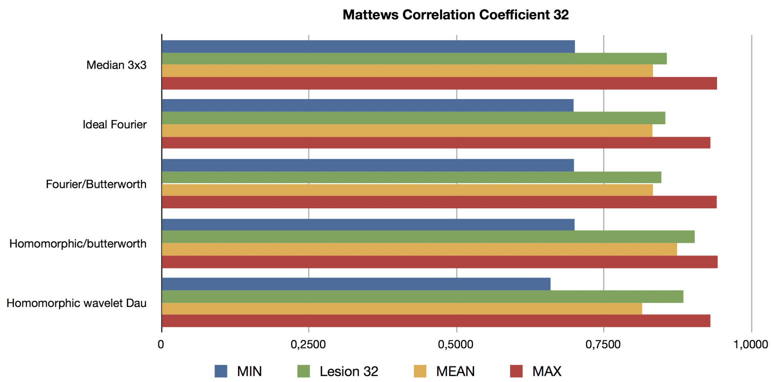

Figure C.5: MR MCC, Case 3, Image 2

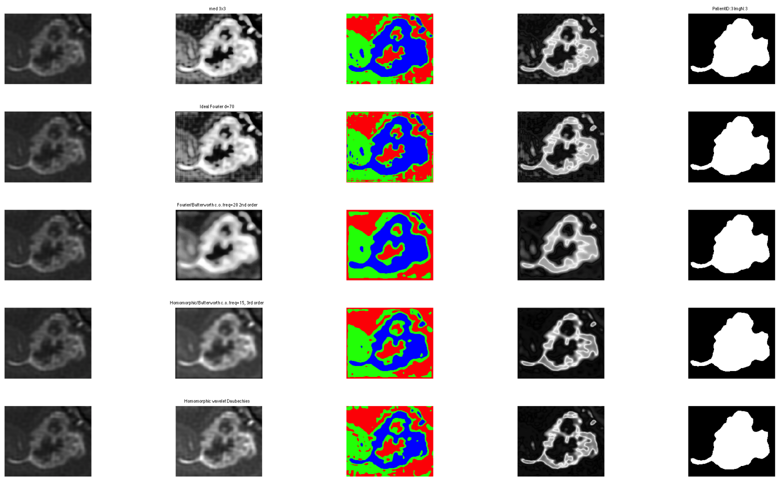

Figure C.6: MR imaging: Case 3, Image 3. In order from top to bottom: Median 3x3, Ideal Fourier, Fourier/Butterworth, Homomorphic/Butterworth, Homomorphic wavelet Daubechies filtering.

MCC 33	Median 3x3	Ideal Fourier	Fourier/Butterworth	Homomorphic/ butterworth	Homomorphic wavelet Dau
MIN	0,7010	0,6987	0,6993	0,7004	0,6597
Lesion 33	0,7478	0,7443	0,7493	0,7004	0,6833
MEAN	0,8332	0,8323	0,8332	0,8741	0,8149
MAX	0,9418	0,9306	0,9413	0,9429	0,9306

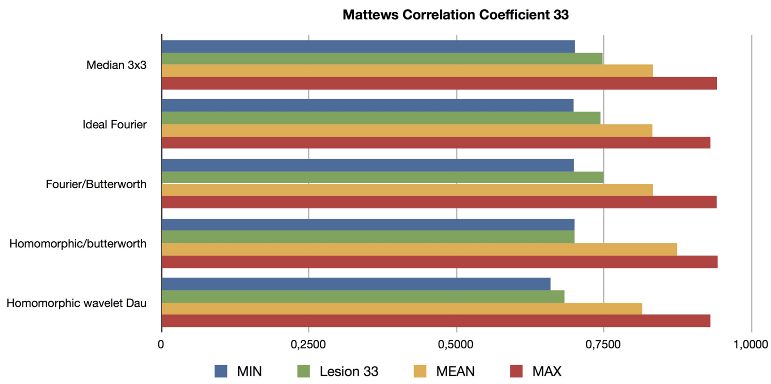

Figure C.7: MR MCC, Case 3, Image 3

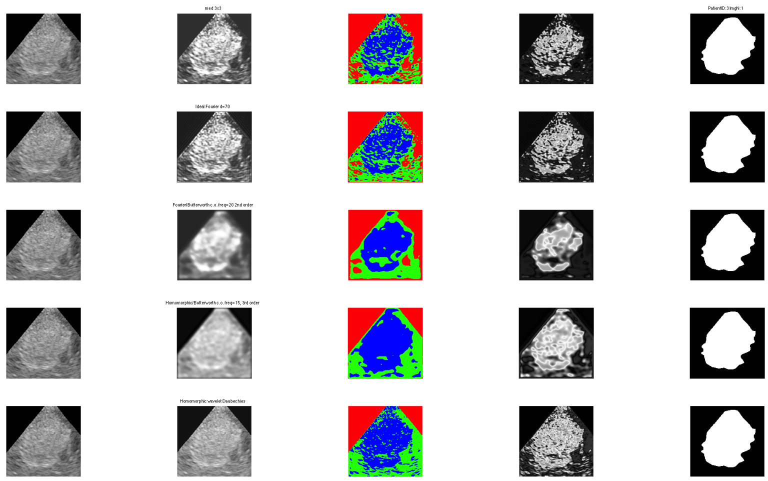

Figure C.8: US imaging: Case 3, Image 1. In order from top to bottom: Median 3x3, Ideal Fourier, Fourier/Butterworth, Homomorphic/Butterworth, Homomorphic wavelet Daubechies filtering.

MCC 31	Median 3x3	Ideal Fourier	Fourier/Butterworth	Homomorphic/ butterworth	Homomorphic wavelet Dau
MIN	0,4836	0,4989	0,5802	0,4478	0,4438
Lesion 31	0,5981	0,5961	0,7140	0,7367	0,6368
MEAN	0,6091	0,5972	0,6867	0,6344	0,5837
MAX	0,7620	0,7115	0,7992	0,7744	0,7115

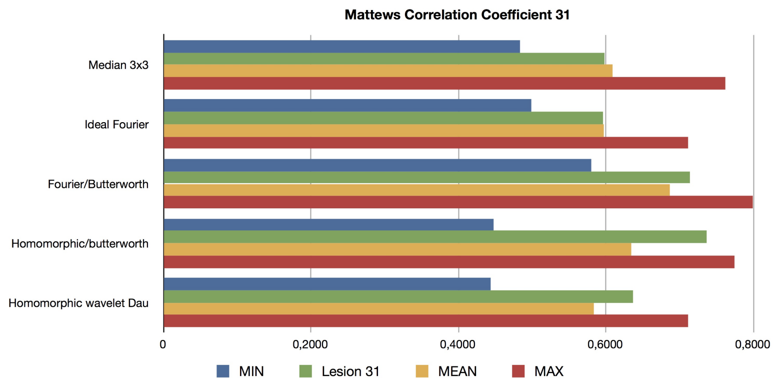

Figure C.9: US MCC, Case 3, Image 1

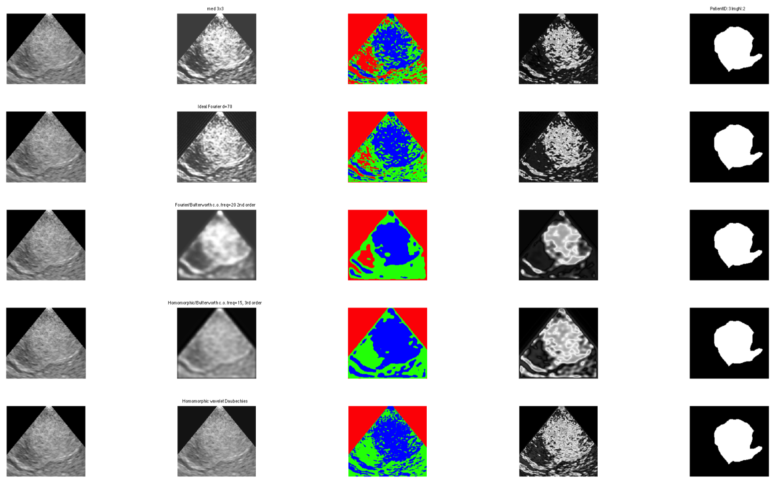

Figure C.10: US imaging: Case 3, Image 2. In order from top to bottom: Median 3x3, Ideal Fourier, Fourier/Butterworth, Homomorphic/Butterworth, Homomorphic wavelet Daubechies filtering.

MCC 32	Median 3x3	Ideal Fourier	Fourier/Butterworth	Homomorphic/ butterworth	Homomorphic wavelet Dau
MIN	0,4836	0,4989	0,5802	0,4478	0,4438
Lesion 32	0,5731	0,5722	0,7804	0,6150	0,5267
MEAN	0,6091	0,5972	0,6867	0,6344	0,5837
MAX	0,7620	0,7115	0,7992	0,7744	0,7115

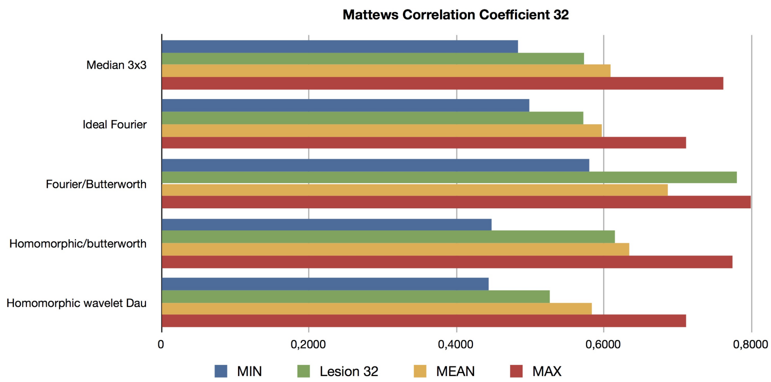

Figure C.11: US MCC, Case 3, Image 2

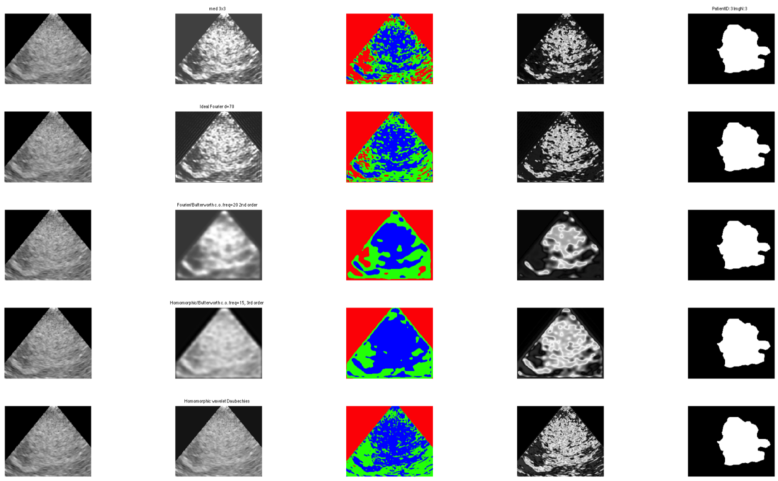

Figure C.12: US imaging: Case 3, Image 3. In order from top to bottom: Median 3x3, Ideal Fourier, Fourier/Butterworth, Homomorphic/Butterworth, Homomorphic wavelet Daubechies filtering.

MCC 33	Median 3x3	Ideal Fourier	Fourier/Butterworth	Homomorphic/ butterworth	Homomorphic wavelet Dau
MIN	0,4836	0,4989	0,5802	0,4478	0,4438
Lesion 33	0,4836	0,4989	0,6451	0,5688	0,4798
MEAN	0,6091	0,5972	0,6867	0,6344	0,5837
MAX	0,7620	0,7115	0,7992	0,7744	0,7115

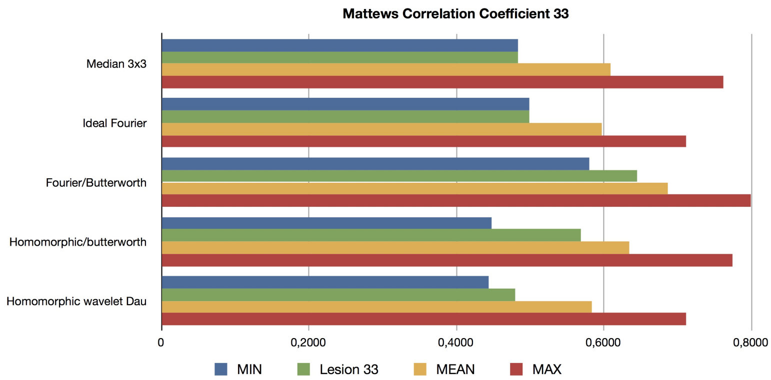

Figure C.13: US MCC, Case 3, Image 3.

Appendix D

Case 4

Surgery information

- Sugeon: Dr. Riccardo Damante
- Data of intervenction: 05/16/2013
- Pathology: Lung metastases
- Gender: Male
- Patient age: 47 years

MRI information

- Magnetic field strenght: 1.5 Tesla
- Voxel dimension (mm x mm x mm): 0.83 x 0.83 x 1.00
- Space between slices (mm): 1.00
- Number of slices: 160
- Slices orientation: Axial
- Acquisition mode: T1 with contrast (Gadolinium)
- Exam data: 04/26/2013

US information

- Wave frequency (MHz): 6.67
- Wave lenght (mm): 0.224
- Pixel dimension (mm x mm): 0.204 x 0.204
- Depth of scan field (mm): 80
- Refresh rate (Hz): 70
- Original image resolution: 800 x 600

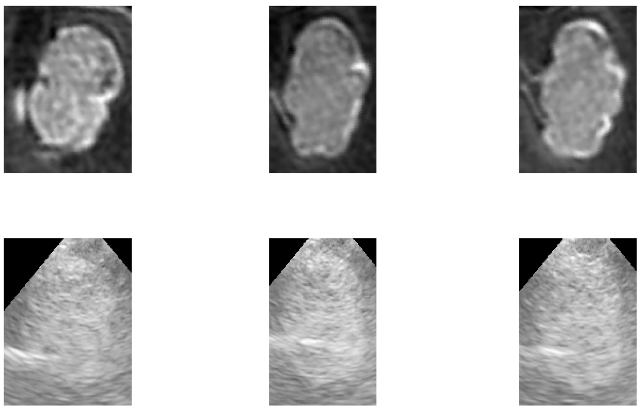

Figure D.1: Case 4. Up: MRI; Down: US.

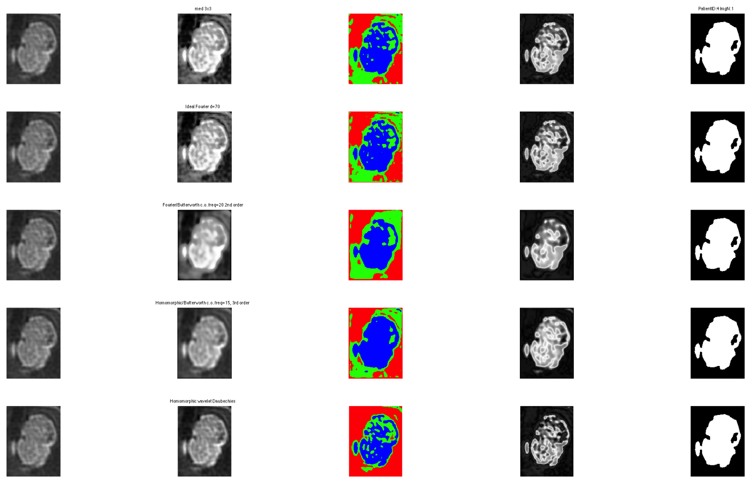

Figure D.2: MR imaging: Case 4, Image 1. In order from top to bottom: Median 3x3, Ideal Fourier, Fourier/Butterworth, Homomorphic/Butterworth, Homomorphic wavelet Daubechies filtering.

MCC 41	Median 3x3	Ideal Fourier	Fourier/Butterworth	Homomorphic/ butterworth	Homomorphic wavelet Dau
MIN	0,7010	0,6987	0,6993	0,7004	0,6597
Lesion 41	0,8438	0,8529	0,8491	0,9429	0,7405
MEAN	0,8332	0,8323	0,8332	0,8741	0,8149
MAX	0,9418	0,9306	0,9413	0,9429	0,9306

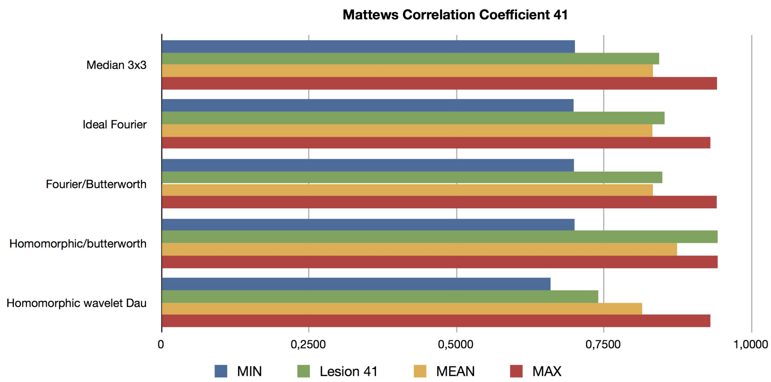

Figure D.3: MR MCC, Case 4, Image 1

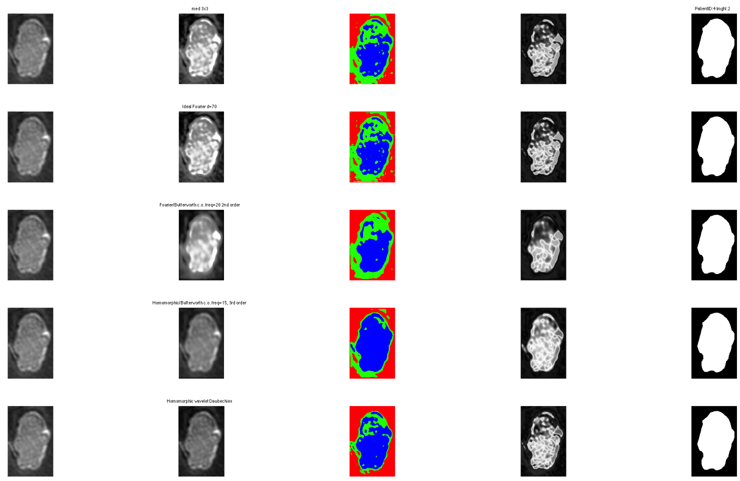

Figure D.4: MR imaging: Case 4, Image 2. In order from top to bottom: Median 3x3, Ideal Fourier, Fourier/Butterworth, Homomorphic/Butterworth, Homomorphic wavelet Daubechies filtering.

MCC 42	Median 3x3	Ideal Fourier	Fourier/Butterworth	Homomorphic/ butterworth	Homomorphic wavelet Dau
MIN	0,7010	0,6987	0,6993	0,7004	0,6597
Lesion 42	0,7010	0,6987	0,6993	0,9049	0,7723
MEAN	0,8332	0,8323	0,8332	0,8741	0,8149
MAX	0,9418	0,9306	0,9413	0,9429	0,9306

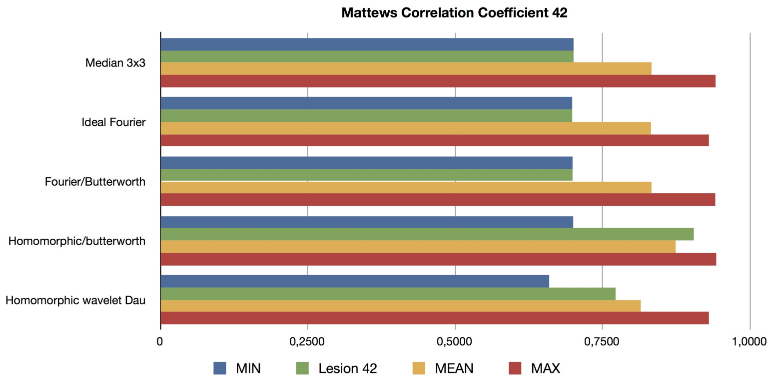

Figure D.5: MR MCC, Case 4, Image 2

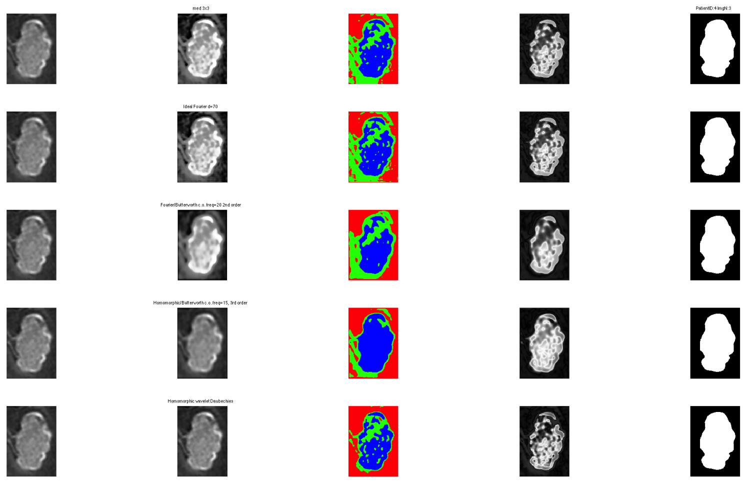

Figure D.6: MR imaging: Case 4, Image 3. In order from top to bottom: Median 3x3, Ideal Fourier, Fourier/Butterworth, Homomorphic/Butterworth, Homomorphic wavelet Daubechies filtering.

MCC 43	Median 3x3	Ideal Fourier	Fourier/Butterworth	Homomorphic/ butterworth	Homomorphic wavelet Dau
MIN	0,7010	0,6987	0,6993	0,7004	0,6597
Lesion 43	0,7759	0,7713	0,7759	0,9254	0,7303
MEAN	0,8332	0,8323	0,8332	0,8741	0,8149
MAX	0,9418	0,9306	0,9413	0,9429	0,9306

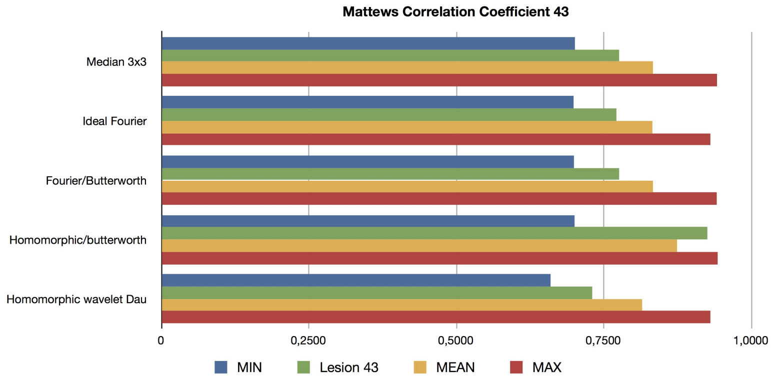

Figure D.7: MR MCC, Case 4, Image 3

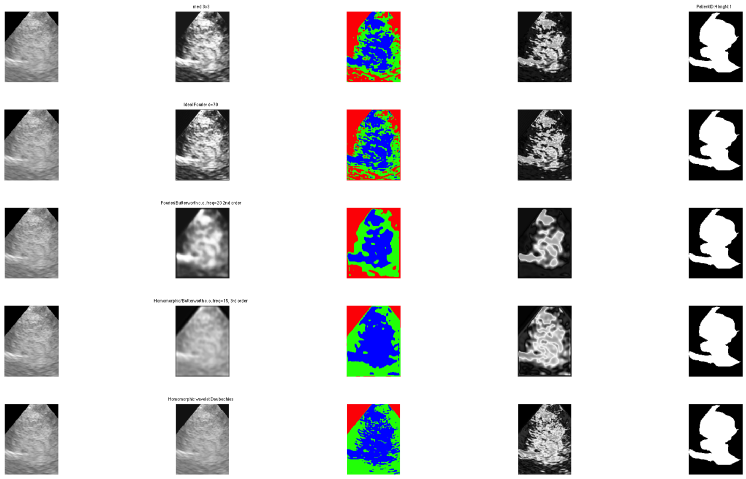

Figure D.8: US imaging: Case 4, Image 1. In order from top to bottom: Median 3x3, Ideal Fourier, Fourier/Butterworth, Homomorphic/Butterworth, Homomorphic wavelet Daubechies filtering.

MCC 41	Median 3x3	Ideal Fourier	Fourier/Butterworth	Homomorphic/ butterworth	Homomorphic wavelet Dau
MIN	0,4836	0,4989	0,5802	0,4478	0,4438
Lesion 41	0,6058	0,5849	0,6207	0,6870	0,6283
MEAN	0,6091	0,5972	0,6867	0,6344	0,5837
MAX	0,7620	0,7115	0,7992	0,7744	0,7115

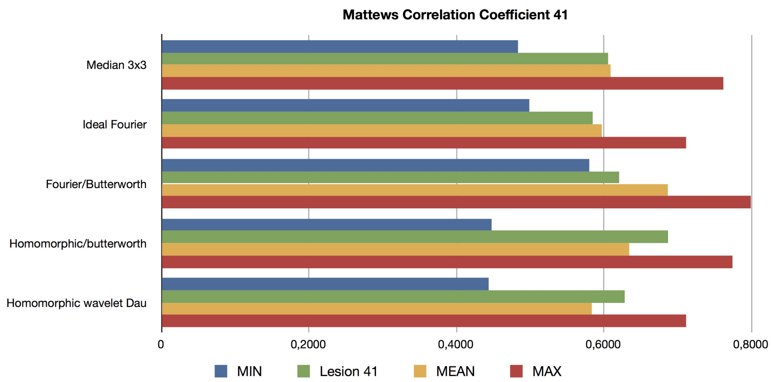

Figure D.9: US MCC, Case 4, Image 1

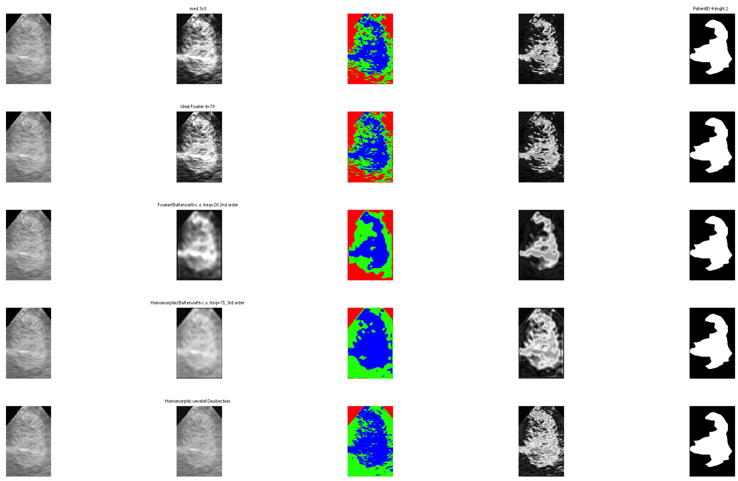

Figure D.10: US imaging: Case 4, Image 2. In order from top to bottom: Median 3x3, Ideal Fourier, Fourier/Butterworth, Homomorphic/Butterworth, Homomorphic wavelet Daubechies filtering.

MCC 42	Median 3x3	Ideal Fourier	Fourier/Butterworth	Homomorphic/ butterworth	Homomorphic wavelet Dau
MIN	0,4836	0,4989	0,5802	0,4478	0,4438
Lesion 42	0,7196	0,6945	0,7992	0,6809	0,6571
MEAN	0,6091	0,5972	0,6867	0,6344	0,5837
MAX	0,7620	0,7115	0,7992	0,7744	0,7115

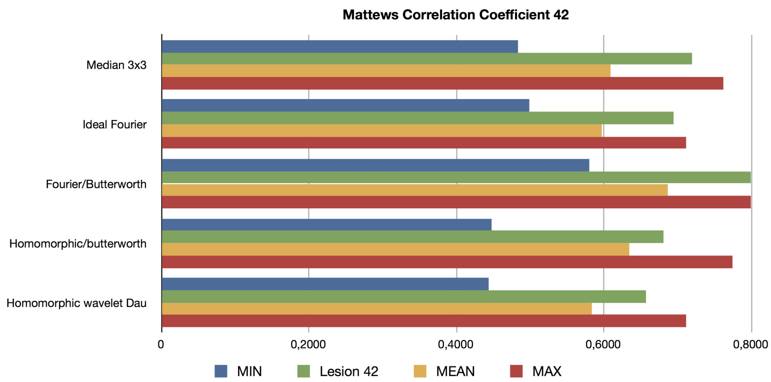

Figure D.11: US MCC, Case 4, Image 2

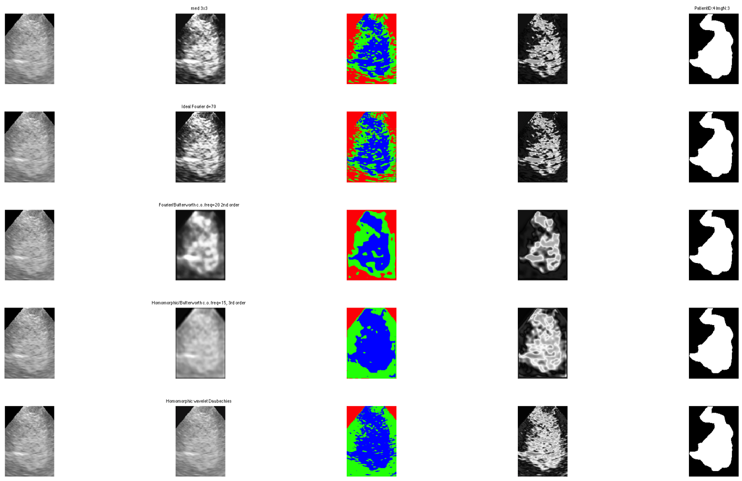

Figure D.12: US imaging: Case 4, Image 3. In order from top to bottom: Median 3x3, Ideal Fourier, Fourier/Butterworth, Homomorphic/Butterworth, Homomorphic wavelet Daubechies filtering.

MCC 43	Median 3x3	Ideal Fourier	Fourier/Butterworth	Homomorphic/ butterworth	Homomorphic wavelet Dau
MIN	0,4836	0,4989	0,5802	0,4478	0,4438
Lesion 43	0,6922	0,6608	0,7404	0,7744	0,7115
MEAN	0,6091	0,5972	0,6867	0,6344	0,5837
MAX	0,7620	0,7115	0,7992	0,7744	0,7115

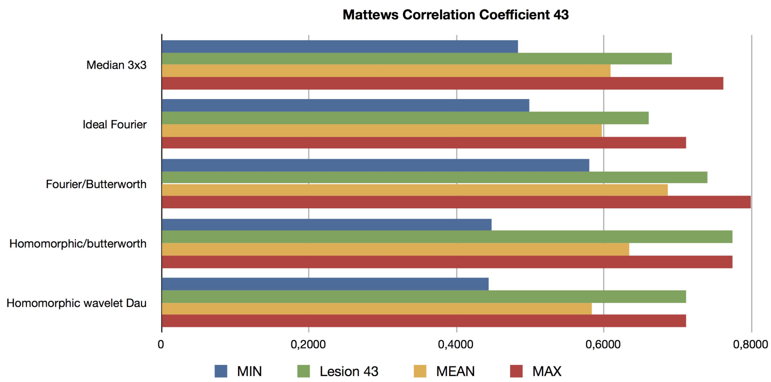

Figure D.13: US MCC, Case 4, Image 3.

Appendix E

Case 5

Surgery information

- Sugeon: Prof. Francesco Sala
- Data of intervenction: 11/06/2013
- Pathology: Metastases
- Gender: Female
- Patient age: 65 years

MRI information

- Magnetic field strenght: 3.0 Tesla
- Voxel dimension (mm x mm x mm): 0.43 x 0.43 x 1.00
- Space between slices (mm): 0.00
- Number of slices: 176
- Slices orientation: Axial
- Acquisition mode: T1 with contrast (Gadolinium)
- Exam data: 05/06/2013

US information

- Wave frequency (MHz): 6.67
- Wave lenght (mm): 0.224
- Pixel dimension (mm x mm): 0.127 x 0.127
- Depth of scan field (mm): 50
- Refresh rate (Hz): 77
- Original image resolution: 800 x 600

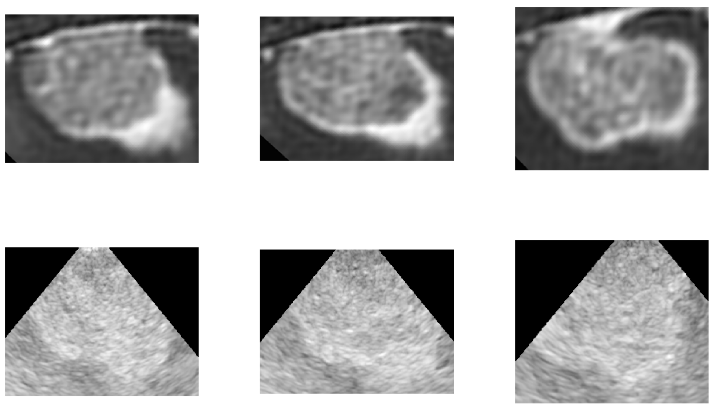

Figure E.1: Case 5. Up: MRI; Down: US.

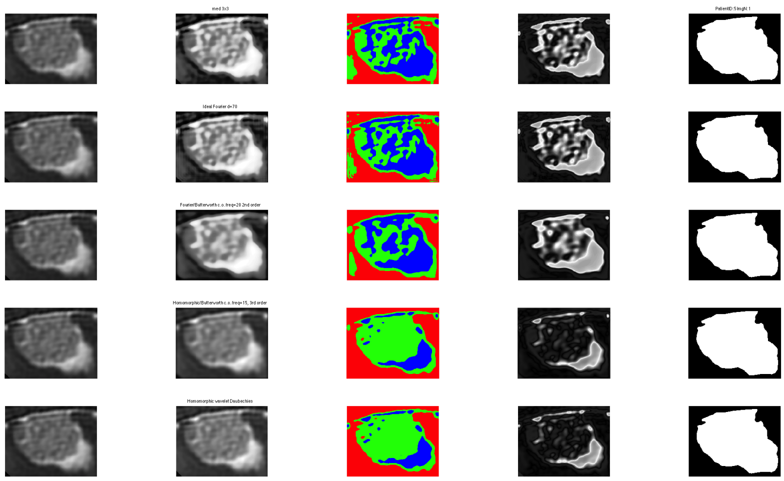

Figure E.2: MR imaging: Case 5, Image 1. In order from top to bottom: Median 3x3, Ideal Fourier, Fourier/Butterworth, Homomorphic/Butterworth, Homomorphic wavelet Daubechies filtering.

MCC 51	Median 3x3	Ideal Fourier	Fourier/Butterworth	Homomorphic/ butterworth	Homomorphic wavelet Dau
MIN	0,7010	0,6987	0,6993	0,7004	0,6597
Lesion 51	0,8205	0,8246	0,8178	0,9148	0,9098
MEAN	0,8332	0,8323	0,8332	0,8741	0,8149
MAX	0,9418	0,9306	0,9413	0,9429	0,9306

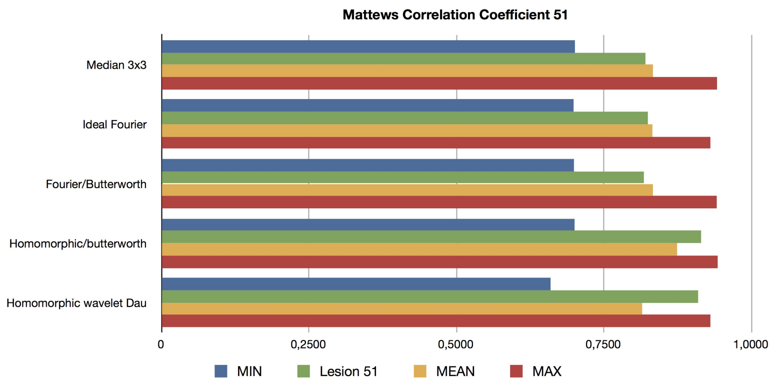

Figure E.3: MR MCC, Case 5, Image 1

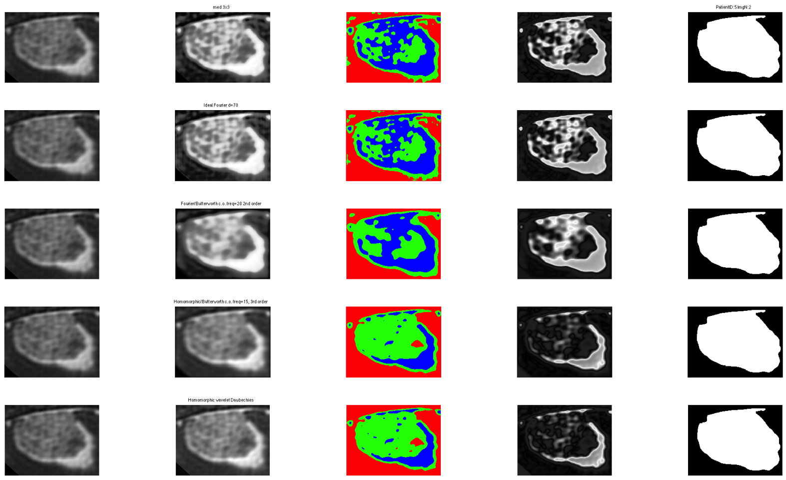

Figure E.4: MR imaging: Case 5, Image 2. In order from top to bottom: Median 3x3, Ideal Fourier, Fourier/Butterworth, Homomorphic/Butterworth, Homomorphic wavelet Daubechies filtering.

MCC 52	Median 3x3	Ideal Fourier	Fourier/Butterworth	Homomorphic/ butterworth	Homomorphic wavelet Dau
MIN	0,7010	0,6987	0,6993	0,7004	0,6597
Lesion 52	0,8263	0,8252	0,8281	0,9021	0,8975
MEAN	0,8332	0,8323	0,8332	0,8741	0,8149
MAX	0,9418	0,9306	0,9413	0,9429	0,9306

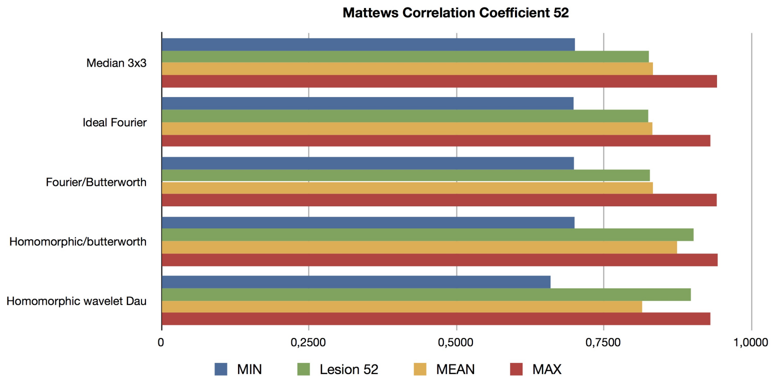

Figure E.5: MR MCC, Case 5, Image 2

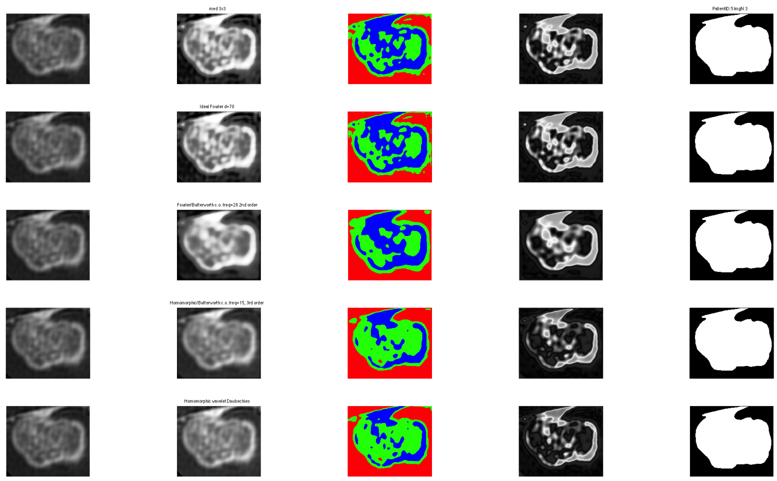

Figure E.6: MR imaging: Case 5, Image 3. In order from top to bottom: Median 3x3, Ideal Fourier, Fourier/Butterworth, Homomorphic/Butterworth, Homomorphic wavelet Daubechies filtering.

MCC 53	Median 3x3	Ideal Fourier	Fourier/Butterworth	Homomorphic/ butterworth	Homomorphic wavelet Dau
MIN	0,7010	0,6987	0,6993	0,7004	0,6597
Lesion 53	0,8383	0,8390	0,8317	0,9407	0,9306
MEAN	0,8332	0,8323	0,8332	0,8741	0,8149
MAX	0,9418	0,9306	0,9413	0,9429	0,9306

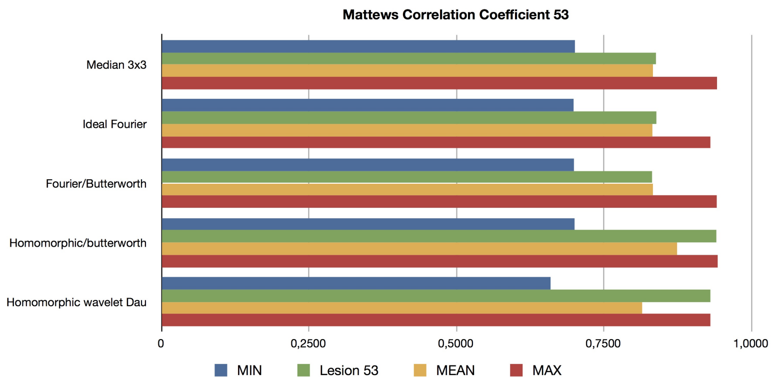

Figure E.7: MR MCC, Case 5, Image 3

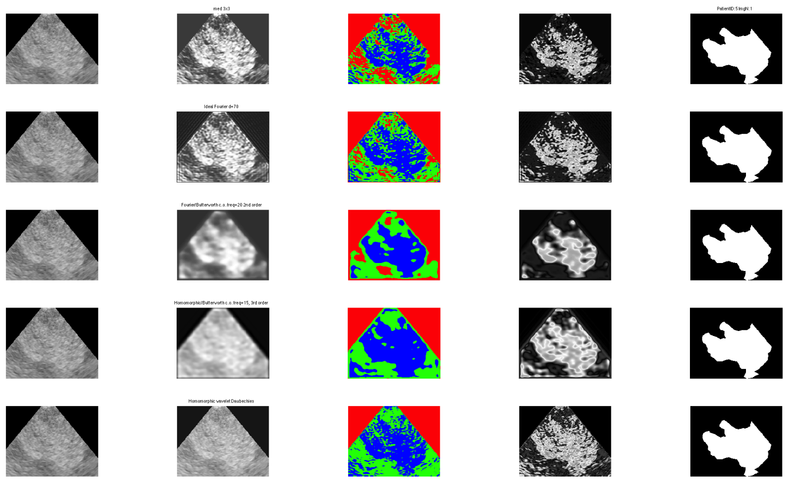

Figure E.8: US imaging: Case 5, Image 1. In order from top to bottom: Median 3x3, Ideal Fourier, Fourier/Butterworth, Homomorphic/Butterworth, Homomorphic wavelet Daubechies filtering.

MCC 51	Median 3x3	Ideal Fourier	Fourier/Butterworth	Homomorphic/ butterworth	Homomorphic wavelet Dau
MIN	0,4836	0,4989	0,5802	0,4478	0,4438
Lesion 51	0,5854	0,5953	0,7465	0,6723	0,5844
MEAN	0,6091	0,5972	0,6867	0,6344	0,5837
MAX	0,7620	0,7115	0,7992	0,7744	0,7115

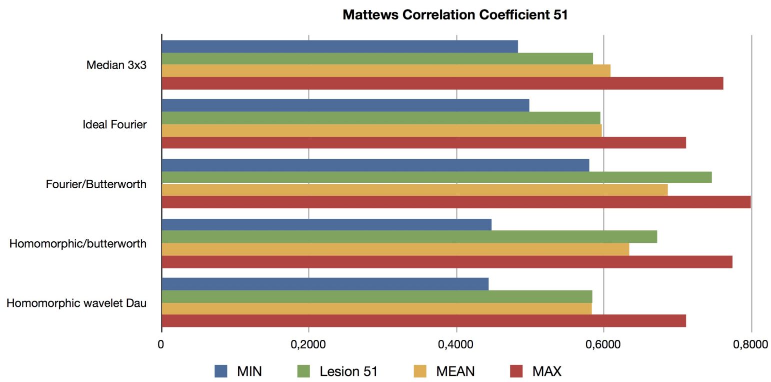

Figure E.9: US MCC, Case 5, Image 1

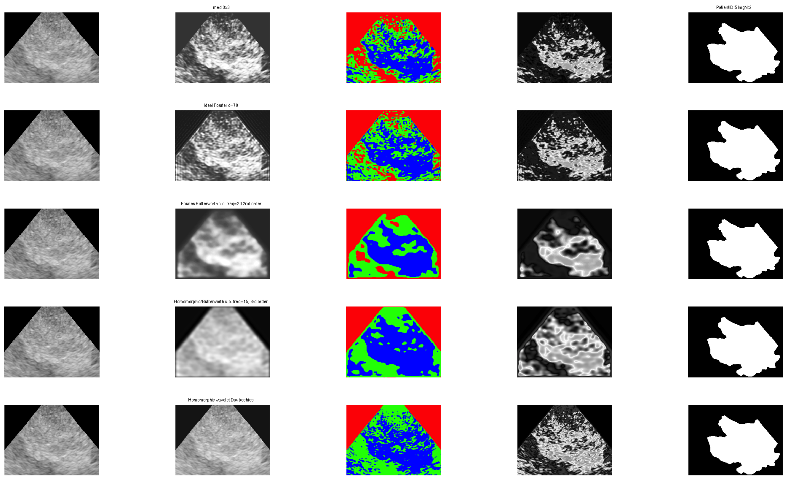

Figure E.10: US imaging: Case 5, Image 2. In order from top to bottom: Median 3x3, Ideal Fourier, Fourier/Butterworth, Homomorphic/Butterworth, Homomorphic wavelet Daubechies filtering.

MCC 52	Median 3x3	Ideal Fourier	Fourier/Butterworth	Homomorphic/ butterworth	Homomorphic wavelet Dau
MIN	0,4836	0,4989	0,5802	0,4478	0,4438
Lesion 52	0,5310	0,5226	0,6162	0,6131	0,5224
MEAN	0,6091	0,5972	0,6867	0,6344	0,5837
MAX	0,7620	0,7115	0,7992	0,7744	0,7115

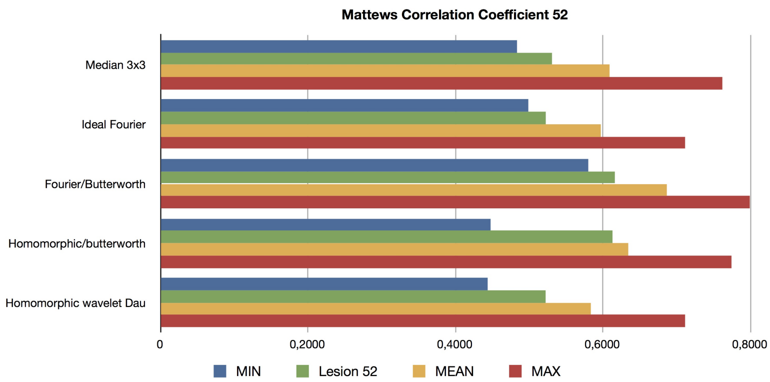

Figure E.11: US MCC, Case 5, Image 2

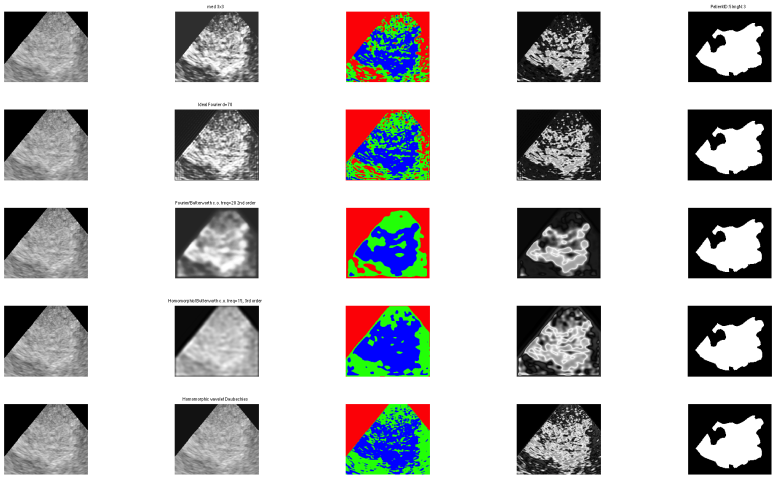

Figure E.12: US imaging: Case 5, Image 3. In order from top to bottom: Median 3x3, Ideal Fourier, Fourier/Butterworth, Homomorphic/Butterworth, Homomorphic wavelet Daubechies filtering.

MCC 53	Median 3x3	Ideal Fourier	Fourier/Butterworth	Homomorphic/ butterworth	Homomorphic wavelet Dau
MIN	0,4836	0,4989	0,5802	0,4478	0,4438
Lesion 53	0,5848	0,5757	0,6754	0,6558	0,5674
MEAN	0,6091	0,5972	0,6867	0,6344	0,5837
MAX	0,7620	0,7115	0,7992	0,7744	0,7115

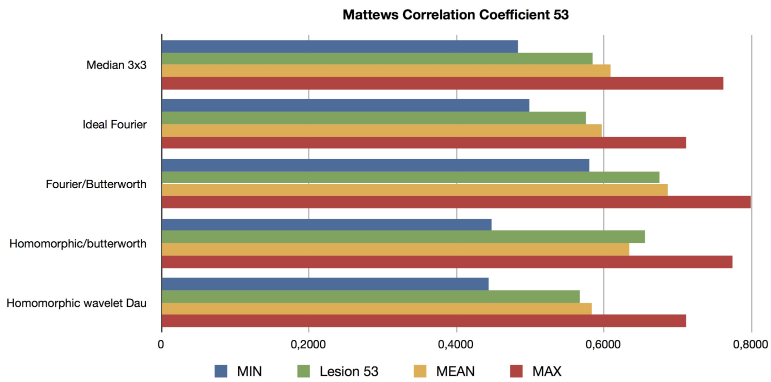

Figure E.13: US MCC, Case 5, Image 3.

Bibliography

[1] URL: http://epp.eurostat.ec.europa.eu/portal/page/portal/government_finance_statistics/data.

[2] URL: http://www.ospedaleuniverona.it/ecm/home/l-azienda/chi-siamo/the-hospital-trust-of-verona.

[3] URL: http://www.genesis.net.au/~ajs/projects/medical_physics/ultrasound/index.html.

[4] URL: http://www.yetkintelesystems.com/en/urun1.htm.

[5] URL: http://www.hindawi.com/journals/bcri/2012/715197/fig1/.

[6] URL: http://www.aloka.com/home.asp.

[7] URL: http://www.aloka.com/products/view_system.asp?id=20.

[8] URL: http://www.hitachi-aloka.co.jp/english/products/ultrasonic/alpha7/alpha7_02.html.

[9] URL: http://www.aloka.com/products/view_category_probes.asp?id=15.

[10] URL: http://www.diffen.com/difference/CT_Scan_vs_MRI.

[11] URL: http://www.mathworks.com/products/matlab/?s_tid=hp_fp_ml.

[12] Yousse A.B. Abd-Elmoniem K.Z. and Y.M. Kadah. "Real-time speckle reduction and coherence enhancement in ultrasound imaging via non linear anisotropic diffusion." In: *IEEE Transactions on Biomedical Engineering* 49.9 (2002), pp. 997–1014.

[13] John Koivukangas at al. "Ultrasound-controlled neuronavigator-guided brain surgery." In: *Journal of Neurosurgery* 79 (1993), pp. 36–42.

[14] Maarouf A. Hammoud et al. "Use of intraoperative ultrasound for localizing tumors and determining the extent of resection- a comparative study with magnetic resonance imaging.pdf." In: *Journal of Neurosurgery* 84 (1996), pp. 737–741.

[15] Ole Vegard Solberg at al. "Freehand 3D Ultrasound Reconstruction Algorithms - A Review." In: *Ultrasound in Medicine and Biology* 33.7 (2007), pp. 991–1009.

[16] Volker M. Tronnier at al. "Comparison of intraoperative MR imaging and 3D-navigated ultrasonography in the detection and resection control of lesions." In: *Neurosurg Focus* 10.3 (2001), pp. 1–5.

[17] Peter Mendel Miroslav Cik Juraj Steno Andrej Steno Martin Karlik. "Navigated three-dimensional intraoperative ultrasound-guided awake resection of low-grade glioma partially infiltrating optic radiation." In: *Acta Neurochirurgica* (2012).

[18] Dermitzakis Aristeidis. *Acoustical Behavior of Single Ultrasound Contrast Agent Microbubbles*. Master's Thesis. 2010.

[19] L.M. Auer and V. van Velthoven. "Intraoperative Ultrasound (US) Imaging. Comparison of Pathomorphological Findings in US and CT." In: *Acta Neurochirurgica* 104 (1990), pp. 84–95.

[20] Eberhard Brunner. "How Ultrasound System Considerations Influence Front-End Component Choice." In: *Analog Dialogue* 36.3 (2002), pp. 1–4.

[21] Silvia Capelli and Carlo Girelli. *Sviluppo di un sistema per il monitoraggio multiparametrico della funzione respiratoria nei neonati.* Bachelor degree thesis. Politecnico di Milano, 2010.

[22] Vincent Chan and Anahi Perlas. *Atlas of Ultrasound-Guided Procedures in Interventional Pain Management.* S.N. Narouze (ed.), 2011.

[23] Yin R. Flynn P. Chen Y. and S. Broschat. "Aggressive region growing for speckle reduction in ultrasound images." In: *Pattern Recognition Letters* 24.4-5 (2003), pp. 667–691.

[24] Marcello Crivellini and Manuela Galli. *Sanità e salute: due storie diverse - Sistemi sanitari e salute nei paesi industrializzati.* Sanità. Viale Monza 106, 20127 Milano, Italy: FrancoAngeli, 2011.

[25] *Extent of Resection as a Prognostic Variable in the Treatment of Gliomas.*

[26] MS Berger. GE Keles B Anderson. "The effect of extent of resection on time to tumor progression and survival in patients with glioblastoma multiforme of the cerebral hemisphere." In: *Surgical neurology* (1999).

[27] Steinar Ommedal Toril A. Nagelhus Hernes Geirmund Unsgaard Aage Gronningsaeter. "Brain Operations Guided by Real-time Two-dimensional Ultrasound: New Possibilities as a Result of Improved Image Quality." In: *Neurosurgery* 51.2 (2002), pp. 402–412.

[28] Tomm Muller Aage Gronningsaeter Toril A. Nagelhua Hernes Geirmund Unsgaard Steinar Ommendal. "Neuronavigation by Intraoperative Three-dimensional Ultrasound: Initial Experience during Brain Tumor Resection." In: *Neurosurgery* 50.804-812 (2002).

[29] K. Helme M. Westphal J. Regelsberger F. Lohmann. "Ultrasound-guided surgery of deep seated brain lesions." In: *European Journal of Ultrasound* 12 (2000), pp. 115–121.

[30] AP King DJ Hawkes JM Blackall GP Penny. "Alignment of sparse freehand 3-D ultrasound with preoperative images of the liver using models of respiratory motion and deformation." In: *IEEE Trans Med Imaging* 24 (2005), pp. 1405–1416.

[31] Kutay M.A. Karaman M. and G. Bozdagi. "An adaptative speckle suppression filter for medical ultrasonic imaging." In: *IEEE Trasactions on Medical Imaging* 14.2 (1995), pp. 283–292.

[32] Kazuhiko Suyama Izumi Nagata Kentaro Hayashi Takayuki Matsuo. "Usefulness of Ultrasonography with a Burr-Hole Transducer During Surgery Through a Burr hole." In: *Neurol Med Chir (Tokyo)* 52 (2012), pp. 165–168.

[33] Matthew J.; Bartlett Jonathan W.; Clegg Shona; Jack Clifford R. Leung Kelvin K.; Clarkson. "Robust atrophy rate measurement in Alzheimer's disease using multi-site serial MRI: Tissue-specific intensity normalization and parameter selection." In: *Neuroimage* 50.2 (2010).

[34] Max A. Viergever Wiro J. Niessen Marloes M.J. Letterboer Peter W.A. Willems. "Brain Shift Estimation in Image-Guided Neurosurgery Using 3-D Ultrasound." In: *IEEE Transaction on biomedical engineering* 52.2 (2005), pp. 268–276.

[35] Wolf-Ingo Steudel Martin Strowitzki Jean Richard Moringlane. "Ultrasound-Based Navigation during Itracranial Burr Hole Procedures: Experience in a Series of 100 Cases." In: *Elseiver Science* (2000).

[36] Saad Masood. *Feasibility of Inter-Modal Rigid Registration.* 2010.

[37] Kaisorn L. chaichana B.s. Muraya GathinJi M.s. FranK J. atteneLLo M.s. Khoi than M.D. aLessanDro oLivi M.D. Jon D. weinGart M.D. henry BreM M.D. Matthew J. McGirt M.D. and M.D. aLFreDo Quiñones-hinoJosa. "Independent association of extent of resection with survival

in patients with malignant brain astrocytoma." In: *Journal of Neurosurgery* 110 (2009), pp. 156–162.

[38] *Metastasis Stage, Adjuvant Treatment, and Residual Tumor Are Prognostic Factors for Medulloblastoma in Children: Conclusions From the Children's Cancer Group 921 Randomized Phase III Study.*

[39] Susan Katz Miller, Dr. Marvin C. Ziskin, and Dr. Wesley L. Nyborg.] *Exposure Criteria for Medical Diagnostic Ultrasound: II. Criteria Based on all Known Mechanisms.* Tech. rep. National Council on Radiation Protection and Measurements, 1991.

[40] Kelverkloglou Panagiota. *Simulation of Ultrasound Brain Cancer Imaging.* 2011.

[41] Terry M. Peters. "Image-guidance for surgical procedures." In: *Institute of Physics Publishing* 51 (2006), R505–R540.

[42] Deforge P. Rakotomamonjy A. and P. Marche. "Wavelet-based speckle noise reduction in ultrasound B-scan images." In: *Ultrasonic Imaging* 22.2 (2000), pp. 73–94.

[43] Aaron Fenster Terry M. Peters Roch M. Comeau Abbas F. Sadikot. "Intraoperative ultrasound for guidance and tissue shift correction in image-guided neurosurgery." In: *Medical Physics* 27 (2000), pp. 787–800.

[44] K Hensel S Hld G Schmitz W Teske S Winter C Dekomien. "[Registration of intraoperative 3D ultrasound with preoperative MRI data for compuer-assisted orthopaedic surgery]." In: *Z Orthop Unfall* 145 (2007), pp. 586–590.

[45] Annika Plate Kai Boetzel Nassir Navab Seyed-Ahmad Ahmadi Tassilo Klein. *Rigid US-MRI Registration.*

[46] Athanasios Karamalis Annika Plate Kai Boetzel Tassilo Klein Seyed-Ahmad Ahmadi Maximilian Baust and Nassir Navab. *Midbrain Segmentation in Transcranial 3D Ultrasound for Parkinson Diagnosis.*

[47] James E.Knake M.D. John E. McGillicuddy M.D. Kevin O. Lillehei M.D. William F. Chandler M.D. and M.D. Terry M. Silver. "Intraoperative use of real-time ultrasonography in neurosurgery." In: *Journal of Neurosurgery* 57 (1982), pp. 157–163.

[48] J Ren G Guiraudon D Boughner TM Peters X Huang NA Hill. "Dynamic 3D ultrasound and MR image registration of the beating heart." In: *MICCAI* (2005), pp. 171–178.

[49] D. Miller W. Tirakotai S. Heinze L. Benes H. Bertalanffy Y. Enchev O. Bozinov and U. Sure. "Image-guided ultrasonography for recurrent cystic gliomas." In: *Acta Neurochirurgica* 148 (2006), pp. 1053–1063.

Ringraziamenti

"Il grazie è abituale sulle labbra di chi non si sente padrone di nulla e comprende che nulla di ciò che ha è suo."

Don Oreste Benzi (1925 - 2007)
Sacerdote Italiano

Il raggiungimento di un obiettivo, tanto più se è un obiettivo importante, è giustamente motivo di gioia. Tuttavia nessuno è in grado di raggiungere alcun traguardo senza l'aiuto, il sostegno e l'amore di chi gli sta accanto. Oggi mi viene attributo il titolo di dottore magistrale in ingegneria biomedica, un titolo che vorrei condividere con tutti voi. Oggi c'è Carlo davanti a questa commissione, un Carlo che sarebbe diverso se mancasse anche una sola delle persone che voglio qui ringraziare. Per questo motivo, qui oggi con me, a ricevere questo titolo, ci sono tutte le persone che porto nel cuore. Ognuno di voi meriterebbe di poter scrivere nel proprio curriculum di questo giorno, poiché ognuno di voi mi ha reso possibile raggiungerlo. Se sono arrivato fino a qui è anche e soprattutto merito delle persone che mi sono state accanto. Tutti voi, con i vostri carismi, mi avete donato qualcosa di straordinario. Chiedo perdono per tutti i miei difetti e chiedo scusa a tutti coloro che dimenticherò di ringraziare nelle prossime righe.

Grazie al prof. Ferrigno e alla dott.ssa De Momi che mi hanno prima proposto questo lavoro di tesi e successivamente mi hanno guidato a distanza nel portarlo avanti. Grazie perché siete riusciti a indirizzare correttamente il mio lavoro verso una strada che da solo, per inesperienza, non avrei saputo perseguire.

Grazie al prof. Foroni che mi ha sempre motivato, anche quando a volte ero deluso. Grazie per tutte le volte che mi ha dato fiducia, mi ha incoraggiato e ha dato valore ai miei piccoli passi in avanti a livello professionale. Grazie per la grande considerazione che ha di me e del mio lavoro anche quando la sento immeritata.

Grazie a Pasquale che mi ha dedicato tempo ed energie. Grazie a quando con la sua lucidità mi ha dato consigli preziosi per il mio lavoro e per il mio futuro. Grazie per il bellissimo lavoro svolto e per il fondamentale aiuto nell'analisi dei dati. La tua esperienza nel campo dell'imaging e, più in generale, della ricerca è stata un pilastro del mio lavoro.

Grazie al dott. Pinna, direttore del reparto di neurochirurgia ospedaliera, che mi ha dato la possibilità di frequentare il suo reparto, di assistere agli interventi e di provare questa nuova tecnologia. Grazie per l'interessamento che ha sempre dimostrato nei confronti del mio studio e del mio lavoro. Grazie anche ai proff. Gerosa e Meglio, direttori del reparto di neurochirurgia clinica, che mi hanno accolto e mi hanno permesso di portare avanti il mio lavoro.

Grazie al prof. Sala e ai dott.ri Musumeci e Damante che hanno voluto provare in prima persona l'ecografo e che mi hanno aiutato a raccogliere i dati. Grazie per aver risposto sempre volentieri alle mie domande, anche a quelle che per un medico possono sembrare banali e scontate. Il nostro diverso percorso di studi non ci ha impedito di collaborare con profitto.

Grazie a tutti gli strutturati del reparto di neurochirurgia di Verona. Oltre che ottimi professionisti siete anche persone con cui è piacevole intrattenersi. Grazie in modo particolare ai dott.ri Soda, Barone, Ricci, Gambin, Cristofori, Longhi, Moscolo, Masotto e Nicolato.

Grazie agli specializzati, agli specializzandi, ai tecnici e a tutti gli operatori, in particolare grazie a Laura, Antonio, Valentina, Angela, Francesco, entrambe le Antonella, Micol, Pietro, Vincenzo e tutti gli altri. Mi avete sempre fatto sentire come uno di voi. Thanks to Sonia for her precious help with the translation.